Chapter 5
Dissipative Particle Dynamics: Foundation, Evolution, Implementation, and Applications

Z. Li, X. Bian, X. Li, M. Deng, Y.-H. Tang, B. Caswell, and G.E. Karniadakis

Abstract Dissipative particle dynamics (DPD) is a particle-based Lagrangian method for simulating dynamic and rheological properties of simple and complex fluids at mesoscopic length and time scales. In this chapter, we present the DPD technique, beginning from its original ad hoc formulation and subsequent theoretical developments. Next, we introduce various extensions of the DPD method that can model non-isothermal processes, diffusion-reaction systems, and ionic fluids. We also present a brief review of programming algorithms for constructing efficient DPD simulation codes as well as existing software packages. Finally, we demonstrate the effectiveness of DPD to solve particle-fluid problems, which may not be tractable by continuum or atomistic approaches.

Keywords Coarse-Graining • Computational biology • Fluctuating hydrodynamics • Fluid mechanics • Lagrangian approach • Mesoscopic method • Multiscale simulation • Particle-based method • Soft matter • Stochastic simulation • Thermostat

MSC2010: 76Z05, 76V05, 74F10, 80A32, 92C35, 74F25, 80A30, 92C45, 92C40

5.1 Introduction

In many applications to soft matter and biological systems, despite of the sustained fast growth of computing power during the past few decades, it is still computationally prohibitive or impractical to simulate dynamics for long temporal scales and large spatial scales with brute-force atomistic simulations [82]. The reason is that the atomistic approaches are limited by the number of atoms/molecules that can be

---

Z. Li • X. Bian • X. Li • M. Deng • Y.-H. Tang • G.E. Karniadakis (✉)
Division of Applied Mathematics, Brown University, Box F, Providence, RI 02912, USA
e-mail: george_karniadakis@brown.edu

B. Caswell
School of Engineering, Brown University, Providence, RI 02912, USA

T. Bodnár et al. (eds.), *Particles in Flows*, Advances in Mathematical
Fluid Mechanics, DOI 10.1007/978-3-319-60282-0_5

included in the simulation, typically $10^4 - 10^8$ corresponding to a length-scale on the order of tens of nanometers, and the maximum time step in atomistic simulations is limited by the smallest oscillation period of the fastest atomic motions in a molecule, which is typically several femtoseconds (10^{-15} s). However, if only mesoscopic structures of molecules or their collective behavior are of practical interest, it may be unnecessary to explicitly take into account all of the atomistic details of materials [110]. To this end, the mesoscopic approach drastically simplifies the atomistic dynamics by eliminating fast degrees of freedom while preserving the behavior of slow entities, and provides an economical simulation path to capture the correct dynamics of complex fluids on larger spatial and temporal scales beyond the capability of conventional atomistic simulations [78]. In recent years, with increasing attention to the research of soft matter and biophysics, mesoscopic modeling has become a rapidly expanding methodology [98] with applications to material science [81, 95], polymer physics [40, 59, 70], rheology of complex fluids [10, 88] and computational biology [55, 56, 93].

Dissipative particle dynamics (DPD) is currently one of the most popular mesoscopic methods [71]. In DPD, a single coarse-grained (CG) particle represents an entire cluster of molecules, with unresolved degrees of freedom approximated by stochastic dynamics [61, 64]. Similar to the molecular dynamics (MD) method, a DPD system consists of many interacting particles with their dynamics computed by time integration of Newton's equation of motion. However, in contrast to MD, DPD has soft interaction potentials allowing for larger integration time steps. As a bottom-up mesoscopic approach, the DPD method smoothly bridges the gap between the microscopic and macroscopic worlds. On the one hand, DPD has its roots in microscopic dynamics as its governing equations can be rigorously derived from the microscopic dynamics by applying the Mori-Zwanzig projection operator [61]. On the other hand, the framework of DPD can be derived from the fluctuating Navier-Stokes equation [25]. The interactions between DPD particles are pairwise so that the total momentum of the DPD system is strictly conserved. By using the Fokker-Planck equation and applying the Mori projection operator, Español [22] and Marsh et al. [77] showed that the hydrodynamic equations of a DPD system recover the continuity and Navier-Stokes equations. Therefore, the DPD method can be considered as a particle-based Lagrangian representation of the continuity and momentum equations at the mesoscopic level.

In this chapter, we will revisit the theory, algorithms and applications of the DPD method. In Sect. 5.2 we consider its theoretical formulation. Beginning with the statistical mechanics behind the DPD method, both bottom-up and top-down derivations of its governing equations as well as the parameterizations will be presented. Next, in Sect. 5.3 we review several extensions of DPD that have been developed in recent years for tackling the challenges in diverse multi-physics applications beyond the capability of the classical DPD method. In Sect. 5.4 we introduce some useful algorithms for computer implementation of DPD simulations. Finally, we present some selected applications in Sect. 5.5 and end with a brief summary in Sect. 5.6.

5.2 Theoretical Formulation and Parameterization

The DPD method was invented intuitively by Kolemann and Hoggerbrugee [39, 44] to study hydrodynamic phenomena at the mesoscale. In the original formulation, DPD has only two types of pairwise forces: dissipative and random forces. Later on Español and Warren [26] further introduced the pairwise conservative force. Meanwhile they also derived the stochastic differential equations (SDE) as the equation of motion (EoM) for the particles. This is a fundamental step putting DPD on a firm physical ground, where the equilibrium invariant distribution of a DPD system is the canonical ensemble of Gibbs if the fluctuation-dissipation theorem (FDT) is satisfied by the DPD inputs. In Sect. 5.2.1, we will introduce the detailed derivations of the FDT for DPD systems.

Furthermore, we describe the projection technique (the Mori projection) in the first part of Sect. 5.2.2, which establishes the correspondence between DPD parameters and thermodynamic properties and transport coefficients of the fluids from the continuum point of view. This is indicated as route A in Fig. 5.1. To connect DPD with a continuum description, one may also interpret DPD as a Lagrangian discretization of the Landau-Lifshitz-Navier-Stokes equation. In this case, it is named as Smoothed DPD or SDPD for brevity. This will be explained in detail in the second part of Sect. 5.2.2, which corresponds to route B in Fig. 5.1. We may further apply the method of BBGKY (Bogoliubov-Born-Green-Kirkwood-Yvon) hierarchy to obtain a kinetic equation for the single particle distribution and then solve it to recover the Navier-Stokes' transport coefficients, as will be explained in Sect. 5.2.3. This corresponds also to the route A in Fig. 5.1. Another simpler alternative to predict the transport coefficients of DPD is by assuming the continuum limit within the cut off radius and take a continuum integral of the DPD parameters as indicated also as the route A in Fig. 5.1. The continuum integral approach together with parameterization of thermodynamic properties (compressibility) are both explained in Sect. 5.2.4. Finally, in Sect. 5.2.5, we revisit some representative work on the fundamental basis for coarse-graining the underlying system of molecular dynamics, including again the projection technique. This time it is the Zwanzig projection instead of the Mori projection. This corresponds to route C in Fig. 5.1.

5.2.1 Fokker-Planck Equation and Fluctuation-Dissipation Theorem

Rather than the *discrete* form from the original DPD paper [39], Español and Warren [26] formulated an EoM for DPD particles as *continuous* stochastic differential equations (SDE)

$$\begin{aligned} \dot{\mathbf{r}}_i &= \dot{\mathbf{p}}_i/m, \\ \dot{\mathbf{p}}_i &= \mathbf{F}_i = \sum_{j\neq i}\mathbf{F}_{ij} = \sum_{j\neq i}\left(\mathbf{F}^C_{ij} + \mathbf{F}^D_{ij} + \mathbf{F}^R_{ij}\right), \end{aligned} \tag{5.1}$$

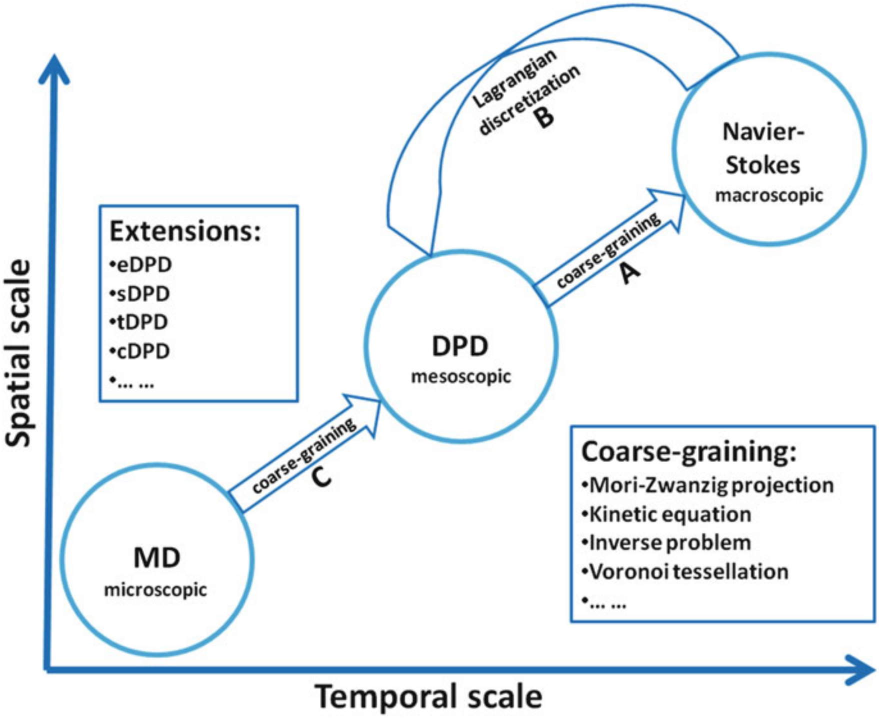

Fig. 5.1 Sketch of the current developments of the dissipative particle dynamics (DPD) method

where $\mathbf{r}_i$ and $\mathbf{p}_i$ are the position and momentum of particle i. Particle index i ranges from 1 to the total number of particles N. The mass m for each particle is taken an identical constant. For Galilean invariance, the forces are postulated to depend only on relative position $\mathbf{r}_{ij} = \mathbf{r}_i - \mathbf{r}_j$ and relative velocity $\mathbf{v}_{ij} = \mathbf{v}_i - \mathbf{v}_j$ of two particles. To preserve linear momentum, forces are antisymmetric and satisfy Newton's third law, that is, $\mathbf{F}_{ij} = -\mathbf{F}_{ji}$. To preserve angular momentum, forces between two particles always lie along the line of centers $\mathbf{e}_{ij} = \mathbf{r}_{ij}/r_{ij}$. Therefore, the three types of forces are expressed as [26, 35]

$$\begin{aligned} \mathbf{F}_{ij}^C &= a w_C(r_{ij})\mathbf{e}_{ij}, \\ \mathbf{F}_{ij}^D &= -\gamma w_D(r_{ij})(\mathbf{e}_{ij} \cdot \mathbf{v}_{ij})\mathbf{e}_{ij}, \\ \mathbf{F}_{ij}^R &= \sigma w_R(r_{ij})\xi_{ij}\mathbf{e}_{ij}, \end{aligned} \tag{5.2}$$

in which a, γ and σ are the strengths of individual forces. Weighting functions w_C, w_D, and w_R are isotropic and depend only on the relative distance $r_{ij} = |\mathbf{r}_{ij}|$ of two particles. $\xi_{ij} = \xi_{ji}$ is a Gaussian white noise with

$$\begin{aligned} &< \xi_{ij}(t) > = 0, \\ &< \xi_{ij}(t)\xi_{kl}(t') > = \left(\delta_{ik}\delta_{jl} + \delta_{il}\delta_{jk}\right)\delta(t-t'), \end{aligned} \tag{5.3}$$

where δ_{ij} is the Kronecker delta and $\delta(t-t')$ is the Dirac delta function [26]. If we replace the forces in Eq. (5.1) by Eq. (5.2), we can write the Langevin equations in a mathematically well-defined form of SDE

$$\begin{aligned} d\mathbf{r}_i &= \frac{\mathbf{p}_i}{m_i}dt, \\ d\mathbf{p}_i &= \left(\sum_{j\neq i}\mathbf{F}_{ij}^C + \sum_{j\neq i}\mathbf{F}_{ij}^D\right)dt + \sum_{j\neq i}\sigma w^R(r_{ij})\mathbf{e}_{ij}dW_{ij}, \end{aligned} \tag{5.4}$$

where $dW_{ij} = dW_{ji}$ are independent increments of the Wiener process and the Itô calculus rule is assumed. Therefore,

$$dW_{ij}dW_{kl} = \left(\delta_{ik}\delta_{jl} + \delta_{il}\delta_{jk}\right)dt. \tag{5.5}$$

In continuum mechanics [46], we know that the conservation law can be expressed as the continuity equation in the differential form as

$$\frac{\partial f(\mathbf{x},t)}{\partial t} + \nabla\cdot[\dot{\mathbf{x}}f(\mathbf{x},t)] = 0, \tag{5.6}$$

which states that in an infinitesimal volume the rate of change of density (e.g., mass density, momentum density, ...) is balanced by the divergence of the corresponding flux. In phase space the relevant coordinate becomes $6N$ dimensional as $\mathbf{x} = (r_1, r_2, \ldots, r_{3N}, p_1, p_2, \ldots, p_{3N})$. Accordingly, the velocity in phase space is then $\dot{\mathbf{x}} = (\dot{r}_1, \dot{r}_2, \ldots, \dot{r}_{3N}, \dot{p}_1, \dot{p}_2, \ldots, \dot{p}_{3N})$, and so $f(\mathbf{x},t)$ is the *probability density function* (PDF) in phase space [32]. Now we may substitute the derivatives in SDE of Eq. (5.4) into Eq. (5.6). By applying the gradient operator ∇ applied on $6N$ dimensions, that is, $\partial/\partial r_i$ and $\partial/\partial p_i$, and after some algebraic manipulations, we obtain the Fokker-Planck equation (FPE) as [26]

$$\frac{\partial f(\mathbf{x},t)}{\partial t} = \mathcal{L}f(\mathbf{x},t) = \mathcal{L}_C f(\mathbf{x},t) + \mathcal{L}_D f(\mathbf{x},t) + \mathcal{L}_R f(\mathbf{x},t), \tag{5.7}$$

where the Fokker-Planck operator $\mathcal{L}$ decomposes into three operators $\mathcal{L}_C$, $\mathcal{L}_D$ and $\mathcal{L}_R$. The individual operators are defined as follows

$$\begin{aligned}
\mathcal{L}_C &\equiv -\left(\sum_i \frac{\mathbf{p}_i}{m} \cdot \frac{\partial}{\partial \mathbf{r}_i} + \sum_{i,j}{}' \mathbf{F}_{ij}^C \cdot \frac{\partial}{\partial \mathbf{p}_i}\right), \\
\mathcal{L}_D &\equiv \sum_{i,j}{}' \mathbf{e}_{ij} \cdot \frac{\partial}{\partial \mathbf{p}_i} \left[\gamma w_D(r_{ij})(\mathbf{e}_{ij} \cdot \mathbf{v}_{ij})\right], \\
\mathcal{L}_R &\equiv \sum_{i,j}{}' \mathbf{e}_{ij} \cdot \frac{\partial}{\partial \mathbf{p}_i} \left[\frac{\sigma^2}{2} w_R^2(r_{ij}) \mathbf{e}_{ij} \cdot \left(\frac{\partial}{\partial \mathbf{p}_i} - \frac{\partial}{\partial \mathbf{p}_j}\right)\right],
\end{aligned} \tag{5.8}$$

where $\sum' \equiv \sum\sum$ with $i \neq j$. The FPE for the DPD system is an extension of the Kramers equation for the Langevin equation of a single particle under an external potential. The FPE is also an extension of the Liouville's equation for the Hamiltonian system of many particles.

We note that the evolution of PDF in the FPE is already averaged so that no random variable appears in Eq. (5.8). The operator $\mathcal{L}_C$ is the classical Liouville operator for a Hamiltonian system interacting with conservative forces $\mathbf{F}^C$ alone, where $\mathbf{F}^C$ is simply the negative gradient of a potential. For a conservative system of particles, it can be shown that the divergence of the PDF is zero, that is, the PDF is *incompressible* and divergence of velocity in Eq. (5.6) is zero. However, due to the dissipative and random forces $\mathbf{F}^D$ and $\mathbf{F}^R$ in DPD, the PDF is generally compressible and these effects are taken into account by the operators $\mathcal{L}_D$ and $\mathcal{L}_R$. We wish to find the steady state solution of Eq. (5.7) for $\partial f/\partial t = 0$, and in particular, the solution is expected to be the Gibbs canonical ensemble:

$$f^{eq}(\mathbf{x}) = \frac{1}{Z} \exp\left[-\beta H(\mathbf{x})\right]. \tag{5.9}$$

Here $\beta = (k_B T)^{-1}$ and the Hamiltonian is the sum of the potential energy and kinetic energy of the system, that is, $H = V(\mathbf{r}) + \sum_i \frac{p_i^2}{2m_i}$. The negative gradient of the potential V gives rise to the conservative force $\mathbf{F}^C$. The partition function Z is there for normalization and is not particularly relevant in this context. Since the canonical ensemble is the equilibrium solution for a conservative system, it is straightforward to obtain $\mathcal{L}_C f^{eq} = 0$. Furthermore, $\mathcal{L}_D f^{eq} + \mathcal{L}_R f^{eq} = 0$ can also be satisfied by postulating two relations as

$$\begin{aligned}
w_D(r) &= [w_R(r)]^2, \\
\sigma^2 &= 2\gamma k_B T.
\end{aligned} \tag{5.10}$$

This is the celebrated fluctuation-dissipation theorem first derived by Español and Warren [26], which is of fundamental importance for a DPD system. With the FDT as a constraint on the input model parameters, the canonical ensemble of the DPD system is warranted in the *continuum* limit, i.e., $dt \to 0$.

Another operator $\tilde{\mathcal{L}}$ related to the Fokker-Planck operator proves to be important later and we shall also briefly introduce it. Given an arbitrary function of phase space coordinates, that is, $a(\mathbf{x})$, we can write down its differential as

$$\begin{aligned} da =& \sum_i \left(\frac{\partial a}{\partial \mathbf{r}_i} \cdot d\mathbf{r}_i + \frac{\partial a}{\partial \mathbf{p}_i} \cdot d\mathbf{p}_i \right) \\ & + \frac{1}{2} \sum_{i,j} \left(\frac{\partial^2 a}{\partial \mathbf{r}_i \partial \mathbf{r}_j} d\mathbf{r}_i d\mathbf{r}_j + \frac{\partial^2 a}{\partial \mathbf{r}_i \partial \mathbf{p}_j} d\mathbf{r}_i d\mathbf{p}_j + \frac{\partial^2 a}{\partial \mathbf{p}_i \partial \mathbf{p}_j} d\mathbf{p}_i d\mathbf{p}_j \right) \\ & + \mathcal{O}(dt^{3/2}) \\ =& \tilde{\mathcal{L}} a dt + \sum_{i,j}{}' \sigma w_R(r_{ij}) \mathbf{e}_{ij} \frac{\partial a}{\partial \mathbf{p}_i} dW_{ij} + \mathcal{O}(dt^{3/2}), \end{aligned} \tag{5.11}$$

where $\tilde{\mathcal{L}}$ is defined as

$$\begin{aligned} \tilde{\mathcal{L}} \equiv & \left(\sum_i \frac{\mathbf{p}_i}{m} \frac{\partial}{\partial \mathbf{r}_i} + \sum_{i,j}{}' \mathbf{F}_{ij}^C \frac{\partial}{\partial \mathbf{p}_i} \right) \\ & + \sum_{i,j}{}' \gamma w_D(r_{ij}) \left[-(\mathbf{e}_{ij} \cdot \mathbf{v}_{ij}) \mathbf{e}_{ij} \cdot \frac{\partial}{\partial \mathbf{p}_i} \right] \\ & + \sum_{i,j}{}' \frac{\sigma^2}{2} w_R^2(r_{ij}) \mathbf{e}_{ij} \cdot \left(\frac{\partial}{\partial \mathbf{p}_i} - \frac{\partial}{\partial \mathbf{p}_j} \right). \end{aligned} \tag{5.12}$$

The SDE of Eq. (5.4) and the Itô calculus rule in Eq. (5.5) were applied to derive Eqs. (5.11) and (5.12). We will need $\tilde{\mathcal{L}}$ to compute the time derivatives of hydrodynamic variables due to the property of Eq. (5.11)

$$\frac{d\langle a \rangle}{dt} = \langle \tilde{\mathcal{L}} a \rangle, \tag{5.13}$$

in which "<>" means ensemble average. It is also noteworthy that DPD satisfies the *detailed balance*

$$\mathcal{L} f^{eq} a = f^{eq} \tilde{\mathcal{L}}^{\epsilon} a, \tag{5.14}$$

where operator $\tilde{\mathcal{L}}^{\epsilon}$ is defined by reversing the sign of velocities in $\tilde{\mathcal{L}}$.

For practical purposes, besides the FDT in Eq. (5.10) on the input parameters, we did not specify the actual values of a, γ and σ, nor did we talk about the functional forms of w_C, w_R and w_R. These discussions are presented in Sects. 5.2.4 and 5.2.5.

In the following section we shall discuss how these input parameters determine the hydrodynamic properties of a DPD system.

5.2.2 Bottom-Up and Top-Down Derivations

Since a DPD system respects Galilean invariance, it only allows for isotropic interactions while preserving conservations of mass and momentum. The equation to be expected to govern on a large spatial-temporal scale is the continuum Navier-Stokes system. This intuitive argument can be put on firm ground by applying the projection operator techniques of Zwanzig and Mori [80, 112, 113]. The projection formalism not only yields the hydrodynamic equations for a DPD system, but also establishes an explicit correspondence between the sound speed and viscosities of the Navier-Stokes and the model parameters of DPD. To this end, the *time-independent* projection operator of Mori [80] was generalized by Español [22] for the non-Hamiltonian system of DPD to derive a linear generalized Langevin equation, from which he obtained the linearized hydrodynamic equations.

We shall revisit a few key steps of the derivations [22]; more details on the technical aspects may be found in [33, 80, 113]. To start with a simplest example, we present the essential idea of projection upon a two dimensional system, that is, two coupled ordinary different equations (ODE).

Projection in a Nutshell

Given a system of two ODEs as follows [113]

$$\frac{dp}{dt} = A_{11}p + A_{12}q, \tag{5.15a}$$

$$\frac{dq}{dt} = A_{21}p + A_{22}q. \tag{5.15b}$$

Suppose that our interest is on p, not q. Then, by solving Eq. (5.15b) for q we have

$$q(t) = e^{A_{22}}q(0) + \int_0^t e^{A_{22}(t-\tau)}A_{21}p(\tau)d\tau. \tag{5.16}$$

Inserting Eq. (5.16) back into Eq. (5.15a), we have

$$\begin{aligned}\frac{dp}{dt} &= A_{11}p + A_{12}\int_0^t e^{A_{22}(t-\tau)}A_{21}p(\tau)d\tau + A_{12}e^{A_{22}t}q(0)\\ &= A_{11}p + \int_0^t K(t-\tau)p(\tau)d\tau + R(t),\end{aligned} \tag{5.17}$$

which has the form of the generalized Langevin equation (GLE). Furthermore, the memory kernel and noise terms are defined as

$$\begin{aligned} K(t) &= A_{12}e^{A_{22}t}A_{21}, \\ R(t) &= A_{12}e^{A_{22}t}q(0). \end{aligned} \tag{5.18}$$

If we are not interested in a specific initial condition $q(0)$, but only in an ensemble of $q(0)$, which has certain statistical distribution, it makes sense to name $R(t)$ as the noise term. In general, given a set of N variables and we are only interested in a subset of them or a set of functions of the N variables, after projection or substitution we are left with equations for the dynamics of a few relevant variables. However, the eliminated variables leave their footprints within the memory kernel and random term.

Next we shall introduce the linear projection adopted by Mori and introduce the concepts of relevant variables and relevant probability density. Subsequently, we apply the Mori formalism to obtain the hydrodynamic equations of DPD. This corresponds to the route A in Fig. 5.1.

The Mori Formalism

First we introduce a scalar product between two functions of phase space coordinates,

$$(\phi, \psi) \equiv \int f^{eq}(\mathbf{x})\phi(\mathbf{x})\psi(\mathbf{x})d\mathbf{x} \equiv tr\left[f^{eq}\phi\psi\right]. \tag{5.19}$$

The technique of projection operators, requires the identification of variables $A_i(\mathbf{x}, t)$ relevant to the macroscopic properties of the system, and subscript i is a free index. In our case, the A_i are hydrodynamic variables to be defined later, with zero equilibrium averages. A *relevant ensemble* has the following form,

$$\bar{f}(\mathbf{x}, t) = \frac{1}{Z}\exp\left[-\beta H + \beta\lambda_i(t)A_i(\mathbf{x}, t)\right], \tag{5.20}$$

where the Einstein convention is assumed on the repeated index i. The thermodynamic parameters λ_i are functions of time to be selected in such a way that the average of A_i performed with the relevant ensemble agrees with the average performed with the original ensemble from the solution of the FPE of Eq. (5.7). Mathematically, this means that the time-dependent average is

$$<A_i(t)> = tr\left[f(t)A_i(t)\right] = tr\left[\bar{f}(t)A_i(t)\right], \tag{5.21}$$

where the $\mathbf{x}$ arguments are omitted for brevity. We further assume that the system is not far from equilibrium, which implies a *linear response* in Eq. (5.20). This allows us to keep the first two terms of a Taylor expansion,

$$\overline{f}(\mathbf{x},t) = \frac{1}{Z}\exp\left[-\beta H\right]\exp\left[\beta\lambda_i(t)A_i(\mathbf{x})\right] \approx f^{eq}(\mathbf{x})\left[1+\beta\lambda_i(t)A_i(\mathbf{x})\right]. \tag{5.22}$$

The linear departures from equilibrium of the two ensembles are defined by,

$$\begin{aligned} f(\mathbf{x},t) &= f^{eq}(\mathbf{x})\left[1+\Psi(\mathbf{x},t)\right], \\ \overline{f}(\mathbf{x},t) &= f^{eq}(\mathbf{x})\left[1+\overline{\Psi}(\mathbf{x},t)\right], \end{aligned} \tag{5.23}$$

where the $\Psi(\mathbf{x},t)$ is constructed in accord with Eq. (5.20) as,

$$\overline{\Psi}(\mathbf{x},t) = \beta\lambda_i(t)A_i(\mathbf{x},t). \tag{5.24}$$

From Eq. (5.21) we can now calculate the average either by use of the original ensemble as

$$\begin{aligned} <A_i(t)> = tr\left[f(\mathbf{x},t)A_i\right] &= \int f(\mathbf{x},t)A_i(\mathbf{x},t)d\mathbf{x} \\ &= \int f^{eq}(\mathbf{x})\left[1+\Psi(\mathbf{x},t)\right]A_i(\mathbf{x},t)d\mathbf{x} \\ &= \int f^{eq}\Psi(\mathbf{x},t)A_i(\mathbf{x},t)d\mathbf{x} \\ &= \left(A_i,\Psi\right), \end{aligned} \tag{5.25}$$

or by use of the relevant ensemble as

$$\begin{aligned} <A_i(t)> = tr\left[\overline{f}(\mathbf{x},t)A_i\right] &= \int \overline{f}(\mathbf{x},t)A_i(\mathbf{x},t)d\mathbf{x} \\ &= \int f^{eq}(\mathbf{x})\left[1+\overline{\Psi}(\mathbf{x},t)\right]A_i(\mathbf{x},t)d\mathbf{x} \\ &= \int f^{eq}\overline{\Psi}(\mathbf{x},t)A_i(\mathbf{x},t)d\mathbf{x} \\ &= \left(A_i,\overline{\Psi}\right), \end{aligned} \tag{5.26}$$

where in both Eqs. (5.25) and (5.26) the equilibrium averages vanish,

$$\int f^{eq}(\mathbf{x})A_i(\mathbf{x},t)d\mathbf{x} = 0,$$

and the scalar product definition Eq. (5.19) has been used. Therefore,

$$\begin{aligned}
<A_i(t)> = (A_i, \Psi) = \left(A_i, \overline{\Psi}\right) &= \int f^{eq}\overline{\Psi}(\mathbf{x}, t)A_i(\mathbf{x}, t)d\mathbf{x} \\
&= \int f^{eq}\beta\lambda_j(t)A_j(\mathbf{x}, t)A_i(\mathbf{x}, t)d\mathbf{x} \\
&= \beta\lambda_j(t)\int f^{eq}A_j(\mathbf{x}, t)A_i(\mathbf{x}, t)d\mathbf{x} \\
&= \beta\lambda_j(t)(A_i, A_j),
\end{aligned} \tag{5.27}$$

where the definitions of the scalar produce and the departure from equilibrium of the relevant ensemble, Eqs. (5.19), (5.24) respectively, are employed. Finally, we have

$$\begin{aligned}
\beta\lambda_j(t) &= (A_i, A_j)^{-1}<A_i(t)> = (A_i, A_j)^{-1}(A_i, \Psi), \\
\overline{\Psi}(\mathbf{x}, t) &= \beta\lambda_j(t)A_i = A_i(A_i, A_j)^{-1}(A_i, \Psi) \equiv \mathcal{P}\Psi(\mathbf{x}, t),
\end{aligned} \tag{5.28}$$

here $\mathcal{P}$ is a *projection operator* that extracts the relevant part of the original ensemble. Accordingly, $\mathcal{Q}\Psi(\mathbf{x}, t) \equiv (1 - \mathcal{P})\Psi(\mathbf{x}, t)$ is the irrelevant part.

From the FPE in Eq. (5.7), we have

$$\begin{aligned}
\frac{\partial f(\mathbf{x}, t)}{\partial t} &= \mathcal{L}f(\mathbf{x}, t), \\
\frac{\partial\{f^{eq}(\mathbf{x})\,[1 + \Psi(\mathbf{x}, t)]\}}{\partial t} &= \mathcal{L}\{f^{eq}(\mathbf{x})\,[1 + \Psi(\mathbf{x}, t)]\}, \\
\frac{\partial\,[f^{eq}\Psi(\mathbf{x}, t)]}{\partial t} &= \mathcal{L}f^{eq}\Psi(\mathbf{x}, t), \\
f^{eq}\frac{\partial\Psi(\mathbf{x}, t)}{\partial t} &= f^{eq}\tilde{\mathcal{L}}^{\epsilon}\Psi(\mathbf{x}, t), \\
\frac{\partial\Psi(\mathbf{x}, t)}{\partial t} &= \tilde{\mathcal{L}}^{\epsilon}\Psi(\mathbf{x}, t),
\end{aligned} \tag{5.29}$$

where detailed balance in Eq. (5.14) is employed. The formal solution to Eq. (5.29) is

$$\Psi(\mathbf{x}, t) = \exp(\tilde{\mathcal{L}}^{\epsilon}t)\Psi(\mathbf{x}, 0), \tag{5.30}$$

in which the operator $\exp(\tilde{\mathcal{L}}^{\epsilon}t)$ is defined in terms of its Taylor expansion. However, if we first solve Eq. (5.29) for the irrelevant part $\mathcal{Q}\Psi(\mathbf{x}, t)$, and then substitute its solution back into the system to obtain the relevant part, we then get

$$\frac{\partial\overline{\Psi}(\mathbf{x}, t)}{\partial t} = \mathcal{P}\tilde{\mathcal{L}}^{\epsilon}\overline{\Psi}(\mathbf{x}, t) + \int_0^t d\tau\mathcal{P}\tilde{\mathcal{L}}^{\epsilon}\exp\left[\mathcal{Q}\tilde{\mathcal{L}}^{\epsilon}(t - \tau)\right]\mathcal{Q}\tilde{\mathcal{L}}^{\epsilon}\overline{\Psi}(\mathbf{x}, \tau). \tag{5.31}$$

Also from Eq. (5.29), we obtain an evolution equation for the relevant variables as

$$\begin{aligned}&\frac{d\langle A_i(\mathbf{x},t)\rangle}{dt}\\&=\left(\tilde{\mathcal{L}}A_i,\overline{\Psi}\right)+\int_0^t d\tau\left(\exp\left[\tilde{\mathcal{L}}\mathcal{Q}\{t-\tau\}\right]\tilde{\mathcal{L}}A_i,\mathcal{Q}\tilde{\mathcal{L}}^{\epsilon}A_j\right)\beta\lambda_j(\tau),\end{aligned}\tag{5.32}$$

which is exact. However, in practice Eq. (5.32) is difficult to apply so that one often tries to further simplify the complex memory kernel by searching for proper relevant variables. With a clear time separation between the memory kernel (fast) and the relevant variables (slow) the Markovian approximation can be invoked so that the equation reads

$$\frac{d\langle A_i(\mathbf{x},t)\rangle}{dt}=\left(\tilde{\mathcal{L}}A_i,\overline{\Psi}\right)+\left\{\int_0^t d\tau\left(\exp\left[\tilde{\mathcal{L}}\mathcal{Q}\tau\right]\tilde{\mathcal{L}}A_i,\mathcal{Q}\tilde{\mathcal{L}}^{\epsilon}A_j\right)\right\}\beta\lambda_j(t).\tag{5.33}$$

Furthermore, it is also extremely difficult to generate the projected dynamics, and in practice, one often approximates the projected dynamics with the real dynamics as $\exp(\tilde{\mathcal{L}}\mathcal{Q}\tau)\approx\exp(\tilde{\mathcal{L}}\tau)$, which can be justified only a posteriori.

Hydrodynamics

If we apply Dirac's δ function to define the relevant variables as those which appear in Navier-Stokes (NS) equations, we have

$$\begin{aligned}\delta\rho(\mathbf{r},t)&=\sum_i m\delta\left[\mathbf{r}-\mathbf{r}_i(t)\right]-\rho_0,\\\mathbf{g}(\mathbf{r},t)&=\sum_i\mathbf{p}_i\delta\left[\mathbf{r}-\mathbf{r}_i(t)\right],\end{aligned}\tag{5.34}$$

here ρ_0 is the equilibrium density so that both the averages of $\delta\rho_{\mathbf{r}}$ and $\mathbf{g}_{\mathbf{r}}$ vanish at equilibrium. Since the energy was not defined as a relevant variable which would appear in the Fourier equations, the classical DPD applies only to isothermal fluids and their flows, in which the energy varies instantaneously and can not be taken as a slow relevant variable.

On following through with the Mori projection introduced previously on these relevant variables, the equation of continuity takes the form

$$\frac{\partial\delta\rho(\mathbf{r},t)}{\partial t}=-\frac{\partial}{\partial\mathbf{r}}\cdot\mathbf{g}(\mathbf{r},t),\tag{5.35}$$

and the momentum equations is [22]

$$\begin{aligned}\frac{\partial \mathbf{g}(\mathbf{r},t)}{\partial t} &= \left(\overline{\Psi}, \tilde{\mathcal{L}}\mathbf{g}(\mathbf{r},t)\right) \\ &\quad + \int_0^t d\tau \int_V d\mathbf{r}' \left(\exp\left[\tilde{\mathcal{L}}\mathcal{Q}(t-\tau)\right]\tilde{\mathcal{L}}\mathbf{g}(\mathbf{r},t), \mathcal{Q}\tilde{\mathcal{L}}^{\epsilon}\mathbf{g}(\mathbf{r}',t)\right)\beta\mathbf{v}(\mathbf{r}',t),\end{aligned} \tag{5.36}$$

where V is the special volume and $\mathbf{v}(\mathbf{r},t)$ is the velocity field. The momentum equation can then be cast into the form of

$$\frac{\partial \mathbf{g}(\mathbf{r},t)}{\partial t} = -c_s^2\nabla\delta\rho(\mathbf{r},t) + \eta\nabla^2\mathbf{v}(\mathbf{r},t) + \left(\zeta - \frac{2\eta}{3}\right)\nabla\nabla\cdot\mathbf{v}(\mathbf{r},t), \tag{5.37}$$

in which the isothermal sound speed $c_s = \partial p/\partial\rho|_T$ and it is only determined by $\mathbf{F}_{ij}^C$ [22]. With the super-indices C and D to denote the contributions of conservative and dissipative forces respectively the shear viscosity $\eta = \eta^C + \eta^D$ and bulk viscosity $\zeta = \zeta^C + \zeta^D$. Each term is further defined as

$$\begin{aligned}\eta^C &= \beta\int_0^{\infty}\frac{1}{V}\left[\sum_{\mu\nu}^{C}(\tau), \mathcal{Q}\sum_{\mu\nu}^{C}\right]d\tau, \\ \left(\zeta^C - \frac{2}{3}\eta^C\right) &= \beta\int_0^{\infty}\frac{1}{V}\left[\sum_{\mu\mu}^{C}(\tau), \mathcal{Q}\sum_{\mu\mu}^{C}\right]d\tau, \\ \eta^D &= \beta\int_0^{\infty}\frac{1}{V}\left[\sum_{\mu\nu}^{D}(\tau), \mathcal{Q}\sum_{\mu\nu}^{D}\right]d\tau, \\ \left(\zeta^D - \frac{2}{3}\eta^D\right) &= \beta\int_0^{\infty}\frac{1}{V}\left[\sum_{\mu\mu}^{D}(\tau), \mathcal{Q}\sum_{\mu\mu}^{D}\right]d\tau.\end{aligned} \tag{5.38}$$

In these summations $\mu \neq \nu$ with no summation on repeated indices. Moreover, the stress tensor contributions are given as

$$\begin{aligned}\sum^{C} &= \sum_i \frac{\mathbf{p}_i}{m}\mathbf{p}_i + \sum_{i,j}\left(\mathbf{r}_i - \mathbf{r}_j\right)\mathbf{F}_{ij}^C, \\ \sum^{D} &= \sum_{i,j}\left(\mathbf{r}_i - \mathbf{r}_j\right)\mathbf{F}_{ij}^D,\end{aligned} \tag{5.39}$$

which follows the identification of the conservative and the dissipative force contributions to the shear and the bulk viscosities respectively.

Such formal derivations via the Mori projection on the SDE of the DPD system provide further insight and support for understanding why DPD satisfies the hydrodynamic equations at large spatial-temporal scales. However, in practice it is not possible to quantify a priori the sound speed and viscosities of a DPD system from the given input parameters without actually running DPD simulations.

Fluctuating Hydrodynamics

To circumvent the difficulty of specifying a priori the equation of state and the transport coefficients of classical DPD, an alternative approach is smooth particle hydrodynamics (SPH) which begins with the Lagrangian discretization of Naiver-Stokes or in general Landau-Lifshitz-Navier-Stokes (LLNS) equations [25]. Given the governing differential equations of NS in Lagrangian form

$$\frac{d\rho}{dt} = -\rho\nabla\cdot\mathbf{v}, \tag{5.40a}$$

$$\rho\frac{d\mathbf{v}}{dt} = -\nabla P + \eta\nabla^2\mathbf{v} + \left(\zeta + \frac{\eta}{3}\right)\nabla\nabla\cdot\mathbf{v}, \tag{5.40b}$$

where d/dt is the substantial derivative (or material derivative), which describes how quantities such as, density field $\rho(\mathbf{r}, t)$, and velocity field $\mathbf{v}(\mathbf{r}, t)$, evolve with time along the trajectory of a point particle $\mathbf{r}$ at time t. Intensive variables, such as the pressure field $P = P^{eq}[\rho(\mathbf{r}, t)]$, are determined by an equation of state under the local equilibrium assumption. For simplicity the shear (dynamic) and bulk viscosities η, ζ are taken as input constants.

The NS equations are discretized by following the methodology of SPH [79]. An arbitrary function $A(\mathbf{r})$ can be formulated in an integral form by convolution with the Dirac δ function as

$$A(\mathbf{r}) = \int A(\mathbf{r}')\delta(\mathbf{r}' - \mathbf{r})d\mathbf{r}'. \tag{5.41}$$

The essence of SPH consists of two steps to evaluate Eq. (5.41): first a *kernel approximation* to replace the Dirac $\delta(r)$ function, and second a *particle summation* to approximate the integration. In the end, an arbitrary function $A(\mathbf{r})$ is expressed in terms of values at a set of N discrete disordered points—the SPH particles.

In SPH, a normalized smoothing function $W(\mathbf{r}' - \mathbf{r}, h)$ is used as the *kernel* with h as its *smoothing length* such that in the limit $h \to 0$ $W(\mathbf{r}' - \mathbf{r}, h)$ tends to the Dirac δ function,

$$\int W(\mathbf{r}' - \mathbf{r}, h)d\mathbf{r} = 1, \quad \lim_{h\to 0} W(\mathbf{r}' - \mathbf{r}, h) = \delta(\mathbf{r}' - \mathbf{r}). \tag{5.42}$$

Note that $W(\mathbf{r}' - \mathbf{r}, h)$ is bell-shaped and radially-symmetric. Therefore, it can be written as a function of a scalar variable: $W(\mathbf{r}' - \mathbf{r}, h) \equiv W(|\mathbf{r}' - \mathbf{r}|, h) \equiv \frac{1}{h^D} w(s)$, where D is the dimension of the problem and $s = |\mathbf{r}' - \mathbf{r}|/h = r/h$. Here we shall not specify any kernel and for practical flow problems different kernels may have different properties. Equations (5.40a) and (5.40b) require the gradient of the kernel function derived from,

$$\nabla W(\mathbf{r}' - \mathbf{r}, h) = -(\mathbf{r}' - \mathbf{r}) G(|\mathbf{r}' - \mathbf{r}|, h), \tag{5.43}$$

with $G \geq 0$, the physical meaning of G will be clarified below.

The volume $\mathcal{V}_i$ is defined as the inverse of the number density d_i, which, in turn, is related to mass m_i and mass density ρ_i as

$$\frac{1}{\mathcal{V}_i} = d_i = \frac{\rho_i}{m_i} = \sum_j W(|\mathbf{r}_i - \mathbf{r}_j|) = \sum_j W_{ij}. \tag{5.44}$$

Recall the hydrodynamic Eqs. (5.40a) and (5.40b), which can now be given in their discrete forms as

$$\dot{\rho}_i = -\rho_i \left(\nabla \cdot \mathbf{v}\right)_i, \tag{5.45a}$$

$$m_i \dot{\mathbf{v}}_i = -\frac{(\nabla P)_i}{d_i} + \frac{\eta (\nabla^2 \mathbf{v})_i}{d_i} + \frac{\eta \left(\nabla \nabla \cdot \mathbf{v}\right)_i}{3 d_i}, \tag{5.45b}$$

where any quantity associated with particle i is denoted with a sub-index i and '$\dot{}$' is an abbreviation for the total (Lagrangian) time derivative.

According to Eqs. (5.44) and (5.45a), we have the following equivalent continuity equations

$$\begin{aligned} \dot{\rho}_i &= -\rho_i \left(\nabla \cdot \mathbf{v}\right)_i \\ \Longleftrightarrow \dot{d}_i &= -d_i \left(\nabla \cdot \mathbf{v}\right)_i \\ \Longleftrightarrow \dot{\mathcal{V}}_i &= \mathcal{V}_i \left(\nabla \cdot \mathbf{v}\right)_i . \end{aligned} \tag{5.46}$$

In the Lagrangian description, each particle moves according to

$$\dot{\mathbf{r}}_i = \mathbf{v}_i. \tag{5.47}$$

Therefore, the time derivative of Eq. (5.44) is given as

$$\dot{d}_i = \sum_j \dot{W}(|\mathbf{r}_i - \mathbf{r}_j|) = \sum_j \left[\nabla W(|\mathbf{r}_i - \mathbf{r}_j|) \cdot (\mathbf{v}_i - \mathbf{v}_j)\right]. \tag{5.48}$$

If we define notations

$$\begin{aligned} \mathbf{r}_{ij} &= \mathbf{r}_i - \mathbf{r}_j, \\ \mathbf{v}_{ij} &= \mathbf{v}_i - \mathbf{v}_j, \\ -G_{ij}\mathbf{r}_{ij} &= \nabla W_{ij} = \nabla W(|\mathbf{r}_i - \mathbf{r}_j|), \end{aligned} \tag{5.49}$$

then Eq. (5.48) becomes

$$\dot{d}_i = \sum_j \left(G_{ij}\mathbf{r}_{ij} \cdot \mathbf{v}_{ij} \right). \tag{5.50}$$

By comparing Eq. (5.50) with Eq. (5.46), we get a SPH representation for the divergence operator of velocity

$$(\nabla \cdot \mathbf{v})_i = \frac{1}{d_i} \sum_j \left(G_{ij}\mathbf{r}_{ij} \cdot \mathbf{v}_{ij} \right). \tag{5.51}$$

The extensive variables of the system are as follows,

$$\begin{aligned} M &= \sum_i m_i, \\ E &= \sum_i \left(\frac{m\mathbf{v}_i^2}{2} + E_i \right), \end{aligned} \tag{5.52}$$

where the total mass M is a sum of the individual masses. The total energy E is sum of the individual kinetic energy $m\mathbf{v}_i^2/2$ and internal energy E_i of each particle i.

Each particle i has the same constant mass $m_i = m$; hence conservation of total mass is $\dot{M} = 0$. E_i is a prescribed function of the particle's own mass m_i, and volume $\mathcal{V}_i$

$$E_i = E^{eq}(m_i, \mathcal{V}_i). \tag{5.53}$$

Its time derivative is given by

$$\dot{E}_i = \frac{\partial E^{eq}}{\partial m_i}\dot{m}_i + \frac{\partial E^{eq}}{\partial \mathcal{V}_i}\dot{\mathcal{V}}_i. \tag{5.54}$$

The thermodynamics equation of state [14] yields the pressure as

$$P_i = -\frac{\partial E^{eq}}{\partial \mathcal{V}_i}. \tag{5.55}$$

Therefore, Eq. (5.54) with constant m_i becomes

$$\dot{E}_i = -P_i \dot{\mathcal{V}}_i. \tag{5.56}$$

As required by the first and second laws of thermodynamics, the SPH representation of an isolated system must satisfy

$$\dot{E} = \sum_i \left(m\mathbf{v}_i \cdot \mathbf{v}_i + \dot{E}_i \right) = 0, \tag{5.57a}$$

$$\dot{S} = \sum_i \dot{S}_i \geq 0. \tag{5.57b}$$

- *Reversible dynamics*: Suppose we deal with an inviscid Euler flow with $\eta = 0$ and $\kappa = 0$, we have

$$\begin{aligned}
\dot{E} &= \sum_i \left(m\dot{\mathbf{v}}_i \cdot \mathbf{v}_i + \dot{E}_i \right) \quad \text{with} \quad \text{Eqs. (5.45b) and (5.56)} \\
&= \sum_i \left[-\frac{(\nabla P)_i}{d_i} \cdot \mathbf{v}_i - P_i \dot{\mathcal{V}}_i \right] \quad \text{with} \quad \text{Eq. (5.46)} \\
&= \sum_i \left[-\frac{(\nabla P)_i}{d_i} \cdot \mathbf{v}_i - \frac{P_i}{d_i} (\nabla \cdot \mathbf{v})_i \right] \\
&= 0,
\end{aligned} \tag{5.58}$$

  which is required by Eq. (5.57a). This leads to

$$\begin{aligned}
&\sum_i \left[-\frac{(\nabla P)_i}{d_i} \cdot \mathbf{v}_i \right] \\
&= \sum_i \left[\frac{P_i}{d_i} (\nabla \cdot \mathbf{v})_i \right] \quad \text{with} \quad \text{Eq. (5.51)} \\
&= \sum_i \left[\frac{P_i}{d_i^2} \sum_j \left(G_{ij} \mathbf{r}_{ij} \cdot \mathbf{v}_{ij} \right) \right] \\
&= \sum_i \left[\frac{P_i}{d_i^2} \sum_j \left(G_{ij} \mathbf{r}_{ij} \cdot \mathbf{v}_i \right) \right] - \sum_i \left[\frac{P_i}{d_i^2} \sum_j \left(G_{ij} \mathbf{r}_{ij} \cdot \mathbf{v}_j \right) \right] \\
&= \sum_i \left[\frac{P_i}{d_i^2} \sum_j \left(G_{ij} \mathbf{r}_{ij} \cdot \mathbf{v}_i \right) \right] + \sum_j \left[\frac{P_j}{d_j^2} \sum_i \left(G_{ij} \mathbf{r}_{ij} \cdot \mathbf{v}_i \right) \right] \\
&= \sum_i \sum_j \left[\left(\frac{P_i}{d_i^2} + \frac{P_j}{d_j^2} \right) G_{ij} \mathbf{r}_{ij} \cdot \mathbf{v}_i \right].
\end{aligned} \tag{5.59}$$

Therefore, a physically faithful SPH representation of pressure gradient operator is proposed as

$$\frac{(\nabla P)_i}{d_i} = \sum_i \left[\left(\frac{P_i}{d_i^2} + \frac{P_j}{d_j^2} \right) G_{ij} \mathbf{r}_{ij} \right]. \tag{5.60}$$

Hence, in the SPH representation, a pairwise conservative force from pressure gradient can be written as

$$\mathbf{F}_{ij}^C = \left(\frac{P_i}{d_i^2} + \frac{P_j}{d_j^2} \right) G_{ij} \mathbf{r}_{ij}. \tag{5.61}$$

In summary, by the density definition in Eq. (5.44) and the position evolution of the Lagrangian description in Eq. (5.47), we get a divergence operator of SPH for velocity in Eq. (5.51) so that continuity equation is accounted for. The velocity divergence operator Eq. (5.51) generates a pressure gradient operator Eq. (5.60) which ensures the total energy of an inviscid fluid to be constant. Further note that using a variational approach, it can be shown that Eqs. (5.44) and (5.60) are also variationally consistent [12].

- *Irreversible dynamics*: Using the kernel approximation, we have the following identity [25]

$$\begin{aligned} &\int d\mathbf{r}' \left[A(\mathbf{r}') - A(\mathbf{r}) \right] G(|\mathbf{r}' - \mathbf{r}|) \left[5 \frac{(\mathbf{r}' - \mathbf{r})^\alpha (\mathbf{r}' - \mathbf{r})^\beta}{(\mathbf{r}' - \mathbf{r})^2} - \delta^{\alpha\beta} \right] \\ &= \nabla^\alpha \nabla^\beta A(\mathbf{r}) + \mathcal{O}(\nabla^4 A h^2), \end{aligned} \tag{5.62}$$

where we have assumed that $A(\mathbf{r})$ is sufficiently smooth on the scale of h. Taking the trace of Eq. (5.62) leads to

$$2 \int d\mathbf{r}' \left[A(\mathbf{r}') - A(\mathbf{r}) \right] G(|\mathbf{r}' - \mathbf{r}|) = \nabla \cdot \nabla A(\mathbf{r}) + \mathcal{O}(\nabla^4 A h^2). \tag{5.63}$$

Note that

$$\int d\mathbf{r}' \rightarrow \sum_j \mathcal{V}_j = \sum_j \frac{1}{d_j}. \tag{5.64}$$

The second derivatives in SPH are discretized as

$$\begin{aligned} \frac{(\nabla^2 \mathbf{v})_i}{d_i} &= -2 \sum_j \left(\frac{G_{ij}}{d_i d_j} \mathbf{v}_{ij} \right), \\ \frac{(\nabla \nabla \cdot \mathbf{v})_i}{d_i} &= -\sum_j \left[\frac{G_{ij}}{d_i d_j} \left(5 \mathbf{e}_{ij} \cdot \mathbf{v}_{ij} \mathbf{e}_{ij} - \mathbf{v}_{ij} \right) \right], \end{aligned} \tag{5.65}$$

where we have introduced the notation

$$\mathbf{e}_{ij} = \frac{\mathbf{r}_i - \mathbf{r}_j}{|\mathbf{r}_i - \mathbf{r}_j|} = \frac{\mathbf{r}_{ij}}{r_{ij}}. \tag{5.66}$$

Finally, the pairwise dissipative force is

$$\mathbf{F}_{ij}^{D} = -\left(\frac{5\eta}{3} - \zeta\right)\frac{G_{ij}}{d_i d_j}\mathbf{v}_{ij} - 5\left(\zeta + \frac{\eta}{3}\right)\frac{G_{ij}}{d_i d_j}\left(\mathbf{e}_{ij}\cdot\mathbf{v}_{ij}\mathbf{e}_{ij}\right). \tag{5.67}$$

One may go ahead and apply the SPH methodology to discretize the random stress part of LLNS, but it is difficult to impose thermodynamic consistency by this route. Although the original stochastic partial different equation (SPDE) of LLNS is thermodynamically consistent, a separate discretization of the viscous and random stresses does not guarantee the same consistency at the discrete level. This inconsistency is avoided by the creation directly at the discrete level of a random force $\mathbf{F}_{ij}^{R}$ consistent with $\mathbf{F}_{ij}^{D}$, as was first done by Español and Revenga [25]. One could also extend the continuous FPE introduced in Sect. 5.2.1 to a discrete version, and so derive a consistent form of $\mathbf{F}_{ij}^{R}$. An elegant alternative is to apply the GENERIC (general equation for the nonequilibrium reversible-irreversible coupling) [84] method, which imposes thermodynamic consistency on any discrete mesoscopic model without the need to involve derivations in phase space directly. Consequently, in GENERIC, all operations and constraints are simply algebraic. Without further derivations, we shall simply provide the pairwise random force as

$$\mathbf{F}_{ij}^{R} = \sum_j \left(A_{ij} d\overline{\overline{\mathbf{W}}}_{ij} + \frac{B_{ij}}{3} tr[d\mathbf{W}_{ij}]\right)\cdot\mathbf{e}_{ij}, \tag{5.68}$$

where $d\mathbf{W}_{ij}$ is matrix of independent increments of the Wiener process, $d\overline{\mathbf{W}}_{ij}$ is the symmetric part of it, and $d\overline{\overline{\mathbf{W}}}_{ij}$ is the traceless symmetric part of it. They are given explicitly by

$$\begin{aligned} d\overline{\mathbf{W}}_{ij} &= \left(d\mathbf{W}_{ij} + d\mathbf{W}_{ij}^{T}\right)/2, \\ d\overline{\overline{\mathbf{W}}}_{ij} &= d\overline{\mathbf{W}}_{ij} - tr[d\mathbf{W}_{ij}]\mathbf{I}/3, \\ tr[d\mathbf{W}_{ij}] &= \sum_{\alpha} d\mathbf{W}^{\alpha\alpha}. \end{aligned} \tag{5.69}$$

Furthermore, the magnitude of noise is given as

$$\begin{aligned} A_{ij} &= \left[4k_B T\left(\frac{5\eta}{3} - \zeta\right)\frac{G_{ij}}{d_i d_j}\right]^{1/2}, \\ B_{ij} &= \left[4k_B T\left(\frac{5\eta}{3} + 8\zeta\right)\frac{G_{ij}}{d_i d_j}\right]^{1/2}. \end{aligned} \tag{5.70}$$

From the SPH discretization of the Navier-Stokes equation and the introduction of the random force corresponding to the fluctuating hydrodynamic equations known as LLNS [46], we get a version of DPD named SDPD. In contrast to the DPD method, the equation of state and transport coefficients are explicitly specified a priori in SDPD. This may avoid some of the difficulties associated with the original DPD mentioned above. This also corresponds to the top-down view of DPD, or the route B on Fig. 5.1. However, from this version of DPD, one cannot expect more than the continuum behavior of the system. Whereas in the original DPD designed by coarse-graining or parameterization, small scale behavior is expected to arise that corresponds to some underlying physical process.

5.2.3 Transport Coefficients from Kinetic Theory

Besides the Mori projection, we may also formulate the transport coefficients of DPD by deriving its kinetic equations. This also corresponds to the route A in Fig. 5.1. Let us introduce the μ-space density, single-particle and pair distribution functions as [76, 77]

$$\begin{aligned}\hat{f}(\mathbf{x},t) &= \sum_i \delta(\mathbf{x}-\mathbf{x}_i),\\ f^s(\mathbf{x},t) &= \left\langle \sum_i \delta(\mathbf{x}-\mathbf{x}_i)\right\rangle = \left\langle \hat{f}(\mathbf{x},t)\right\rangle,\\ f^2(\mathbf{x},\mathbf{x}',t) &= \left\langle \sum_{i,j}{}' \delta(\mathbf{x}-\mathbf{x}_i)\delta(\mathbf{x}-\mathbf{x}_j)\right\rangle.\end{aligned} \tag{5.71}$$

We apply Eqs. (5.11)–(5.71) and neglect the conservative force (corresponding to the high γ limit), we get

$$\begin{aligned}\frac{\partial f^s(\mathbf{x},t)}{\partial t} =& -\nabla\cdot\left\langle \sum_i \mathbf{v}_i\delta(\mathbf{x}-\mathbf{x}_i)\right\rangle\\ &+\gamma\frac{\partial}{\partial \mathbf{v}}\cdot\left\langle \sum_{i,j}{}'\delta(\mathbf{x}-\mathbf{x}_i)w^D(r_{ij})(\mathbf{e}_{ij}\cdot\mathbf{v}_{ij})\mathbf{e}_{ij}\right\rangle\\ &+\frac{\sigma^2}{2}\frac{\partial^2}{\partial\mathbf{v}\partial\mathbf{v}}:\left\langle \sum_{i,j}{}'\delta(\mathbf{x}-\mathbf{x}_i)w^D(r_{ij})\mathbf{e}_{ij}\mathbf{e}_{ij}\right\rangle,\end{aligned} \tag{5.72}$$

where the contraction ":" of tensors is defined as $A{:}B = \sum_{ij} A_{ij}B_{ji}$ and $\nabla = \partial/\partial\mathbf{r}$. We perform the integrals over all variables except $\mathbf{x}_i$ and $\mathbf{x}_j$,

$$\begin{aligned}&\frac{\partial f^s(\mathbf{x},t)}{\partial t} + \mathbf{v}\cdot f^s(\mathbf{x},t)\\ &= \gamma \int d\mathbf{v}' \int d\mathbf{R}\hat{\mathbf{R}}\hat{\mathbf{R}} w^D(\hat{\mathbf{R}}){:} \left\{ \frac{\partial}{\partial \mathbf{v}}(\mathbf{v}-\mathbf{v}') + \frac{\sigma^2}{2\gamma}\frac{\partial^2}{\partial\mathbf{v}\partial\mathbf{v}} \right\} f^2(\mathbf{x},\mathbf{x}',t),\end{aligned} \tag{5.73}$$

where $\mathbf{x} = (\mathbf{r},\mathbf{v})$, $\mathbf{x}' = (\mathbf{r}',\mathbf{v}')$, $\mathbf{R} = \mathbf{r}-\mathbf{r}'$ and $\hat{\mathbf{R}} = \mathbf{R}/|\mathbf{R}|$. This is the first equation of the BBGKY (Bogoliubov-Born-Green-Kirkwood-Yvon) hierarchy [37]. Note that the difference here is we apply the Fokker-Planck operator for a dissipative system instead of the Louville operator for a Hamiltonian system. If we assume molecular chaos to be

$$f^2(\mathbf{x},\mathbf{x}',t) \approx f^s(\mathbf{x},t) f^s(\mathbf{x}',t), \tag{5.74}$$

then we arrive at a nonlinear integro-partial differential equation,

$$\begin{aligned}&\frac{\partial f^s(\mathbf{x},t)}{\partial t} + \mathbf{v}\cdot f^s(\mathbf{x},t)\\ &= \gamma \int d\mathbf{v}' \int d\mathbf{R}\hat{\mathbf{R}}\hat{\mathbf{R}} w^D(\hat{\mathbf{R}}) f(\mathbf{r}',\mathbf{v}',t){:} \left\{ \frac{\partial}{\partial \mathbf{v}}(\mathbf{v}-\mathbf{v}') + \frac{\sigma^2}{2\gamma}\frac{\partial^2}{\partial\mathbf{v}\partial\mathbf{v}} \right\} f(\mathbf{r},\mathbf{v},t).\end{aligned} \tag{5.75}$$

Following the Chapman-Enskog method, we solve Eq. (5.75) as a power series in a small parameter μ on the hydrodynamic scale, i.e., $f = f_0 + \mu f_1 + \ldots$; then, we define a mean free time as $t_0 = 1/(\gamma n r_c)$, where n is the number density of a DPD system, and define a mean thermal velocity as $v_0 = \sqrt{k_B T/m}$. Hence, the small parameter is $\mu = t_0 v_0 \nabla$, essentially $\sim 1/\gamma$ in the high friction limit. The first two terms f_0 and f_1 suffice to estimate the Navier-Stokes transport coefficients as follows,

$$\eta_K = \frac{d k_B T}{2[w]\gamma}, \quad \zeta_K = \frac{k_B T}{\gamma[w]}, \tag{5.76}$$

where subscript "K" denotes the kinetic contributions. From the contribution of the dissipative force we have

$$\eta_D = \frac{m\gamma n^2[r_c^2 w g_0]}{2d(d+2)}, \quad \zeta_D = \frac{m\gamma n^2[r_c^2 w g_0]}{2d^2}, \tag{5.77}$$

where the square brackets mean a spatial integral as $[\ldots] = \int \ldots d\mathbf{r}$.

5.2.4 Parameterization

The parameterization of input parameters for a particular DPD simulation falls generally into two approaches: one approach is to solve an inverse problem and the other approach is to directly coarse-grain from an underlying MD system. The first approach generally initiates a loop of processes involving trial simulations and tuning input parameters until the desired properties are simulated by the DPD system. Although not accurately, the kinetic equations (neglecting conservative force) from the last section indeed provide a guideline of tuning the DPD parameters. We may also apply the kinetic equations further here to provide a guideline for selecting the finite time step Δt of DPD. This part largely follows the methodologies introduced in [75]. Furthermore, we shall also present the continuum integral approximation [35], which provides an alternative reference to tune the input parameters. Nevertheless, with either the kinetic equations or the continuum integral approximation, one may need a few trial simulations to solve the inverse problem. This can be done systematically by applying the Bayesian framework, but this topic is beyond the scope of this chapter.

The direct or forward way of coarse-graining will be presented in Sect. 5.2.5.

Timestep for a Constant Temperature and Noise Level

In Sect. 5.2.1, we learnt that, at $\Delta t \to 0$, the temperature is well defined if the input parameters of DPD satisfy the FDT given by Eq. (5.10). Here we try to find out how the finite time step Δt affects the temperature, since one advantage of DPD is the use of a larger time step than that of MD.

We define the one-particle distribution function for DPD as

$$f^{(1)}(\mathbf{x}, t) = \sum_i \int d\mathbf{x} \delta(\mathbf{r} - \mathbf{r}_i(t)) \delta(\mathbf{p} - \mathbf{p}_i(t)) f(\mathbf{x}, t), \tag{5.78}$$

where $f(\mathbf{x}, t)$ is the distribution function in the $6N$ phase-space introduced above. For simplicity, if we ignore the conservative force in DPD as is in the original form introduced by Hoogerbrugge and Koelman [39], the equilibrium distribution is the Gibbs distribution for the momentum

$$f^{eq}(\mathbf{p}) = \frac{1}{Z} \exp\left(-\beta \sum_i \frac{\mathbf{p}_i^2}{2m}\right). \tag{5.79}$$

In a simulation with a discrete time step Δt, the changes in position and momentum for particle i are $\Delta \mathbf{r}_i(t)$ and $\Delta \mathbf{p}_i(t)$, then the change in $f^{(1)}(\mathbf{x}, t)$ from

t to $t + \Delta t$ is

$$\begin{aligned}
&\Delta f^{(1)}(t)\\
&= f^{(1)}(\mathbf{x}, t + \Delta t) - f^{(1)}(\mathbf{x}, t)\\
&= \sum_i \int d\mathbf{x} \left[\delta(\mathbf{r} - \mathbf{r}_i - \Delta\mathbf{r}_i)\delta(\mathbf{p} - \mathbf{p}_i - \Delta\mathbf{p}_i) - \delta(\mathbf{r} - \mathbf{r}_i)\delta(\mathbf{p} - \mathbf{p}_i)\right] f(\mathbf{x}),
\end{aligned} \tag{5.80}$$

where t is suppressed in the last expression to save space. We can expand the terms under the integral of Eq. (5.80) by Taylor series. Keeping only up to second partial derivatives, we can have an expression for the differential $\Delta f^{(1)}$. The first moment of $\Delta f^{(1)}$ is

$$\begin{aligned}
\Delta \int d\mathbf{p} \int d\mathbf{r} f^{(1)}\mathbf{p} &= \int d\mathbf{p} \int d\mathbf{r} \left(\sum_i \int d\mathbf{x} f^{eq} \delta(\mathbf{r} - \mathbf{r}_i)\delta(\mathbf{p} - \mathbf{p}_i)\Delta\mathbf{p}_i\right)\\
&= 0,
\end{aligned} \tag{5.81}$$

which follows from the momentum conservation of DPD. The second moment of $\Delta f^{(1)}$ is

$$\begin{aligned}
&\Delta \int d\mathbf{p} \int d\mathbf{r} f^{(1)}\mathbf{p}^2\\
&= -2\gamma \Delta t k_B T n \left[w_D\right] + \sigma^2 \Delta t \left[w_R^2\right] + \frac{k_B T \gamma^2 \Delta t^2}{m} \left\{ 2n \left[w_D^2\right] + \frac{n^2 \left[w_D\right]^2}{d} \right\},
\end{aligned} \tag{5.82}$$

where d is the number of space dimensions and the square brackets denote the integral

$$[w(\mathbf{r})] = \int d\mathbf{r} w(\mathbf{r}). \tag{5.83}$$

To have an invariant one-particle distribution, Eq. (5.82) must be zero, therefore,

$$m k_B T = \frac{A_3}{A_1(2 - A_1 n \Delta t) - A_2 \Delta t}, \tag{5.84}$$

where

$$A_1 = \frac{\gamma}{md}\left[w_D\right], \quad A_2 = \frac{2\gamma^2}{m^2 d}\left[w_D^2\right], \quad A_3 = \frac{\sigma^2}{d}\left[w_R^2\right]. \tag{5.85}$$

For the distribution function in Eq. (5.79), higher moments are related to lower ones as

$$\int d\mathbf{p} f^{(1)} p^{n+2} \propto \int d\mathbf{p} f^{(1)} p^{n}, \tag{5.86}$$

and so if the first and second moments remain constant then all moments are constant.

We shall briefly discuss the implications of Eq. (5.85) as follows [75].

- For a special case of Eq. (5.85) with $\Delta t = 0$, we then have $mk_BT = A_3/(2A_1)$. This recovers Eq. (5.10), which was obtained from the equilibrium solutions of Fokker-Planck equation correspond to the SDE of DPD.
- For a given set of input parameters of DPD $(\gamma, \sigma, w_D, w_R, n)$, the measured temperature of the system will increase as the time step becomes larger. Furthermore, $1/(k_BT)$ is a linearly monotonic function of Δt. For example, one way to measure the equilibrium temperature is to calculate the averaged kinetic energy of the particles. Then, from the equipartition theorem one obtains temperature as

$$k_BT = \left\langle \mathbf{v}^2 \right\rangle /3. \tag{5.87}$$

- For a given set of input parameters, if $\Delta t > \Delta t_c$, the denominator of Eq. 5.85 becomes negative and the system will become unstable, where

$$\Delta t_c = (2A_1)/(nA_1^2 + A_2). \tag{5.88}$$

- Once a value of Δt is selected, the density can not exceed a critical density

$$n_c = (2A_1 - A_2\Delta t)/(A_1^2 \Delta t), \tag{5.89}$$

  for a stable simulation.
- The choice of larger γ (and σ) will amplify the effects of a finite Δt.

The analysis above ignored the conservative force for the simplification of the equilibrium solution of $f^{eq}(\mathbf{x})$. To select a proper Δt for a practical simulation with conservative force, one may draw similar conclusions by running actual trial simulations and measure the temperature by Eq. (5.87). Depending on the level of the artificial temperature increase we are willing to accept in the simulation we can then pick the appropriate Δt.

In our experience with random number generation, there is no statistical difference between using uniform-distributed and Gaussian-distributed random numbers. In practice the uniform distribution is preferred for the random forces, as it is computationally less expensive. From Eq. (5.85), it is also clear that the temperature increases as the noise level as σ^2. But the value of σ does not change the range of Δt over which the system is stable. However, with higher σ, γ is larger due to the FDT (5.10) and this accelerates the process of a DPD system changing from a deviated temperature k_BT' to the target temperature k_BT.

Repulsive Parameter in the Conservative Force

For modeling a correct thermodynamic state of a liquid, a DPD system must have the correct fluctuations, which are determined by the compressibility of the liquid [37]. Therefore, the repulsive force parameter a in Eq. (5.2) is selected to recover the compressibility of realistic fluids [35]. By applying the virial theorem, we obtain the pressure of a DPD system as

$$\begin{aligned} p &= \rho k_BT + \frac{1}{3V}\left\langle \sum_{i<j}(\mathbf{r}_i - \mathbf{r}_j)\cdot \mathbf{f}_i \right\rangle \\ &= \rho k_BT + \frac{1}{3V}\left\langle \sum_{i<j}(\mathbf{r}_i - \mathbf{r}_j)\cdot \mathbf{F}_{ij}^c \right\rangle \\ &= \rho k_BT + \frac{2\pi}{3}\rho^2 \int_0^{r_c} rf(r)g(r)r^2dr, \end{aligned} \tag{5.90}$$

where $g(r)$ is the radial distribution function of DPD particles, ρ the number density of DPD particles and r_c the cutoff radius beyond which $f(r)$ vanishes. For a wide range of parameters, the pressure can be approximated for high densities ($\rho > 2$) as

$$p = \rho k_BT + \alpha a\rho^2 (\alpha = 0.101 \pm 0.001). \tag{5.91}$$

The compressibility of a DPD fluid is computed by $\kappa_c^{-1} = (\partial p/\partial\rho)_T/k_BT$. To match the compressibility of a DPD fluid to that of a realistic fluid, the dimensionless compressibility is defined by

$$\kappa_c^{-1} = \frac{[L]^3}{\rho k_BT\beta_T}, \tag{5.92}$$

where β_T is the isothermal compressibility of the fluid of interest and $[L]$ the length scale and ρ the number of DPD particles in a volume of $[L]^3$. For example, the liquid water at 300 K has a thermal energy of $k_BT = 4.142 \times 10^{-21}\,\mathrm{kg\,m^2\,s^{-2}}$ and a compressibility of $\beta_T = 4.503 \times 10^{-10}\,\mathrm{m\,s^2/kg}$. Let $\rho = 3$ be the number density of a DPD system where one DPD particle represents a water molecule, a length scale $[L] = 0.448$ nm is determined so that the DPD system matches the number density of water molecule. Substituting these values into Eq. (5.92) gives $\kappa_c^{-1} = 16.0$. Therefore, the repulsive force parameter is $a = k_BT(\kappa_c^{-1} - 1.0)/2\alpha\rho \approx 75.0k_BT/\rho$ with $\alpha = 0.101 \pm 0.001$ for liquid water [35]. It is worth notable that the expression $a = 75.0k_BT/\rho$ is obtained based on a choice of $[L] = 0.448$ nm. Whenever the coarse-graining level or the length scale $[L]$ is changed, a_{ij} should be modified accordingly to recover the correct compressibility of the fluid. Otherwise, the value of κ_c^{-1} will be underestimated, and hence the DPD fluid's sound speed will be lower than expected.

Dissipative Coefficient

We consider a fluid undergoing uniform linear flow $v_\alpha = e_{\alpha\beta} r_\beta$. From the Irving-Kirkwood formula [41], we know that the stress has contributions from both a kinetic part due to particle transfer across streamlines and a dynamic part due to inter-particle forces. We first consider the second part due to forces. In particular, the one arising from the dissipative force is

$$\sigma_{\alpha\beta} = \frac{1}{V} \left\langle \sum_{i>j} r_{ij\alpha} \mathbf{F}^D_{ij\beta} \right\rangle, \tag{5.93}$$

where the expression for $\mathbf{F}^D_{ij}$ is given in Eq. (5.2). If we assume a uniform density without a particular structure for the particles, that is, $g(r) = 1$, we can then replace the summation by an integral as

$$\sigma_{\alpha\beta} = \frac{2\pi\gamma\rho^2}{15} \int_0^\infty drr^4 \gamma w_D(r) \left[e_{\alpha\beta} + e_{\beta\alpha} + \delta_{\beta\alpha} e_{\gamma\gamma} \right]. \tag{5.94}$$

Therefore, the viscosity due to dissipative contribution is

$$\eta^D = \frac{2\pi\gamma\rho^2}{15} \int_0^\infty drr^4 w_D(r). \tag{5.95}$$

For any specific weight function $w_D(r)$ chosen, the viscosity can be calculated in a straightforward way.

Next we derive the kinetic contribution to viscosity due to the diffusion of the particles. The Langevin equation for a single particle without conservative forces reads as,

$$\frac{d\mathbf{v}_i}{dt} = \sum_{j \neq i} \mathbf{F}^D_{ij} + \sum_{j \neq i} \mathbf{F}^R_{ij}. \tag{5.96}$$

Since the friction force is linear in the velocity difference, we may write

$$\frac{d\mathbf{v}_i}{dt} + \frac{\mathbf{v}_i}{\tau} = \mathbf{F}^R, \tag{5.97}$$

where

$$\frac{1}{\tau} = \sum_{j\neq i} \gamma w_D(r_{ij}) \frac{\hat{\mathbf{r}}_{ij}\cdot\hat{\mathbf{r}}_{ij}}{3}, \quad \mathbf{F}^R = \sum_{j\neq i} \sigma w_R(r_{ij})\theta_{ij}\hat{\mathbf{r}}_{ij}. \tag{5.98}$$

We further replace the sum by integral and get

$$\begin{aligned} \frac{1}{\tau} &= \frac{4\pi\gamma\rho}{3}\int_0^\infty drr^2 w_D(r), \\ \left\langle \mathbf{F}^R \right\rangle &= 0, \\ \left\langle \mathbf{F}^R(t)\cdot\mathbf{F}^R(t')\right\rangle &= 4\pi\sigma^2\rho\int_0^\infty drr^2\left[w_R(r)\right]\delta(t-t'). \end{aligned} \tag{5.99}$$

We can solve the Langevin equation Eq. (5.96) straightforwardly to obtain the time correlation of velocity as

$$\langle \mathbf{v}_i(0)\cdot\mathbf{v}_i(t)\rangle = 3k_BT\exp\left(-t/\tau\right). \tag{5.100}$$

Thereafter, the diffusion coefficient is obtained as

$$D = \frac{1}{3}\int_0^\infty dt\,\langle \mathbf{v}_i(0)\cdot\mathbf{v}_i(t)\rangle = \tau k_BT. \tag{5.101}$$

According to the kinetic theory, the viscosity contribution due to the particle diffusion reads

$$\eta^K = \rho\left\langle \mathbf{v}^2\right\rangle\tau/3. \tag{5.102}$$

The total viscosity is simply the sum of η^D and η^K. Therefore, given Eqs. (5.95) and (5.102), one may estimate the input parameters to achieve a desired viscosity of a DPD system.

5.2.5 *The Zwanzig Formalism for Coarse-Graining*

We have applied the Mori formalism in Sect. 5.2.2 to get the linear GLE or the linearized hydrodynamic equations, where the correspondence between thermodynamic response and transport coefficients of the NS equations and DPD parameters are established. Here we introduce another projection adopted by Zwanzig [38, 43, 50, 61, 112, 113], from which a non-linear GLE is obtained. It can be shown that Zwanzig's approach is more general and in fact Mori's approach is an approximation to Zwanzig's near equilibrium [33].

We shall introduce the microdynamics described by a Hamiltonian, which has Gibbsian statistics. Furthermore, we derive two equivalent ways of projection. Firstly, we work on the relevant density adopted by Zwanzig [111]. Secondly, we work on the relevant variables directly [38].

Microdynamics

Given N particles (atoms or molecules) of a Hamiltonian system, a phase space point is defined as $\mathbf{Z}(t) = [Z_1(t), \ldots, Z_{6N}(t)] = [\mathbf{r}_1(t), \ldots, \mathbf{r}_N(t), \mathbf{p}_1(t), \ldots, \mathbf{p}_N(t)]$ where $\mathbf{r}_i$ and $\mathbf{p}_i$ are the position and momentum of ith particle in three dimensions. The dynamics of N atoms is governed by Hamilton's equations of motion

$$\dot{\mathbf{r}}_i = \frac{\partial \mathcal{H}}{\partial \mathbf{p}_i}, \quad \dot{\mathbf{p}}_i = -\frac{\partial \mathcal{H}}{\partial \mathbf{r}_i}, \tag{5.103}$$

where $\mathcal{H}$ is the Hamiltonian of the system defined as the sum of kinetic energy and potential energy of the particles

$$\mathcal{H}(\mathbf{r}_1, \ldots, \mathbf{r}_N, \mathbf{p}_1, \ldots \mathbf{p}_N) = K(\mathbf{p}_1, \ldots \mathbf{p}_N) + V(\mathbf{r}_1, \ldots \mathbf{r}_N), \tag{5.104}$$

where $K = \sum_i^N \frac{\mathbf{p}_i^2}{2m}$ with m as the particle mass, and V is yet to be specified. In particular, given the initial condition $\mathbf{Z}(0) = \mathbf{z}$, the evolution of dynamics for $\mathbf{Z}(t)$ is determined.

Generally, we are not interested in $\mathbf{Z}(t)$ *per se*, but in a set of M functions defined on the phase space $\mathbf{A}(\mathbf{Z}(t)) \equiv [A_1(\mathbf{Z}(t)), \ldots, A_M(\mathbf{Z}(t))] \equiv \mathbf{a}(t, z)$, where $\mathbf{a}$ is introduced to indicate the explicit dependence on initial condition $\mathbf{z}$. The evolution of dynamics of $\mathbf{a}$ is

$$\frac{\partial \mathbf{a}(t, \mathbf{z})}{\partial t} = \mathcal{L}\mathbf{a}(t, \mathbf{z}), \tag{5.105}$$

in which $\mathcal{L}$ is the Liouville operator defined in Sect. 5.2.2, and it was referred to as $\mathcal{L}_C$ in the context of a dissipative system. Here we simply omit the subscript C without ambiguity. The formal solution to Eq. (5.105) is

$$\mathbf{a}(t, \mathbf{z}) = \exp\{t\mathcal{L}\}\mathbf{a}(0, \mathbf{z}) = \exp\{t\mathcal{L}\}\mathbf{A}(\mathbf{z}), \tag{5.106}$$

where the exponential operator is defined via its Taylor expansions. Inserting Eq. (5.106) into Eq. (5.105) we get

$$\frac{\partial \mathbf{a}(t, \mathbf{z})}{\partial t} = \mathcal{L}\mathbf{a}(t, \mathbf{z}) = \mathcal{L}\exp\{t\mathcal{L}\}\mathbf{A}(\mathbf{z}) = \exp\{t\mathcal{L}\}\mathcal{L}\mathbf{A}(\mathbf{z}), \tag{5.107}$$

where $\mathcal{L}$ and $\exp\{t\mathcal{L}\}$ commute.

We have also the Liouville equation for the PDF of particle microdynamics as

$$i\frac{\partial f(t)}{\partial t} = \mathcal{L}_C f(t), \tag{5.108}$$

which has the formal solution as $f(t) = \exp(-i\mathcal{L}t)$. Note that the PDF here describes the microdynamics of a Hamiltonian system, in contrast to the PDF for the dissipative system of DPD particles in Sect. 5.2.1.

The Zwanzig Formalism: Relevant Density

We introduce an operator $\mathcal{P}$ [111], which is used to divide an ensemble density $f(t)$ into a relevant part $f_1(t) = \mathcal{P}f(t)$ and an irrelevant part $f_2(t) = (1 - \mathcal{P})f(t)$,

$$f(t) = f_1(t) + f_2(t). \tag{5.109}$$

Here $\mathcal{P}$ is a linear operator and time-independent so that $\mathcal{P}$ and $\partial/\partial t$ commute. Therefore, the Liouville's equation can be decomposed into a pair of equations

$$\begin{aligned} \mathcal{P}[i(\partial f/\partial t)] &= i(\partial f_1/\partial t) = \mathcal{P}L(f_1 + f_2), \\ (1-\mathcal{P})[i(\partial f/\partial t)] &= i(\partial f_2/\partial t) = (1-\mathcal{P})L(f_1 + f_2). \end{aligned} \tag{5.110}$$

The second equation is a first-order inhomogeneous equation and can be solved in terms of $f_2(0)$ and $f_1(t)$ in a straightforward manner [113] to obtain:

$$\begin{aligned} f_2(t) =& \exp[-it(1-\mathcal{P})\mathcal{L}]f_2(0) \\ & - i\int_0^t ds \exp[-is(1-\mathcal{P})\mathcal{L}]\,(1-\mathcal{P})\mathcal{L}f_1(t-s). \end{aligned} \tag{5.111}$$

Substitute $f_2(t)$ into the first equation we get

$$\begin{aligned} i\frac{\partial f_1(t)}{\partial t} =& \mathcal{P}Lf_1(t) \\ & - i\int_0^t ds\mathcal{P}\mathcal{L}\exp[-is(1-\mathcal{P})\mathcal{L}]\,(1-\mathcal{P})\mathcal{L}f_1(t-s) \\ & + \mathcal{P}\mathcal{L}\exp[-it(1-\mathcal{P})\mathcal{L}]f_2(0), \end{aligned} \tag{5.112}$$

which is the evolution equation for the relevant density.

The Zwanzig Formalism: Relevant Variable

More specifically, if we are interested in the statistical properties of $A(\mathbf{a}(t, \mathbf{z})) \equiv A(\mathbf{Z}(t))$, with initial condition $\mathbf{Z}(0) = \mathbf{z}$ satisfying $\mathbf{A}(\mathbf{z}) = \boldsymbol{\alpha}$. That is, the initial condition of $\mathbf{z}$ is distributed according to the equilibrium density $f^{eq}(\mathbf{z})$, such as $f^{eq}(\mathbf{z}) = \Omega_0^{-1}\delta(\mathcal{H}(\mathbf{z}) - E)$ in the microcanonical ensemble and Ω_0 is the normalization factor, and meanwhile $f^{eq}(\mathbf{z})$ is conditional on the initial condition $\mathbf{A}(\mathbf{z}) = \boldsymbol{\alpha}$. Zwanzig's approach allows us to write an exact integro-differential equation with random coefficients and when the equation is solved with different realizations, the ensemble of $\mathbf{A}(\mathbf{Z}(\mathbf{t}))$ is generated.

We introduce a conditional expectation operator $\mathcal{P}_\alpha$, whose action to an arbitrary phase-space function $F(\mathbf{z})$ at $\mathbf{A}(\mathbf{z}) = \boldsymbol{\alpha}$ gives the conditional equilibrium expectation of $F(\mathbf{z})$ as [38]

$$\mathcal{P}_{\boldsymbol{\alpha}} F(\mathbf{z}) = \frac{1}{\Omega(\boldsymbol{\alpha})} \int F(\mathbf{z}) f^{eq}(\mathbf{z}) \delta(\mathbf{A}(\mathbf{z}) - \boldsymbol{\alpha})) d\mathbf{z}, \tag{5.113}$$

where the probability density of $\mathbf{A}(\mathbf{z})$ is defined as

$$\Omega(\boldsymbol{\alpha}) = \int f^{eq}(\mathbf{z}) \delta(\mathbf{A}(\mathbf{z}) - \boldsymbol{\alpha}) d\mathbf{z}. \tag{5.114}$$

Let $\mathcal{Q}_{\mathbf{A}(\mathbf{z})} = 1 - \mathcal{P}_{\mathbf{A}(\mathbf{z})}$ and insert 1 into Eq. (5.107) we get

$$\frac{\partial \mathbf{a}(t,z)}{\partial t} = \exp\{t\mathcal{L}\}\mathcal{L}\mathbf{A}(\mathbf{z}) = \exp\{t\mathcal{L}\}\mathcal{P}_{\mathbf{A}(\mathbf{z})}\mathcal{L}\mathbf{A} + \exp\{t\mathcal{L}\}\mathcal{Q}_{\mathbf{A}(\mathbf{z})}\mathcal{L}\mathbf{A}. \tag{5.115}$$

Recall the Duhamel-Dyson identity as already applied in Sect. 5.2.2

$$\exp\{t\mathcal{L}\} = \exp\{t\mathcal{Q}_{\mathbf{A}(\mathbf{z})}\mathcal{L}\} + \int_0^t ds \exp\{(t-s)\mathcal{L}\}\mathcal{P}_{\mathbf{A}(\mathbf{z})}\mathcal{L} \exp\{s\mathcal{Q}_{\mathbf{A}(\mathbf{z})}\mathcal{L}\}, \tag{5.116}$$

which can be verified by differentiation [33, 113]. If we apply Eq. (5.116) to replace the second term in Eq. (5.115), we get

$$\frac{\partial \mathbf{a}(t,z)}{\partial t} = \exp\{t\mathcal{L}\}\mathcal{P}_{\mathbf{A}(\mathbf{z})}\mathcal{L}\mathbf{A} + \int_0^t ds \exp\{(t-s)\mathcal{L}\}\mathcal{P}_{\mathbf{A}(\mathbf{z})}\mathcal{L}\tilde{\mathbf{R}}(s,\cdot) + \tilde{\mathbf{R}}(t,\mathbf{z}), \tag{5.117}$$

with

$$\tilde{\mathbf{R}}(t,\mathbf{z}) = \exp\{t\mathcal{Q}_{\mathbf{A}(\mathbf{z})}\mathcal{L}\}\mathcal{L}\mathbf{A} = \mathcal{Q}_{\mathbf{A}} \exp\{t\mathcal{Q}_{\mathbf{A}(\mathbf{z})}\mathcal{L}\}\mathcal{L}\mathbf{A}. \tag{5.118}$$

Equation (5.117) is the evolution equation for relevant variables. Lei et al. [50] have applied it to derive a set of equations of motion for mesoscopic particles, each of which represents a cluster of constrained MD particles. The resultant equation of motion has the same form as DPD. Hijón et al. [38] and Li et al. [61] also applied the Mori-Zwanzig formalism to coarse-grain a system of homogeneous star polymer melts, where each DPD particle represents the center of mass of individual star polymer. In the context of coarse-graining, the parameters such as a, γ (σ) and weighting functions w_C, w_D (w_R) for DPD depend on the properties of the underlying MD system at a specific state point performed. Typically, we have numerical values for DPD input parameters obtained from the MD values.

5.3 Extensions of Dissipative Particle Dynamics

The classical DPD model was initially proposed as a minimal working version for mesoscopic simulation of fluids. It only considers the momentum equation governing the evolution of flow field, which precludes the classical DPD method from modeling some specific problems, e.g., liquid-vapor coexistence in one-component multiphase fluid systems, heat flow in non-isothermal systems and diffusion-reaction process in biological systems. To this end, several extensions of the DPD method have been developed in recent years for tackling the challenges in diverse applications involving multiple physical fields (i.e., flow field, thermal field and concentration field), which are beyond the capability of classical DPD model.

In this section, we will introduce some of them, including the many-body DPD (mDPD) model for multiphase flows [85], the energy-conserving DPD (eDPD) model for non-isothermal systems [6, 23] and the transport DPD (tDPD) model for advection-diffusion-reaction processes [66], as shown by the "DPD Alphabet" in Fig. 5.2. The eDPD model is the first extension of DPD proposed by Avalos et al. [6]

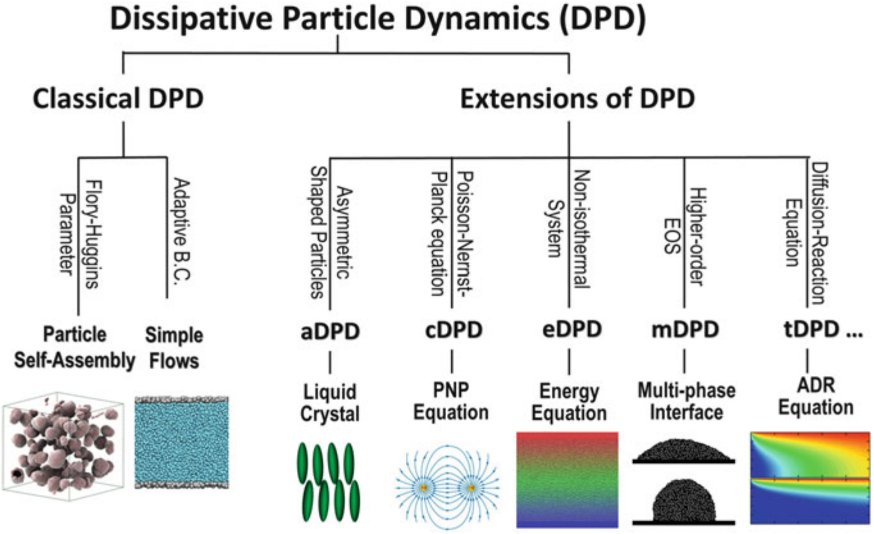

Fig. 5.2 State of the art of the DPD method ("DPD Alphabet"), in which the classical DPD model is widely used for studying hydrodynamics of isothermal fluid systems while various extensions of DPD have been developed for modeling different phenomena in multiphysics applications

and Español [23] independently in 1997, the mDPD model is another extension of DPD initialized by Pagonabarraga and Frenkel [85] in 2001 and subsequently specified by Warren [106] in 2003, and the tDPD model was developed by Li et al. [66] in 2015.

5.3.1 *Energy-Conserving DPD (eDPD) for Non-Isothermal Systems*

The dissipative force or force of friction between DPD particles reduces their velocity difference and thus dissipates the thermal kinetic energy of the system, while the random force generates a stochastic force on each DPD particle that inputs kinetic energy into the system. In the classical DPD model, the dissipative and random forces together satisfy the fluctuation-dissipation theorem and so act as a thermostat to maintain the system at a constant temperature [26]. The evolution equation for the macroscopic energy density in a DPD system does not have the form of a local conservation equation [77], but contains source and sink terms corresponding to the random and dissipative forces, respectively, and hence the total energy of the system is not conserved [6]. As a result, the classical DPD method is limited to isothermal systems and can neither sustain temperature gradients nor can it model heat transfer [23].

To extend the isothermal DPD equations to modeling heat transport in non-isothermal fluid systems, energy conservation is satisfied in DPD by introducing the internal energy as an additional property of the system [23, 96]. Therefore, an energy-conserving DPD model was developed and is known in the literature as eDPD [62, 95]. As in classical DPD, each eDPD particle is considered to be coarse-grained representation of a group of molecules rather than individual atoms. The time evolution of an eDPD particle i with mass m_i is governed by the conservation of momentum and energy, which is described by the following set of equations [23, 62]:

$$m_i \frac{\mathrm{d}^2\mathbf{r}_i}{\mathrm{d}t^2} = m_i \frac{\mathrm{d}\mathbf{v}_i}{\mathrm{d}t} = \mathbf{F}_i = \sum_{i \neq j} (\mathbf{F}_{ij}^C + \mathbf{F}_{ij}^D + \mathbf{F}_{ij}^R), \tag{5.119a}$$

$$C_v \frac{\mathrm{d}T_i}{\mathrm{d}t} = q_i = \sum_{i \neq j} (q_{ij}^C + q_{ij}^V + q_{ij}^R), \tag{5.119b}$$

where t, $\mathbf{r}_i$, $\mathbf{v}_i$ and $\mathbf{F}_i$ denote time, and position, velocity, force vectors, respectively, T_i the temperature, C_v the thermal capacity of eDPD particles and q_i the heat flux between particles. The summation of forces is carried out over all other particles within a cutoff radius r_c, beyond which the forces are considered to be zero.

The three components of $\mathbf{F}_i$, including the conservative force $\mathbf{F}_{ij}^C$, dissipative force $\mathbf{F}_{ij}^D$ and random forces $\mathbf{F}_{ij}^R$, are given by Eq. (5.2) [35]. For an eDPD system in local thermodynamic equilibrium, a Fokker-Planck equation, mathematically identical to the stochastic equations of Eqs. (5.119a) and (5.119b), can now be derived [23]. The solution of the FPE gives the relationship between the dissipative force and random force, which requires $\sigma_{ij}^2 = 4\gamma_{ij}k_BT_iT_j/(T_i + T_j)$ and $w_D(r) = w_R^2(r)$. The key aspect of eDPD is that the temperature T_i is defined on each particle, and the fluctuation-dissipation theorem is applied locally based on the particle temperature T_i rather than the thermodynamic temperature of the system. As a result, eDPD allows temperature gradients and can be used in non-isothermal problems, where thermal transport plays a critical role.

The heat fluxes between particles accounting for the thermal conduction q^C, viscous heating q^V, and random heat flux q^R are given by Qiao and He [95] and Li et al. [62]:

$$\begin{aligned}
q_i^C &= \sum_{j\neq i} k_{ij} w_{CT}(r_{ij}) \left(T_i^{-1} - T_j^{-1}\right), \\
q_i^V &= \frac{1}{2C_v} \sum_{j\neq i} \left\{ w_D(r_{ij}) \left[\gamma_{ij} \left(\mathbf{e}_{ij}\mathbf{v}_{ij}\right)^2 - \sigma_{ij}^2/m_i\right] - \sigma_{ij} w_R(r_{ij}) \mathbf{e}_{ij}\mathbf{v}_{ij}\zeta_{ij} \right\}, \\
q_i^R &= \sum_{j\neq i} \beta_{ij} w_{RT}(r_{ij}) \xi_{ij}^e,
\end{aligned} \tag{5.120}$$

where the expression of thermal conduction q^C contains T^{-1} rather than T because the thermodynamic quantity conjugated to the internal energy is the inverse of the temperature rather than the temperature itself [35]. The parameters k_{ij} and β_{ij} determine the strength of the thermal conduction and the random heat flux, respectively. In particular, k_{ij} plays the role of a thermal conductivity given as $k_{ij} = C_v^2\kappa(T_i + T_j)^2/4k_B$ in which κ is interpreted as a mesoscale heat friction coefficient [95, 96], and $\beta_{ij}^2 = 2k_Bk_{ij}$. The weight functions $w_{CT}(r)$ and $w_{RT}(r)$ in Eq. (5.120) are given as $w_{CT}(r) = w_{RT}^2(r) = (1 - r/r_{ct})^{s_T}$ in which s_T is the exponent of the weight functions and r_{ct} is a cutoff radius for heat fluxes. The case of $s_T = 2.0$ corresponds to the typical quadratic weighting function [35].

For an eDPD particle, the characteristic scale of the kinetic energy related to its momentum is k_BT, while the characteristic scale of the internal energy related to its temperature is C_vT. To convert the kinetic energy into the internal energy, we need a scaling factor k_BT/C_vT. Therefore, the viscous heating q_i^V given by Eq. (5.120) has a factor $1/C_v$ when the kinetic energy k_BT has been rescaled into the unit. Also, the factor 2 in the denominator means that the heat generated by non-conservative interactions is distributed evenly to both particles of a pair. By performing practical eDPD simulations, Li et al. [62] verified the energy conservation of the eDPD system.

The transport properties including diffusivity and viscosity of the eDPD fluid are output properties instead of input parameters. Groot and Warren [35] and Marsh et al. [77] have investigated the expressions of the diffusivity and the viscosity in terms of DPD parameters. With the interaction between particles described by Eq. (5.2), they are given by Groot and Warren [35] and Marsh et al. [77]

$$\begin{aligned} D &= k_B T \left(\frac{4\pi\gamma\rho}{3} \int_0^{\infty} r^2 g(r) w_D(r) dr \right)^{-1}, \\ \nu &= \frac{D}{2} + \frac{2\pi\gamma\rho}{15} \int_0^{\infty} r^4 g(r) w_D(r) dr, \end{aligned} \tag{5.121}$$

where $g(r)$ is the radial distribution function of DPD particles. A rough analytical prediction of the diffusivity and the kinematic viscosity can be obtained by assuming $g(r) = 1.0$ corresponding to ideal gases [35]. Substituting $w_D(r) = w_R^2(r) = (1 - r/r_c)^s$ into Eq. (5.121), the diffusivity and kinematic viscosity of the eDPD fluid can be approximated by:

$$\begin{aligned} D &= \frac{3k_B T(s+1)(s+2)(s+3)}{8\pi\gamma\rho r_c^3}, \\ \nu &= \frac{3k_B T(s+1)(s+2)(s+3)}{16\pi\gamma\rho r_c^3} + \frac{16\pi\gamma\rho r_c^5}{5(s+1)(s+2)(s+3)(s+4)(s+5)}. \end{aligned} \tag{5.122}$$

Equation (5.122) indicates that both the diffusivity D and the kinematic viscosity ν of the eDPD fluid increase with the increase of temperature when other variables in Eq. (5.122) are kept constant. However, for most of the simple liquids such as water, ethanol and glycerin, the diffusivity increases but the kinematic viscosity decreases with increasing temperature. In order to simulate the flow dynamics of such liquids, at least one of the parameters ρ, r_c, γ and s should be function of temperature so that the eDPD model can reproduce the correct dynamic behavior of non-isothermal fluid systems. After studying the sensitivity of D and ν, the exponent of the weighting function s is defined as a function of temperature for modeling the temperature-dependent diffusion and viscosity of eDPD fluids. For details on choosing the function for s, readers are referred to [52, 62].

In addition, if the variation of fluid density with temperature is also considered, a temperature-dependent conservative coefficient $a(T)$ is required to capture the effect of temperature on the fluid density. More specifically, let both the fluid density $\rho(T)$ and compressibility $\kappa_c^{-1}(T)$ be functions of temperature obtainable from experimental data. The temperature-dependent conservative coefficient is determined by $a(T) = k_B T(\kappa_c^{-1}(T) - 1)/2\alpha\rho(T)$ in which $\alpha = 0.101 \pm 0.001$. For example, the density of a DPD fluid with constant a is invariant with respect to temperature, while $a(T) = 75k_B T/\rho$ yield a linear dependence of density on temperature [62].

Similar to the diffusivity and the kinematic viscosity, the thermal conductivity is also an output property. For an eDPD system whose transport of energy is dominated by the dissipative interactions of Eq. (5.120), the macroscopic thermal conductivity

λ can be calculated by Mackie et al. [74]:

$$\lambda = \frac{2\pi}{3}\frac{\rho^2}{T^2}\int_0^{r_c} r^4 k w_{CT}(r) g(r) dr, \tag{5.123}$$

where $k = C_v^2 \kappa T^2 / k_B$ and $w_{CT}(r)$ the weight function used in Eq. (5.120). Given $w_{CT}(r) = (1 - r/r_c)^{s_T}$ an analytical estimate for the thermal conductivity λ can be obtained by assuming the radial pair distribution function $g(r) = 1.0$ corresponding to ideal gases, and it is given as:

$$\lambda = \frac{16\pi\rho^2\kappa C_v^2 r_c^5}{k_B(s_T+1)(s_T+2)(s_T+3)(s_T+4)(s_T+5)}. \tag{5.124}$$

In particular, when the typical quadratic weight function $(1 - r/r_c)^2$ is employed for $w_{CT}(r)$ with $s_T = 2.0$, then Eq. (5.124) becomes

$$\lambda = \frac{2\pi\rho^2}{315 k_B}\kappa C_v^2 r_c^5. \tag{5.125}$$

The definition of the Prandtl number is $\mathrm{Pr} = \rho\nu C_v/\lambda$, which is a temperature-dependent dimensionless number and its value can be obtained from available experimental data. After replacing λ by Pr in Eq. (5.125), we have a formula for determining the mesoscale heat friction κ for the eDPD system given by:

$$\kappa = \frac{315 k_B \nu}{2\pi\rho C_v r_c^5}\frac{1}{\mathrm{Pr}}, \tag{5.126}$$

where ν is the kinematic viscosity which can be roughly approximated by Eq. (5.121) or given by the computed kinematic viscosity. The expression of Eq. (5.126) is obtained from the typical quadratic weight function $w_{CT}(r) = (1 - r/r_c)^2$ and a similar formula can be derived from Eq. (5.123) when a different weight function is employed.

By including the energy equation in the DPD framework, the eDPD method has been successfully used in diverse applications involving thermal fields. For example, Li et al. [62] considered the coupling of the flow and the thermal fields, where an eDPD simulation of a Poiseuille flow confined between a hot wall and a cold wall was performed. Since the hotter fluid is less viscous than the colder fluid, the variation of the viscosity perpendicular to the flow direction leads to an asymmetric velocity profile. As a result, the peak of the velocity profile shifts to the hotter side, as shown in Fig. 5.3a. Li et al. [65] also applied the eDPD method to modeling of thermoresponsive polymers. Because of the energy conservation in eDPD, they demonstrated that eDPD simulations are able to correctly capture not only the transient behavior of polymer precipitation from solvent induced by temperature changes, as shown in Fig. 5.3b, but also the energy variation associated with the phase transition process. Moreover, natural convection in microchannels [1]

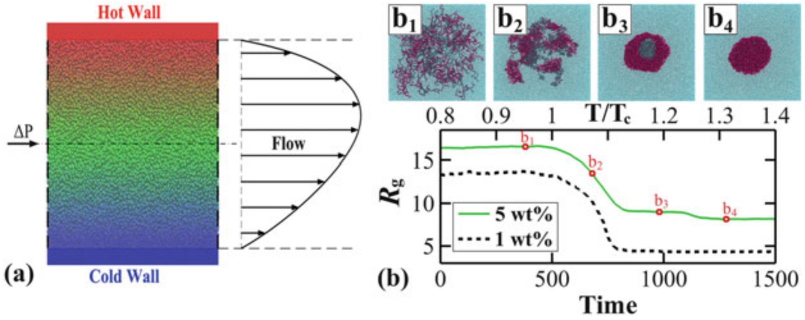

Fig. 5.3 (**a**) An eDPD simulation [62] of the Poiseuille flow combined with the heat conduction between a cold wall T_C and a hot wall T_H. (**b**) eDPD modeling of thermoresponsive microgels [65]. Lines show the evolution of gyration radius R_g and (*b1–b4*) show cross sections of their transient microstructure corresponding to the changes of R_g during heating. Images (**b**) is adapted with permissions from [65]

and in eccentric annulus [15], thermal conduction of nanofluids [95] and doubly thermoresponsive self-assemblies [102], to name but a few, have been also studied using eDPD simulations.

5.3.2 Many-Body DPD (mDPD) for Multiphase Flows

The conservative force between particles i and j is given as $\mathbf{F}_{ij}^C = a w_c(r_{ij})\mathbf{e}_{ij}$ in the classical DPD model, where a is a repulsive force parameter and $w_c(r_{ij})$ is a soft and unspecific weight function. A common choice of the weight function is $w_c(r_{ij}) = 1 - r_{ij}/r_c$ for $r_{ij} \leq r_c$ and vanishes beyond the cutoff radius r_c. For a single-component DPD fluid with a purely repulsive conservative force, the equation of state (EOS) of the system can be computed by Groot and Warren [35]

$$\begin{aligned} p &= \rho k_B T + \frac{1}{3V}\left\langle \sum_{j>i} (\mathbf{r}_i - \mathbf{r}_j)\cdot \mathbf{F}_{ij}^C \right\rangle \\ &= \rho k_B T + a\rho^2 \cdot \frac{2\pi}{3}\int_0^\infty w_c(r)g(r)r^3 dr, \end{aligned} \tag{5.127}$$

where $g(r)$ is the RDF, and ρ is the number density of DPD particles. The first term in the EOS is an ideal gas term, and the second term is the excess pressure. In the mean-field theory, Eq. (5.127) can be simplified by employing the RDF of the idea gas $g(r) = 1$,

$$p = \rho k_B T + \alpha_{\mathrm{MF}} a \rho^2, \tag{5.128}$$

where $\alpha_{\mathrm{MF}} = \frac{2\pi}{3}\int_0^\infty w_c(r)r^3 dr$. Given a weighting function $w_c(r) = 1 - r/r_c$ with a cutoff radius $r_c = 1$, we arrive at $\alpha_{\mathrm{MF}} = \pi/30$. The realistic EOS of a DPD fluid can be computed by performing a series of DPD simulations at various densities. The computed EOS of DPD fluids is in the form of $p \approx \rho k_B T + \alpha a \rho^2$ with a coefficient $\alpha = 0.101 \pm 0.001$ very close to the mean-field prediction $\alpha_{\mathrm{MF}} = \pi/30 = 0.1047$, which is perfectly quadratic in the density [35]. This monotonic function of EOS does not have a van der Waals loop and excludes the possibility of modeling phenomena involving vapor-liquid coexistence and free-surfaces of single-component fluids. To this end, Pagonabarraga and Frenkel [85] defined the free energy ψ of an inhomogeneous system with density $\rho(\mathbf{r})$ as $\psi = \int \rho(\mathbf{r})\varphi(\rho(\mathbf{r}))\, d\mathbf{r}$, where $\varphi(\rho)$ is the local free energy per particle associated to the local configuration of particles rather than a mechanical potential energy. If the free energy determines the relevant energy for a given configuration of DPD particles, then the force acting on each particle can be derived as the variation of such energy when the corresponding particle is displaced. However, the ideal contribution to the free energy of the system has already been accounted for by the dissipative and random forces. Therefore, only the excess free energy is involved in the conservative interaction between DPD particles. Let $\psi_{\mathrm{ex}}(\rho)$ be the excess component of the total free energy $\psi(\rho)$, the conservative force acting on a particle i is written as $\mathbf{F}_i = -\frac{\partial}{\partial \mathbf{r}_i}\sum_j \psi_{\mathrm{ex}}(\rho_j) = \sum_j \mathbf{F}_{ij}$. Then, the conservative force between a pair of particles i and j depends not only on their relative positions, but also on their local densities. This defines the many-body DPD (mDPD) model [106].

Let $\phi(\rho)$ be an unspecified function of density, the density-dependent conservative force is written as,

$$\mathbf{F}_{ij}^C = \frac{1}{2}\left[\phi(\rho_i) + \phi(\rho_j)\right] w_c(r_{ij})\mathbf{e}_{ij}, \tag{5.129}$$

for a one-component fluid. The local density ρ_i of a particle i is taken to be the instantaneously weighted average $\rho_i = \sum_{i \neq j} w_\rho(r_{ij})$ with a weight function $w_\rho(r_{ij}) = 15(1 - r_{ij}/r_c)^2/(2\pi r_c^3)$, which is normalized so that $\int_0^\infty d^3\mathbf{r} w_\rho(r) = 1$. It is obvious that if $\phi(\rho) \equiv a$, the method with Eq. (5.129) reduces exactly to the classical DPD model. By the mean-field theory, the modified force law of Eq. (5.129) should give an EOS

$$p_{\mathrm{MF}} = \rho k_B T + \alpha_{\mathrm{MF}}\phi(\rho)\rho^2, \tag{5.130}$$

where $\alpha_{\mathrm{MF}} = \pi/30$ for the standard choice of $w_c(r)$. Since $\phi(\rho)$ is an unspecified function of density, in principle, an arbitrary dependence of EOS on density can be recovered. However, having a van der Waals loop in the EOS is not sufficient to stabilize the vapor-liquid interface. Pagonabarraga and Frenkel [85] discussed that a simple many-body DPD model with a single interaction range may not yield a stable interface. To simulate the vapor-liquid coexistence with mDPD, one must also give consideration to the ranges of interactions. In the approach developed by Warren [106], the density-dependent conservative force is introduced empirically with a different cut-off radius r_d, and can be written as,

$$\mathbf{F}_{ij}^{C} = Aw_c(r_{ij})\mathbf{e}_{ij} + B(\rho_i + \rho_j)w_d(r_{ij})\mathbf{e}_{ij}, \tag{5.131}$$

where the first term with a negative coefficient $A < 0$ stands for an attractive force within an interaction range r_c, and the second term with $B > 0$ is the density-dependent repulsive force within an interaction range r_d. Then, the mean-field EOS is

$$p_{\mathrm{MF}} = \rho k_B T + \alpha_{\mathrm{MF}}(A\rho^2 + 2Br_d^4\rho^3). \tag{5.132}$$

Thus, given $A < 0$ and $B > 0$, this EOS has the potential to contain a van der Waals loop for modeling vapor-liquid coexistence.

Using numerical experiments, Warren [106] explored a wider parameter space for the mDPD model with the conservative force given by Eq. (5.131). By defining a function $\Phi = (p - \rho k_B T - \alpha A\rho^2 - 2\alpha Br_d^4\rho^3)/Br_d^4$, the data of the mDPD fluids collapse onto a straight line, as shown in Fig. 5.4a. The computed EOS can be fitted by

$$p = \rho k_B T + \alpha A\rho^2 + 2\alpha Br_d^4(\rho^3 - c\rho^2 + d), \tag{5.133}$$

where $\alpha = 0.101 \pm 0.001$, $c = 4.16 \pm 0.02$, and $d = 18 \pm 1$. Let ρ_V and ρ_L be vapor and liquid coexistence densities, respectively, then a phase separation can be observed in a range of densities $\rho_V < \rho < \rho_L$. In principle, integration of the EOS gives the free-energy density from which predictions can be made about ρ_V and

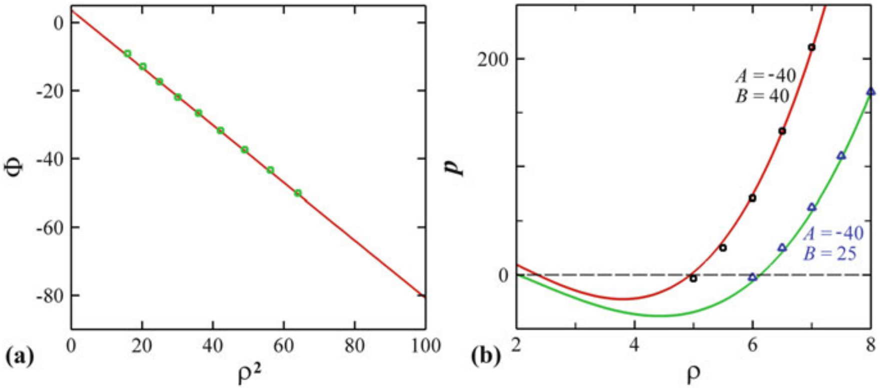

Fig. 5.4 (**a**) Data collapse of pressure against density for $\rho_L < \rho \leq 8, A = -40 \sim -20, B = 25$ or $40, k_BT = r_c = 1, r_d = 0.75$. The ordinate is the function $\Phi = (p - \rho k_B T - \alpha A\rho^2 - 2\alpha Br_d^4\rho^3)/Br_d^4$. The straight line is a fit to data given by Eq. (5.133). (**b**) Pressure as a function of density for the two selected parameter sets $A = -40, B = 40$ or $25, r_d = 0.75, k_BT = r_c = 1.0$. The lines are the predictions of the fitted EOS in the form of Eq. (5.133). Data are from [106]

ρ_L. Unfortunately, the EOS must deviate from the above fitted form of Eq. (5.133) for $\rho \ll 1$. Therefore, the vapor phase is inadequately characterized. If the case $\rho_L \geq 1$ in coexistence with a very dilute vapor is of practical interest, it would be easier to use the EOS to predict the point where the pressure vanishes as an estimate of the coexisting liquid phase density, i.e., $p(\rho_L) = 0$. Using this, the numerical experiments performed by Warren [106] obtained the liquid densities of the order $\rho_L \sim 5$ for $-A \sim B \sim 30$. Figure 5.4b plots the computed EOS of two DPD fluids with parameters $A = -40, B = 40$ or $25, r_d = 0.75, k_BT = r_c = 1.0$. The two parameter sets are distinguished by the different values of the liquid densities, i.e., $\rho_L = 5.08 \pm 0.01$ for $B = 40$ and $\rho_L = 6.05 \pm 0.01$ for $B = 25$, as indicated in Fig. 5.4b by $p(\rho_L) = 0$. The coexisting vapor density $\rho_L \ll 1$, so these parameters are suitable for free-surface simulations.

Ever since its inception, the mDPD model has been applied to simulations of various wetting phenomena and multiphase flows. For example, Arienti et al. [5] investigated the performance of the mDPD model at vapor/liquid and liquid/solid interfaces and simulated the dynamics of droplets entering an inverted Y-shaped fracture junction, as shown in Fig. 5.5a. Li et al. [60] performed mDPD simulations of the manipulation of a liquid droplet on solid surfaces driven by a linear gradient of wettability. They explored the internal three-dimensional velocity field with transverse flow in a moving droplet, as shown in Fig. 5.5b. Li et al. [58] also studied droplet oscillations in AC electrowetting using mDPD simulations. Wang and Chen [105] used mDPD to simulate droplets sliding across micropillars and investigated how the pillars with different intrinsic wettability influence the movement of droplets, as shown in Fig. 5.5c, which describes the evolution of the advancing and receding contact angle with time as well as five snapshots of the droplet sliding across multiple micropillars.

The essential concept of the mDPD model is to construct a density-dependent conservative force, which yields EOS with a van der Waals loop for modeling vapor-liquid coexistence. In the strategy proposed by Warren, an empirical expression of the conservative force is first introduced, and then the mDPD model is calibrated to determine the true EOS and thermodynamic properties of the mDPD fluid. Alternatively, following the original formulations of mDPD proposed by Pagonabarraga and Frenkel [85], Tiwari and Abraham [103] used an opposite strategy to construct the conservative force for the mDPD model. They started from a van der Waals equation of state and formulated the conservative force in the context of the mean-field theory.

Using the mean-field approximation for intermolecular attraction, the free energy per particle is given by

$$\psi = \int_{r>\sigma} u_{\text{att}}(r)\rho(\mathbf{r})d\mathbf{r}, \tag{5.134}$$

where $u_{\text{att}}(r)$ is the attractive component of the interaction potential, r the separation distance of particles and σ the diameter of particles for excluded volume. Expanding $\rho(\mathbf{r})$ in Eq. (5.134) about $\mathbf{r}$ and assuming that the gradient of ρ is small, only the even

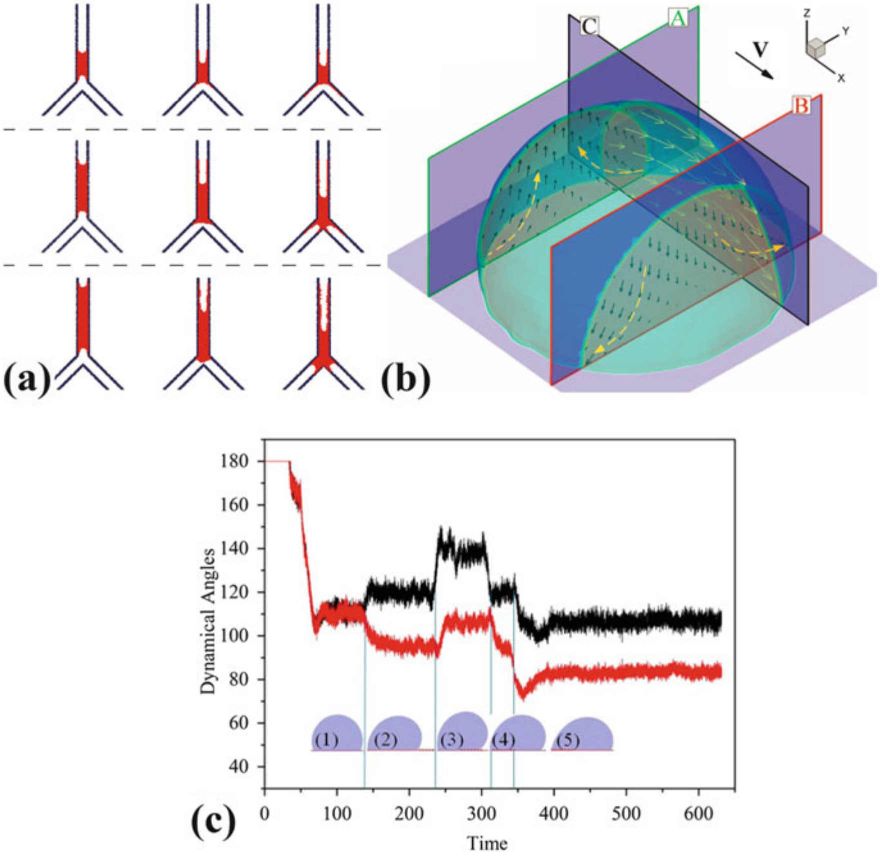

Fig. 5.5 (**a**) mDPD simulations of droplets with different sizes entering an inverted Y-shaped fracture junction. (**b**) Three-dimensional velocity field inside a moving droplet, where the vector V denotes the direction of movement. (**c**) Advancing and receding contact angle evolution versus time for a droplet sliding over pillars. Images (**a**), (**b**) and (**c**) are adapted with permissions from [5, 60, 105]

derivatives of density survive and the leading two terms are

$$\psi = -\mu\rho - \kappa\nabla^2\rho, \tag{5.135}$$

in which $\mu = -\int_{r>\sigma} u_{\text{att}}(r)d\mathbf{r}$ and $\kappa = -\frac{1}{6}\int_{r>\sigma} r^2 u_{\text{att}}(r)d\mathbf{r}$. The parameters μ and κ arise due to the long-range attractive forces and give rise to the weak attraction and surface tension, respectively, between the mDPD particles at the coarse-grained level. Then, the form of the conservative force $\mathbf{F}^C$, which gives rise to phase segregation and surface tension in a liquid-vapor system, is given by

$$\mathbf{F}^C = -\nabla\psi_{\text{ex}} + \mathbf{F}^S, \tag{5.136}$$

with ψ_{ex} being the excess part of the free energy ψ. $\mathbf{F}^S = \kappa \nabla \nabla^2 \rho$ represents the surface tension component that comes from the second term in Eq. (5.135). Here, only the contribution from the excess part is considered in the conservative force because the ideal part has already been considered through the random and dissipative forces. If the EOS of the mDPD fluids is described by the van der Waals equation of state, then

$$p = \frac{\rho k_B T}{1 - b\rho} - a\rho^2, \tag{5.137}$$

where a and b are the parameters for the EOS. More specifically, the parameter a accounts for the long-range attractive behavior, while the parameter b is responsible for excluded volume effects. Then, the free energy ψ of particles can be derived from Eq. (5.137) by $p = -\partial \psi / \partial v$ where p is the pressure and $v = \rho^{-1}$ the specific volume,

$$\psi = \psi_{\text{ex}} + k_B T \ln \rho = -k_B T \ln(1 - b\rho) - a\rho + k_B T \ln \rho, \tag{5.138}$$

where the first term is responsible for repulsion between the particles, the second term originates from the attractive part of interaction potential, and the last term is the ideal gas part. Substituting the excess free energy ψ_{ex} into Eq. (5.136), we obtain

$$\mathbf{F}^C = -\nabla \left[k_B T \ln(1 - b\rho) + a\rho \right] + \kappa \nabla \nabla^2 \rho. \tag{5.139}$$

It is clear that the conservative force in the form of Eq. (5.139) is also density-dependent. For mDPD system consisting of discrete particles, the density in the vicinity of a particle i is computed as a weighted average of contributions from its neighbors, i.e., $\rho_i = \sum_j w_\rho(r_{ij})$, where the weighting function $w_\rho(r_{ij})$ can be the widely used smoothing kernels in the smoothed particle hydrodynamics (SPH) method [79]. For example, the Lucy kernel reads

$$w_\rho(r, r_c) = \begin{cases} \frac{105}{16\pi r_c^3} \left(1 + \frac{3r}{r_c}\right) \left(1 - \frac{r}{r_c}\right)^3, & r \leq r_c \\ 0. & r > r_c \end{cases} \tag{5.140}$$

Let $w_\rho^{(1)}(r)$ and $w_\rho^{(3)}(r)$ be the first and third derivatives of the weight function of Eq. (5.140) with respect to the particle separation r. Then, the conservative force for a pair of particles i and j takes the final form

$$\mathbf{F}_{ij}^C = \left\{ -\left(\frac{b k_B T}{1 - b\rho_i} + \frac{b k_B T}{1 - b\rho_j} - 2a \right) w_\rho^{(1)}(r_{ij}) + \kappa w_\rho^{(3)}(r_{ij}) \right\} \mathbf{e}_{ij}. \tag{5.141}$$

With parameters $a = 3.012 \times 10^{-3}$, $b = 2.5 \times 10^{-2}$, $k_B T = 2.1 \times 10^{-2}$ and $r_c = 1.11$ in DPD units, Tiwari and Abraham [103] successfully validated the mDPD model with the two-dimensional Young–Laplace equation $\Delta p = p_{\text{in}} - p_{\text{out}} = \sigma_{\text{lv}} / R$ where

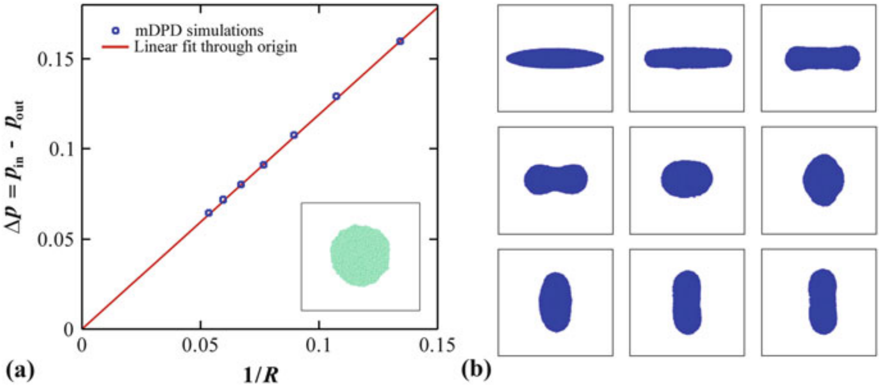

Fig. 5.6 (**a**) Validation of the mDPD model with the two-dimensional Young–Laplace equation $\Delta p = p_{\mathrm{in}} - p_{\mathrm{out}} = \sigma_{\mathrm{lv}}/R$. The *inset* shows the setup of mDPD simulations for a two-dimensional droplet in a periodic box. (**b**) Snapshots of large-amplitude oscillations of liquid cylinder with an initial aspect ratio of 5. (**a**) and (**b**) are adapted with permission from [103]

σ_{lv} is the liquid-vapor interfacial tension and R the equilibrium radius of the droplet, as shown in Fig. 5.6a, and simulated large-amplitude oscillations of liquid cylinders, as shown in Fig. 5.6b.

Surface tension is one of the most important fluid properties relevant to the liquid-vapor coexistence. Although the magnitude of surface tension is determined by the interactions between mDPD particles, it is an output property of the mDPD system rather than an input parameter. The exact value of the surface tension needs to be computed from mDPD simulations. Several methods can be applied to compute the surface tension of a mDPD fluid. The first one is to compute the pressure difference between the inside and the outside of a droplet for various radii. According to the Young–Laplace equation, i.e., $\Delta p = p_{\mathrm{in}} - p_{\mathrm{out}} = 2\sigma_{\mathrm{lv}}/R$ for three-dimensional droplets, the surface tension σ_{lv} is determined by the slope of the line $\Delta p \sim R^{-1}$, as shown in Fig. 5.6a. The second one is the pendant drop method, which is also widely used in experimental tensiometers. To set up the pendant droplet in mDPD simulations, a vertical cylindrical column of fluid at a density close to the equilibrium liquid density is equilibrated. A "support" needs to be constructed by "freezing" particles at the top of the column as a solid wall. By applying a gravitational body force onto each mDPD particle, the liquid forms a pendant droplet after the system reaches equilibrium. Then, a numerical fit of the theoretical drop shape to the shape obtained by mDPD simulations eventually yields the surface tension [106]. The third method is the easiest one that only needs a thin liquid film in a periodic computational box. The surface tension is computed from the standard mechanical definition of the pressure tensor using the Irving–Kirkwood expression,

$$\sigma_{\mathrm{lv}} = \int \left[p_{\mathrm{zz}} - \frac{1}{2}(p_{\mathrm{xx}} + p_{\mathrm{yy}}) \right] dz, \tag{5.142}$$

where $p_{\mathrm{xx}}, p_{\mathrm{yy}}$ and p_{zz} are the three diagonal components of the pressure tensor, with x and y parallel to the planar interface and z normal to it. More practically, let Λ be the surface area of the planar surface of the liquid film, then the surface tension is computed by

$$\sigma_{\mathrm{lv}} = \left\langle \frac{1}{2\Lambda} \sum_{i \neq j} \left[\mathbf{r}_{ij,x}\mathbf{F}_{ij,x} - \frac{1}{2}(\mathbf{r}_{ij,y}\mathbf{F}_{ij,y} + \mathbf{r}_{ij,z}\mathbf{F}_{ij,z}) \right] \right\rangle, \tag{5.143}$$

where the factor 2 in the denominator accounts for the fact that the liquid film has two interfaces, $\mathbf{r}_{ij,\beta}$ and $\mathbf{F}_{ij,\beta}$ are the β-component (β is x, y or z) of $\mathbf{r}_{ij}$ and $\mathbf{F}_{ij}$, respectively.

In the last decade, the mDPD model proposed by Warren [106] has been more widely used in diverse applications than Tiwari's mDPD model [103]. The reason may lie in the convenience of Warren's approach in modeling solid-liquid interfacial tensions. More specifically, Warren employed empirical expressions of the conservative force in Eq. (5.131), where the coefficients A and B can be defined as species-dependent parameters. For instance, let A_{ll} and B_{ll} be the coefficients for liquid-liquid interaction while A_{sl} and B_{sl} for solid-liquid interaction, the solid-liquid interfacial tension can be easily changed just by varying A_{sl} and B_{sl}, which generates various wetting phenomena of droplets on solid substrates. However, Tiwari's mDPD model starts from the van der Waals equation of state, which does not easily model solid-liquid interfaces. Moreover, the van der Waals model describes vapor-liquid equilibrium over very limited ranges of temperature. The famous loops provide only a qualitative representation of the two-phase boundary in PVT space. Therefore, Warren's approach has been successfully applied to various wetting problems involving solid-liquid interfacial tensions, while Tiwari's approach has been only applied to fluids in periodic boxes.

5.3.3 Transport DPD (tDPD) for Advection-Diffusion-Reaction

The classical DPD system has only equations governing the evolution of density and velocity fields but no evolution equations for describing the concentration field, which precludes the classical DPD method from modeling diffusion-reaction processes, i.e., two of the most fundamental processes in biological systems [21]. More specifically, proteins in an aqueous solution diffuse in a living cell due to Brownian motion, and some collisions of appropriate proteins may lead to chemical reactions. Moreover, most biological functions depend highly on the concentrations of specific proteins, ions or other biochemical factors [4], whose transports at the cellular and subcellular levels are crucial to corresponding biological processes in living systems. Therefore, it is important to include the advection-diffusion-reaction (ADR) equation in the DPD model when diffusion and reactions are involved. To this end, Li et al. [66] developed a transport dissipative particle dynamics model named tDPD for mesoscopic problems involving ADR processes.

Similar to classical DPD method, in tDPD each particle is associated with extra variables for carrying concentrations in addition to other quantities such as position and momentum. The transport of concentration is modeled by a Fickian flux and a random flux between tDPD particles. More specifically, the time evolution of a tDPD particle i with unit mass $m_i \equiv 1$ is governed by the conservation of momentum and concentration, which is described by the following set of equations

$$\begin{aligned} \frac{\mathrm{d}^2\mathbf{r}_i}{\mathrm{d}t^2} &= \frac{\mathrm{d}\mathbf{v}_i}{\mathrm{d}t} = \mathbf{F}_i = \sum_{i\neq j}(\mathbf{F}_{ij}^C + \mathbf{F}_{ij}^D + \mathbf{F}_{ij}^R) + \mathbf{F}_i^{ext}, \\ \frac{\mathrm{d}C_i}{\mathrm{d}t} &= Q_i = \sum_{i\neq j}(Q_{ij}^D + Q_{ij}^R) + Q_i^S, \end{aligned} \tag{5.144}$$

where t, $\mathbf{r}_i$, $\mathbf{v}_i$ and $\mathbf{F}_i$ denote time, and position, velocity, force vectors, respectively. $\mathbf{F}_i^{ext}$ is the force on particle i from an external force field. Just as in the standard DPD model, the pairwise interaction between tDPD particles i and j consists of the conservative force $\mathbf{F}_{ij}^C = a_{ij}w_C(r_{ij})\mathbf{e}_{ij}$, dissipative force $\mathbf{F}_{ij}^D = -\gamma_{ij}w_D(r_{ij})(\mathbf{e}_{ij} \cdot \mathbf{v}_{ij})\mathbf{e}_{ij}$ and random force $\mathbf{F}_{ij}^R = \sigma_{ij}w_R(r_{ij})\xi_{ij}\mathbf{e}_{ij}$. C_i represents the concentration of one species defined as the number of a chemical species carried by a tDPD particle i and Q_i the corresponding concentration flux. The total concentration flux on a particle i accounts for the Fickian flux Q_{ij}^D, the random flux Q_{ij}^R and a source term Q_{ij}^S due to chemical reactions. Since tDPD particles have unit mass, this definition of concentration is equivalent to the concentration in terms of chemical species per unit mass. Then, the volume concentration, i.e. chemical species per unit volume, is ρC_i where ρ is the number density of tDPD particles. We note that C_i can be a vector $\mathbf{C}_i$ containing N components i.e. $\{C_1, C_2, \ldots, C_N\}_i$ when N chemical species are considered.

The driving force for diffusion of each species is the gradient of chemical potential $Q = -DC\nabla\mu/RT$ in which D is the diffusion coefficient, R the universal gas constant, T the absolute temperature and μ the chemical potential given by $\mu = \mu_0 + RT \ln C$ for dilute solutions [83]. By substituting the chemical potential into the expression of driving force, we find that the diffusion driving force is proportional to the concentration gradient ∇C, which corresponds to a concentration difference between two neighboring tDPD particles. It follows that the Fickian flux

Q_{ij}^D and random flux Q_{ij}^R in the tDPD model are given by

$$Q_{ij}^D = -\kappa_{ij} w_{DC}(r_{ij}) \left(C_i - C_j \right), \tag{5.145a}$$

$$Q_{ij}^R = \epsilon_{ij} w_{RC}(r_{ij}) \xi_{ij}, \tag{5.145b}$$

where κ_{ij} and ϵ_{ij} determine the strength of the Fickian and random fluxes, and ξ_{ij} is the Gaussian white noise [26]. $w_{DC}(r)$ and $w_{RC}(r)$ are weight functions with a cutoff radius r_{cc}. The Fickian friction parameter κ plays the analogous role for concentration differences between tDPD particles as γ does for momentum. In general, the concentration friction κ is a $N \times N$ matrix when the interdiffusivities of N different chemical species are involved. However, considering N chemical species in dilute solution and neglecting the interdiffusivities of different species, the system is then reduced to a set of uncoupled diffusion equations with independent diffusivities between species, and hence κ becomes a diagonal matrix [8].

By applying the local-equilibrium assumption to the tDPD system, the random term Q_{ij}^R is related to the dissipative term Q_{ij}^D by satisfying the fluctuation-dissipation theorem [66, 83]

$$\epsilon_{ij}^2 = m_s^2 \kappa_{ij} \rho (C_i + C_j), \quad w_{DC}(r_{ij}) = w_{RC}^2(r_{ij}), \tag{5.146}$$

where m_s the mass of a single solute molecule, C_i and C_j are the concentrations on particle i and j, respectively. For detailed derivations for obtaining Eq. (5.146), readers are referred to [66]. In general, the mass of a single solute molecule m_s is much smaller than the mass of a tDPD particle m, which is chosen as mass unit. Consequently, the magnitude of ϵ is small at $m_s \ll m$, which indicates that the contribution of the random flux Q_{ij}^R to the total diffusion coefficient D is negligible unless m_s becomes comparable to m in nanoscale systems.

The macroscopic properties including viscosity and diffusivity of a tDPD system are output properties rather than input parameters. Since the stochastic forces on tDPD particles yield random movements, the effective diffusion coefficient D is the result of contributions from the random diffusion D^ξ and the Fickian diffusion D^F. In general, the random contribution D^ξ is a combined result of the random movements of tDPD particles and random flux Q_{ij}^R in Eq. (5.145b). However, the variance of random flux Q_{ij}^R has a small prefactor m_s^2 as given by Eq. (5.146). In practical applications, the contribution of the random flux Q_{ij}^R to D^ξ is negligible, which has been confirmed by Kordilla et al. [45] Thus, in the mathematical derivations in this section, we consider that D^ξ is due to the random movements of tDPD particles. In particular, for a tDPD system in thermal equilibrium, the diffusion coefficient D^ξ induced by the random movements of tDPD particles can be calculated by Groot and Warren [35]

$$D^\xi = \frac{3k_BT}{4\pi\gamma\rho \cdot \int_0^{r_c} r^2 w_D(r) g(r) dr}, \tag{5.147}$$

where r_c is the cutoff radius for forces. Also, the macroscopic diffusion coefficient D^F due to the Fickian flux can be computed by Mackie et al. [74]

$$D^F = \frac{2\pi\kappa\rho}{3}\int_0^{r_{cc}} r^4 w_{DC}(r)g(r)dr, \tag{5.148}$$

in which κ is the Fickian friction coefficient and r_{cc} is the cutoff radius for concentration flux. Let $w_D(r) = (1 - r/r_c)^{s_1}$ and $w_{DC}(r) = (1 - r/r_{cc})^{s_2}$ be the weight functions of the dissipative force $\mathbf{F}_{ij}^D$ and of the Fickian flux Q_{ij}^D, respectively. When the radial distribution function of ideal gas $g(r) = 1.0$ is employed, both D^ξ and D^F can be evaluated analytically

$$\begin{aligned} D =& D^\xi + D^F \\ =& \frac{3k_BT(s_1+1)(s_1+2)(s_1+3)}{8\pi\gamma\rho r_c^3} \\ &+ \frac{16\pi\kappa\rho r_{cc}^5}{(s_2+1)(s_2+2)(s_2+3)(s_2+4)(s_2+5)}, \end{aligned} \tag{5.149}$$

where s_1 and s_2 are the exponents of $w_D(r)$ and $w_{DC}(r)$. Equation (5.149) provides a relationship between the macroscopic effective diffusion coefficient D (which can be experimentally measured) and parameters in the tDPD model. Equation (5.149) indicates that the effective diffusion coefficient D is a linear function of the parameter κ, and the minimum value of the effective diffusion coefficient $D_{\min} = D^\xi$ is obtained at $\kappa = 0$. Since the radial distribution function $g(r) = 1$ corresponding to the ideal gas is used, Eq. (5.149) provides a rough prediction of the effective diffusion coefficient D. The accurate value of D can only be obtained by computations in tDPD simulations.

Li et al. [66] proposed a numerical diffusivity benchmark to compute the accurate value of D of tDPD systems, which shares the same strategy of reverse Poiseuille flow as a numerical viscometer [7] and computation of the thermal conductivity in eDPD [62]. For a tDPD fluid with constant diffusion coefficient, the ADR equation is given by $dC/dt = D\nabla^2 C + Q^S$ where D is the diffusion coefficient and Q^S a source term. For steady state problems, the ADR equation is simplified to $D\nabla^2 C = -Q^S$, which is the same as the governing equation of Poiseuille flow driven by a body force $\upsilon\nabla^2\mathbf{V} = -g$. To obtain the accurate value of the effective diffusion coefficient, one needs to perform a tDPD simulation in a computational domain with periodic boundary conditions. Let $z = 0$ be a plane subdividing the fluid system into two equal domains in z-direction. A small concentration source $+Q^S$ is applied in the domain of $z > 0$ while a concentration sink with same magnitude $-Q^S$ is applied in the other domain $z < 0$, as shown in Fig. 5.7a. Because of the periodic boundary conditions, the concentration of the tDPD fluid is constrained to be invariable at the plane $z = 0$. When the diffusion coefficient D is constant, the steady state solution

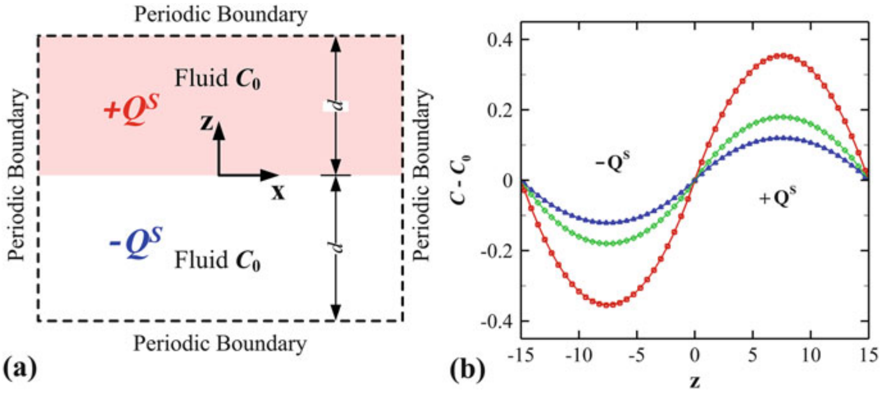

Fig. 5.7 (**a**) Schematic geometry for the numerical diffusivity meter using fully periodic boundary conditions. (**b**) Concentration profiles obtained by running tDPD simulations for different Fickian friction coefficients κ. (**b**) is adapted with permission from [66]

of the concentration profile is given by

$$C(z) = \frac{Q^S z}{2D}(d - |z|) + C_0, \tag{5.150}$$

where Q^S is the source term, C_0 the initial concentration of the tDPD system, and d the half length of the computational domain in z-direction. The concentration profiles can be easily obtained by running the tDPD simulation to the steady state. Figure 5.7b shows the concentration profiles obtained from tDPD simulations for different Fickian friction coefficients κ, in which the lines are the best-fitting parabolas for each case. Then, the effective diffusion coefficient can be determined by fitting the concentration profile with the analytical solution given by Eq. (5.150). It is obvious that the effective diffusion coefficient D can be significantly changed by varying the Fickian friction coefficient κ.

Boundary conditions are crucial for the investigation of diffusion-reaction processes in wall-bounded systems. Usually, defining stationary particles to represent solid objects is a common treatment in classical DPD simulations [108]. However, those solid walls made up by discrete frozen particles induce unwanted temperature and density fluctuations in the vicinity of the walls [90]. Alternatively, Li et al. [66] used effective boundary fluxes to impose Dirichlet and Neumann boundary conditions for concentration in the tDPD systems.

Dirichlet Boundary Condition

Since the fluid particles do not penetrate into wall boundaries, the random movements of fluid particles do not have any contributions to the boundary concentration flux. Therefore, the effective boundary concentration flux is induced only by the Fickian flux. For a fluid particle i in the vicinity of a wall boundary, the effective Fickian concentration flux on particle i from the wall can be calculated [66] by

$$
\begin{aligned}
Q_{D,i}^{W}(h) &= 2\pi\rho \int_{z=h}^{r_{cc}} \int_{x=0}^{\sqrt{{r_{cc}}^2-z^2}} Q^{D}(r)g(r)xdxdz \\
&= 2\pi\rho \int_{z=h}^{r_{cc}} \int_{x=0}^{\sqrt{{r_{cc}}^2-z^2}} -\kappa \cdot w_{DC}(r) \cdot \frac{z}{h}(C_i - C_w) \cdot g(r)xdxdz \\
&= 2\pi\rho\kappa\, (C_w - C_i) \cdot \varphi(h),
\end{aligned}
\tag{5.151}
$$

where C_i is the concentration of particle i, C_w the expected concentration at the wall surface, and h the distance of the particle i away from the wall surface. Here, $\varphi(h)$ is a function of h, which is defined as

$$
\varphi(h) = \int_{z=h}^{r_{cc}} \int_{x=0}^{\sqrt{{r_{cc}}^2-z^2}} w_{DC}(r)g(r)\frac{zx}{h} \cdot dx \cdot dz. \tag{5.152}
$$

Equation (5.151) reveals that the boundary concentration flux is determined by the concentration difference between particle i and the wall, and also their distance. Given a radial distribution function $g(r)$ and the weight function $w_{DC}(r)$, the function $\varphi(h)$ can be evaluated through Eq. (5.152). As the distance h approaches to zero, the magnitude of $\varphi(h)$ goes to infinity. In practical tDPD simulations, a truncation of $\varphi(h)$ at small distances can be used to stabilize the simulation, i.e., setting $\varphi(h < 0.01r_{cc}) = \varphi(0.01r_{cc})$.

Neumann Boundary Condition

To consider the effective flux along the normal direction of wall surface, we integrate the effect of concentration flux from the wall boundary and define a distance dependent function given by

$$
\Phi(h) = \int_{z=h}^{r_{cc}} \int_{x=0}^{\sqrt{{r_{cc}}^2-z^2}} w_{DC}(r)g(r)\frac{zx}{r}dxdz. \tag{5.153}
$$

The normalized $\Phi(h)$ is defined as $\overline{\Phi}(h) = \Phi(h)/\int_0^{r_{cc}} \Phi(x)dx$. Then, the integral of $\overline{\Phi}(h)$ is equal to one. Using the computed $g(r)$ and the expression of $w_{DC}(r)$, the function $\overline{\Phi}(h)$ can be obtained through Eq. (5.153). To impose a Neumann boundary condition $dC/dn = \Lambda$ at a wall boundary, it is equivalent to applying a concentration flux $Q^W = D\Lambda$ across the boundary. In practice, the flux Q^W is distributed onto the fluid particles in the vicinity of the wall weighted by $\overline{\Phi}(h)$. Let ρ be the number density of the fluid particles, the volume concentration is ρC

because the concentration C in tDPD is defined as the number of a chemical species per particle. Then, any fluid particle i close to the wall receives a concentration flux from the wall boundary given by

$$Q_i^W(h) = D\Lambda\rho \cdot \overline{\Phi}(h). \tag{5.154}$$

One-dimensional test cases have been performed in [66] to check the effectiveness and the accuracy of using the effective boundary fluxes for implementation of the Dirichlet and Neumann boundary conditions. Figure 5.8(a1) illustrates the initial condition $C(x, 0) = 0$ and the boundary conditions for the test case of the Dirichlet boundary condition. By solving a one-dimensional diffusion equation $dC/dt = D\nabla^2 C$ with boundary conditions of $C(0, t) = 0$ and $C(L_x, t) = C_0$, an analytical solution for the transient concentration profile can be obtained [66]

$$C(x, t) = \frac{C_0 x}{L_x} + \sum_{n=1}^{\infty} \frac{2C_0}{n\pi}(-1)^n \sin(\beta_n x) \exp\left(-D\beta_n^2 t\right), \tag{5.155}$$

where $\beta_n = n\pi/L_x$ with L_x being the length of the computational domain in the x-direction, D the diffusion coefficient. Figure 5.8(b1) shows a comparison between the concentration profiles obtained using tDPD and theoretical solution Eq. (5.155) at several times including the steady state solution. The results are in good agreement, which validates the effective boundary flux of Eq. (5.151) for imposing the correct Dirichlet boundary condition in the tDPD simulation.

Figure 5.8(a2) shows a similar setup as the previous test case but different wall boundary conditions for the Neumann boundary condition. Considering a

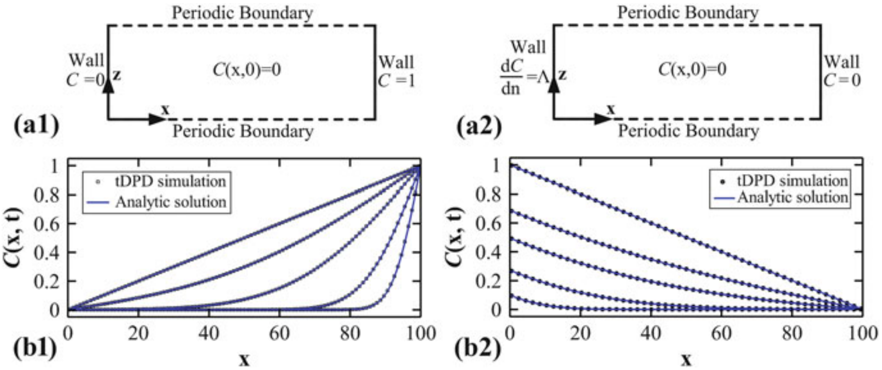

Fig. 5.8 Initial condition and boundary conditions for the one-dimensional diffusion with (**a1**) the Dirichlet boundary condition and (**a2**) the Neumann boundary condition. The corresponding transient concentration profiles and comparison with theoretical solutions are shown in (**b1**) and (**b2**). These plots are adapted with permission from [66]

concentration flux at the left wall $x = 0$, we apply the a Neumann boundary condition $dC/dn = \Lambda$ at $x = 0$. Also, the right wall at $x = L_x$ has a fixed concentration $C(100, t) = 0$. By solving a one-dimensional diffusion equation $dC/dt = D\nabla^2 C$ with boundary conditions of $dC(0, t)/dx = \Lambda$ and $C(L_x, t) = 0$, we have the theoretical solution for the transient concentration profile given by Li et al. [66]

$$C(x, t) = \Lambda(x - L_x) + \frac{4\Lambda}{L_x} \sum_{n=1,\mathrm{odd}}^{\infty} \beta_n^{-2} \sin^2\left(\frac{n\pi}{4}\right) \cos\left(\beta_n x\right) \exp\left(-D\beta_n^2 t\right), \tag{5.156}$$

where $\beta_n = n\pi/(2L_x)$ with L_x being the length of the computational domain in the x-direction, D the diffusion coefficient. Figure 5.8(b2) compares the transient concentration profiles obtained using tDPD with the theoretical solution Eq. (5.156). The excellent agreement between the tDPD results and the theoretical solution confirms the validity of the effective boundary flux of Eq. (5.154) for imposing the correct Neumann boundary condition.

The particle-based tDPD method satisfies the conservation of concentration automatically and provides an economical way to solve ADR equations with a large number of species. It has been reported [66] that the tDPD solution of a 25-species coagulation model is only twice as computationally expensive as the conventional DPD simulation of hydrodynamics alone, unlike the continuum model requiring more than 20 Poisson/Helmholtz solvers making the computational cost over ten times higher than the Navier-Stokes solver. This low additional cost for solving ADR equations indicates the promising potential of tDPD in biological applications involving multiple biochemical species at the mesoscale.

5.3.4 *Other Extensions*

In addition to eDPD, mDPD and tDPD models, there are some other extensions of DPD developed for different purposes. Examples include:

1. Fluid particle model (FPM): It is a generalization of the classical DPD method developed by Español [24]. FPM considers both linear and angular momenta of the particles and includes both central and noncentral forces between particles, while the classical DPD method considers only linear momentum and includes only central forces. By introducing torques and angular velocities of the particles, both linear and angular momenta of FPM are conserved.
2. Single-particle DPD model: It is based on FPM with modified colloid-solvent pairwise potentials [86]. In this model, each spherical colloidal particle can be represented by a single FPM particle rather than a cluster of particles. As a result,

it shows high computational efficiency in studying the dynamical and rheological properties of colloidal suspensions in simple fluid solvents.

3. Anisotropic single-particle DPD model (aDPD): It is a further development of the single-particle DPD model [20]. By introducing a shape matrix indicating the particle size and shape, aDPD formulates the conservative and dissipative interactions between anisotropic DPD particles using a linear mapping from the original single-particle DPD model of isotropic spherical particles, while the random forces are properly formulated by satisfying the fluctuation-dissipation theorem. Consequently, aDPD enables the DPD method to efficiently model the colloidal ellipsoids under the effect of thermal fluctuation. Examples include the orientation-dependent diffusion of an anisotropic particle, and the isotropic-nematic transition in an ellipsoidal suspension induced by the changes of volume fraction or the aspect ratio of ellipsoid particles.
4. Charged DPD model (cDPD): It was developed by Deng et al. [19] based on tDPD for simulating mesoscopic electrokinetic phenomena governed by the stochastic Poisson-Nernst-Planck and the Navier-Stokes equations. By introducing extra degrees of freedom for the ionic concentration and the electrostatic potential associated with each DPD particle, cDPD models the diffusion of ionic species driven by the ionic concentration gradient, electrostatic potential gradient and thermal fluctuations through pairwise fluxes between DPD particles, while the electrostatic potential is obtained by solving the Poisson equation on the moving DPD particles iteratively at each time-step. Since both the fluctuations of momentum and ionic concentration are systematically included in cDPD without any grid-based algorithms, it is a flexible and powerful method in studying complex fluids with electrostatic interactions at the micro- and nano-scales.
5. Smoothed DPD (SDPD) model: It is a top-down approach [25] developed from smoothed particle hydrodynamics (SPH). SDPD starts from continuum equations while other DPD models are bottom-up approaches starting from microscopic dynamics. As a matter of fact, SDPD is a Lagrangian discrete model for simulating Navier-Stokes hydrodynamics that includes thermal fluctuations consistently. Unlike these bottom-up DPD methods, the parameters in the governing equations of SDPD have clear physical meanings. Its inputs are the viscosity, equation of state, temperature and other parameters required by the fluctuating Navier-Stokes equations. However, since the constitutive equations and macroscale properties of the system must be given as inputs, SDPD works well with simple fluids but loses its effectiveness in modeling complex fluids and materials, which may not have a known constitutive equation.

Motivated by tackling different challenges in the mesoscopic modeling, the various extensions of DPD have been developed and constitute the “DPD Alphabet”, as shown in Fig. 5.2. These new developed DPD models dramatically extend the capability of the DPD simulations beyond the classical DPD, which makes DPD a more promising mesoscopic method for diverse applications.

5.4 Computer Implementation

A DPD program shares the structure with an atomistic molecular dynamics simulator, and iterates over a time stepping loop consists of four stages: force evaluation, position/velocity update, parallel communication, and data collection.

5.4.1 Pairwise Search

Due to the short-range nature of the DPD pairwise force, the evaluation is usually assisted with the use of a spatial searching algorithm, which loops over all pairs of particles that are within the cutoff distance r_c. One of the classical approaches used by the most DPD software, as well as many other existing MD software, is to use a Verlet list, which is essentially a table storing the indices of particles within a given distance r_v for each particle in the system. r_v is usually chosen to be slightly larger than r_c such that the list does not need to be updated for every time step. As a trade-off the list will contain some extra particles which are not within r_c.

The Verlet list can be constructed naively by a $O(N^2)$ pairwise search, but more efficiently with the help of a cell list. The cell list algorithm makes use of a uniform lattice to partition the system into many nearly-cubic cells, and stores the indices of the particles that are located within each cell. The cells are numbered consecutively along the axes, allowing the index of cell that each particle belongs to be determined by simply dividing the particle's coordinate by the length of the cells and then flooring to the nearest integer.

Given a system of N particles occupying a volume of $L_x \times L_y \times L_z$, a Verlet list can be constructed from a cell list using $O(N)$ time and storage by looping over each particle, first finding the cell that the particle belongs to, and then comparing against other particles in this cell as well as particles in all 26 immediate neighboring cells. The cell list itself takes $O(L_x L_y L_z + N)$ storage and $O(N)$ time to construct as shown by Algorithm 1. Alternatively, the cell list can be used directly for computing the pairwise force [97] and may delivery better performance on massively parallel processors where memory bandwidth is more precious than computing power.

5.4.2 Force Computation

The conservative force is usually defined directly using a weight function, or through the differentiation of a potential function. The computation of the conservative force is relatively straightforward because it only affects static properties such as radial distribution function and compressibility. In fact, several splitting integration schemes evaluate the dissipative and random force separately from the conservative force.

Algorithm 1 The cell list algorithm

```
Method RectilinearCelllist( Np: integer,
                            ncell: integer[3],
                            cell_size: integer[3],
                            coord: real[N][3] )
  Ncell     = ncell[0] * ncell[1] * ncell[2]
  bin_size  = zeros[Ncell] # O(L^3) space
  local_seq = integer[N]   # O(N)   space
  cid       = integer[N]   # O(N)   space

  # Get cell id and cell-local index for each particle
  # Count cell size
  for i = 0:N
    # operator ./: element-wise division
    cell_xyz = floor( coord[i] ./ cell_size )
    cid[i] = cell_xyz[0] + cell_xyz[1] * ncell[0] + cell_xyz[2] * ncell[1] *
     ncell[2]
    local_seq[i] = bin_size[ cid[i] ]
    ++bin_size[ cid[i] ]

  # O(N) prefix sum for the starting index of each cell
  bin_start = zeros[Ncell] # O(L^3) space
  for i = 1:Ncell
    bin_start[i] = bin_start[i-1] + bin_size[i-1]

  # Scatter particle indices into corresponding cell
  cell_list = integer[N]  # O(N) space
  for i = 0:N
    cell_list[ bin_start[ cid[i] ] + local_seq[i] ] = i

  return cell_list, bin_start
```

The dissipative force is usually evaluated together with the random force, due to the common arithmetics for computing the weight function as dictated by the fluctuation-dissipative theorem. However, the most prevalent and convenient approach is to still evaluate the dissipative and random force alongside the conservative force, because this saves the work for the pairwise searching, a dominant workload in DPD simulations.

It is a common practice in molecular dynamics simulation to omit the pairwise interactions between particles that are connected by bonds. For example, in the CHARMM force field the pairwise interaction between atoms separated by less than three bonds are not computed, because the interaction is assumed to be already considered by the bonded potential. The same principle could be applied to DPD, but a careful consideration must be made on whether to also exclude the dissipative and random terms. The decision to include the dissipative and random force can be justified by noting that the conservative bonded force may only serve the role of the DPD conservative force. The friction and random effects thus are still needed between particles that are bonded, but may be based on different weight functions or coefficients.

The random force in DPD need to be handled carefully for distributed-memory parallelization, which is usually done with a domain decomposition scheme that divides the simulation box into non-overlapping subregions. The force on particles within each subregion can be computed locally on each processor. The force between subregions can be computed with the help of *ghost* particles, which are the local images of remote particles from neighboring processors that are within the cutoff of each subregion. A *forward* communication is responsible for the exchange of the ghost particles. A *backward* communication process is necessary if we are to take advantage of the Newton's 3rd law of action and reaction, which is widely used in serial DPD programs to speed up the force computation. The extra communication stages may actually compromise parallel efficiency on massively parallel clusters due to the overhead for sending and synchronizing over the messages. The computation for pairwise interactions across subregions can be duplicated in order to eliminate the *backward* communication stage. This overhead does not incur network communication and should be negligible as long as the area-to-volume ratio of the subregion remains reasonably large. However, the random term need to be handled carefully in this case because the reproduction of the same random number between the a pair of particles spanning two processors is necessary to ensure momentum conservation. This is usually handled by using a stateless random number generator that crunches in situ a global random variable, which changes over time steps but remains the same across all processors within a time step, with some per-particle signature that is persistent on each particle [2, 89, 101]. As long as the same signature is presented, the same random number can be recovered for each of the particles on two different processors. A common choice for the signature is the *id* of the particle. Alternatively, the signature may be computed from a blend of the highly volatile bits of the particles' degrees of freedom such as position and velocity, which serves as a source of entropy.

5.4.3 Numerical Optimization

In [26], the random numbers between pairs of particles are assumed to be delta-correlated, symmetric Gaussian *i.i.d.* random variables with zero mean and unit variance. However, the generation of Gaussian random numbers is less straightforward and more expensive, despite the existence of highly efficient algorithms such as the Box-Muller method. The non-compact nature of the Gaussian distribution makes it possible for extremely large forces to occur regardless of magnitude. This can cause numerical instability in practice and hence requires treatment such as re-generation or truncation. However, due to the law of large numbers, any random variable with the same mean and variance could lead to the same stochastic differential equation for DPD and thus can lead to the same invariant distribution indistinguishable from that driven by a Gaussian term. This observation liberates us to use much cheaper random number generators, e.g. one that generates numbers uniformly distributed on $[-\sqrt{3}, \sqrt{3})$. Other possibilities include the arcsin distribution on $[-\sqrt{2}, \sqrt{2})$, which can be generated using the logistic map with only floating point operations. This fits better to the architectural characteristics of general purpose graphics processing units with less integer arithmetic throughput.

An effective approach to achieve high Schmidt number in DPD simulation is to increase the power s of the dissipative weight function $w_D(r_{ij}) = (1 - r_{ij}/r_c)^s$ in Eq. (5.2). If the power is non-integral, a general transcendental function that evaluates the result of w^s is needed. This function is among one of the slowest math functions in every programming language, because it has to be evaluated as $w^s = e^{s \cdot \ln w}$ using the identity $x = e^{\ln x}$, and in turn involves the evaluation of the natural logarithm and exponential function. In order to conform to the IEEE floating point standard, a generic implementation of the functions as provided in most programming languages has to deal with the full range of inputs as well as possible exceptions, which triggers instruction branching and reduced CPU efficiency. The process, however, can be sped up by exploiting the limited range of the weight function and the power. The possibility that the base or the exponent being 0 can be precluded by the cutoff testing prior to the function call; it is also unlikely that the base or the exponent would be NaN or Inf unless there are serious problems in the underlying physics of the model. As such, both the logarithm and exponential component of the power function can be implemented using a Chebyshev polynomial expansion with accuracy up to the last digit of the floating point number [101].

5.4.4 Time Integration

The velocity Verlet (VV) algorithm is the most commonly used algorithm for integrating DPD systems due to their symplecticity, numerical stability, and ease of implementation. It integrates position using half-step values of velocity. The form most frequently used in molecular dynamics simulations is:

$$\begin{aligned}
v(t + \frac{\Delta t}{2}) &= v(t) + \frac{\Delta t}{2} t \cdot a(t), \\
r(t + \Delta t) &= r(t) + \Delta t \cdot v(t + \frac{\Delta t}{2}), \\
a(t + \Delta t) &= F(r(t + \Delta t)), \\
v(t + \Delta t) &= v(t + \frac{\Delta t}{2}) + \frac{\Delta t}{2} \cdot a(t + \Delta t).
\end{aligned} \tag{5.157}$$

However, due to the dependence of the dissipative force on particle velocity, the scheme in DPD is of the form:

$$
\begin{aligned}
v(t+\frac{\Delta t}{2}) &= v(t) + \frac{\Delta t}{2} t \cdot a(t),\\
r(t+\Delta t) &= r(t) + \Delta t \cdot v(t+\frac{\Delta t}{2}),\\
a(t+\Delta t) &= F\Big[r(t+\Delta t), v(t+\frac{\Delta t}{2})\Big],\\
v(t+\Delta t) &= v(t+\frac{\Delta t}{2}) + \frac{\Delta t}{2} \cdot a(t+\Delta t).
\end{aligned}
\tag{5.158}
$$

There is a temporal misalignment between the position and velocity used for the force. As such, the modified velocity Verlet algorithm aims to improve the stability of the integrator by using an extrapolated version of the velocity for the force evaluation [35]:

$$
\begin{aligned}
v(t+\frac{\Delta t}{2}) &= v(t) + \frac{\Delta t}{2} t \cdot a(t),\\
r(t+\Delta t) &= r(t) + \Delta t \cdot v(t+\frac{\Delta t}{2}),\\
a(t+\Delta t) &= F\Big[r(t+\Delta t), v(t) + \lambda \cdot \Delta t \cdot a(t)\Big],\\
v(t+\Delta t) &= v(t+\frac{\Delta t}{2}) + \frac{\Delta t}{2} \cdot a(t+\Delta t),
\end{aligned}
\tag{5.159}
$$

where $\lambda \in [0, 1]$ is a parameter that depends on the specific choice of DPD parameter, and need to be tuned case-by-case. There also exist more advanced time integrators that are based on iterative or splitting techniques, such as DPD-VV [9], Shardlow splitting scheme [99], the pairwise Noose-Hoover-Langevin method [53], and the pairwise adaptive Langevin method [54].

5.5 Applications

The DPD method was invented more than two decades ago for simulating complex fluids at the mesoscale [39]. Ever since its inception, DPD modeling has found a wide spectrum of applications including simple fluids hydrodynamics, polymer solutions and melts, biological membranes, colloidal suspensions and blood flow [34, 72]. This section will briefly introduce a few examples of DPD applications.

5.5.1 Single-Phase Fluid Flow

DPD provides the correct hydrodynamic behavior of fluids at the mesoscale, which is of fundamental importance for particles in flow and colloidal/polymer suspensions. In the following, we briefly introduce the implementation of boundary conditions for wall-bounded flows in DPD, and present two examples of single-phase fluid flow.

No-Slip Boundary Condition in DPD

In fluid dynamics, the tangential component of the fluid velocity at the solid boundary is always equal to that of the solid boundary, thus, the no-slip boundary condition is usually used in modeling of wall-bounded flows. When one performs DPD simulation of Couette flow or Poiseuille flow in a microchannel or microtube, the soft repulsion between two particles cannot prevent fluid particles from penetrating solid boundaries, and thus extra effort is required to impose the no-slip boundary condition.

To impose a wall boundary condition in DPD, layers of particles at the solid walls are usually frozen (velocity of these particles are set to zero) to model solid walls. To prevent the penetration of fluid particles into the solid walls, a proper reflection, such as bounce-back reflection, specular reflection, or Maxwellian reflection, at the fluid-solid interface are usually implemented. In order to enforce the no-slip boundary condition at the fluid–solid interface, the DPD repulsive forces from wall particles are adjusted appropriately according to the wall density n_w [90],

$$F^W = a_e \left(0.0303 n_w^2 + 0.5617 n_w - 0.8536\right). \tag{5.160}$$

In this implementation, the average force acting on the DPD particles from the solid wall in the near-wall region is equal to the average force from the fluid.

In addition, interaction of liquids with solid walls causes layering of the fluid, which is responsible for the large density fluctuations near the wall. These fluctuations are physical and thus desirable in simulations, but they may be erroneous in some other simulations; for example, spurious density fluctuations have been observed in particle systems such as stochastic rotational dynamics, MD and DPD simulations. Thus, one needs to control the density fluctuations in wall-bounded DPD systems.

An adaptive boundary condition (ABC) [91] has been developed and applied to fluid particles in the vicinity of the walls in order to control fluid density fluctuations near the solid walls. In the ABC method, the magnitude of the adaptive force, $F^W(i_b)$, depends on the distance of the fluid particles to the solid walls and is update simultaneously during the simulations according to the estimated density fluctuations,

$$F^W_{\text{new}}(i_b) = F^W_{\text{old}}(i_b) + C_W\left(\frac{\sum_{i=i_a}^{i_b}\rho_s(i)}{\sum_{i=i_a}^{i_b}\rho_d(i)} - 1\right), \tag{5.161}$$

where C_W is a weighting factor.

The no-slip boundary condition in shear flow can also be implemented by numerical periodicity, such as the use of Lees–Edwards boundary conditions [47]. Instead of including physical wall boundary, Lees and Edwards [47] proposed a simple and ingenious modification to the standard periodic boundary condition for particle-based simulations of shear flow. In particular, particles is considered as being embedded in a fluid which has a constant velocity gradient to maintain the system under a shear stress in a steady state. Once a particle leaves the simulation box in the direction parallel to the velocity gradient, it will be reintroduced into the box from the opposite boundary with a displacement and a velocity shift in the flow direction. Although the Lees–Edwards boundary conditions have been successfully used in many MD and DPD simulations [3, 87], it can only be applied to fluid systems in steady states with constant shear rates.

Couette Flow

In fluid dynamics, Couette flow is a simple shear flow of a viscous fluid between two parallel walls, one of which is moving relative to the other. The constitutive relation for Couette flow can be expressed as,

$$\tau_{yx} = -\mu\frac{du}{dy}, \tag{5.162}$$

where τ_{yx} is the shear stress, and du/dy is the velocity gradient in the y direction, and μ the dynamic viscosity. In DPD, the friction between the fluid and the moving wall particles causes the fluid to shear. Figure 5.9a shows the simulation results of transient development to the steady-state Couette flow. The DPD results agree well with the analytical solution for different times. A notable aspect of this simple shear flow is that the shear stress is constant throughout the flow domain. Thus, Couette flow is frequently used to measure the viscosity of a fluid.

Poiseuille Flow

Poiseuille flow is a steady viscous fluid flow driven by an effective pressure gradient established between the two ends of a long duct, usually a pipe, of uniform circular cross-section. For a fluid flow through a pipe of radius R and length L, in the presence of a uniform pressure gradient $\Delta P/L$, the velocity of the fluid at a specified

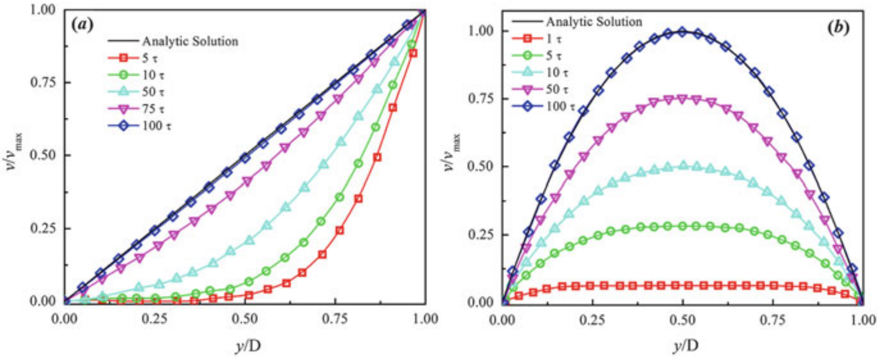

Fig. 5.9 Time evolution of the velocity profiles in (**a**) Couette and (**b**) Poiseuille flows, in which τ denotes the DPD time unit

distance r from the center of the pipe, v(r), is given by,

$$v(r) = \frac{\Delta P}{4L\eta}(R^2 - r^2), \tag{5.163}$$

in which η is the fluid viscosity. In DPD, Poiseuille flow can be obtained by applying a body force to the DPD fluid. Figure 5.9b shows the simulation results of development of Poiseuille flow. The fluid velocity in a pipe changes from zero at the wall surface because of the no-slip condition to a maximum v_{max} at the pipe center.

In DPD modeling of Poiseuille flow, it is also worth to mention the periodic (or reverse) Poiseuille flow method developed by Backer et al. [7], which is also commonly used to estimate the viscosity of the DPD fluid. The method produces counter-flowing Poiseuille flows by uniform body forces in opposite directions along two-halves of a computational domain. The absence of density artifacts makes this method useful for studying the bulk Poiseuille flow.

5.5.2 Blood Flow

Blood is a complex fluid exhibiting intriguing dynamic and its rheology depends on the flowrate and volume fraction of suspending particles especially the red blood cells (RBCs). In recent years, particle-based RBC models have attracted increasing attention in multiscale modeling of blood flows. In particle-based approaches, the motion of particles is flow governed by the interactions between discrete particles. Early attempts focused on simulating blood flow with RBC being an elastic particle, whose inner skeleton is represented by a rectangular lattice connected by elastic springs. More recently, DPD was employed in a systematic coarse-grained procedure for modeling RBCs [92], which served as a basis of a general multiscale RBC (MS-RBC) model that included membrane viscosity and external/internal fluid viscosity contrast [28]. In the MS-RBC model, the membrane of RBC is represented by a two-dimensional triangulated network with a collection of DPD particles, while constraints on the area and volume conservation of RBC are imposed to mimic the area–preserving lipid bilayer and the incompressible interior fluid. Specifically, the elastic part of bond is represented by

$$V_s = \sum_{j \in 1 \ldots N_s} \left[\frac{k_B T l_m (3x_j^2 - 2x_j^3)}{4p(1 - x_j)} + \frac{k_p}{(n-1) l_j^{n-1}} \right], \tag{5.164}$$

where l_j is the length of the spring j, l_m is the maximum spring extension, $x_j = l_j / l_m$, p is the persistence length, $k_B T$ is the energy unit, k_p is the spring constant, and n is a specified exponent. The membrane viscosity is imposed by introducing a viscous force on each spring. The bending resistance of the RBC membrane is modeled by

$$V_b = \sum_{j \in 1 \ldots N_s} k_b \left[1 - cos(\theta_j - \theta_0) \right], \tag{5.165}$$

in which k_b is the bending constant, θ_j is the instantaneous angle between two adjacent triangles having the common edge j, and θ_0 is the spontaneous angle. In addition, the RBC model includes the area and volume conservation constraints, which mimic the area-incompressibility of the lipid bilayer and the incompressibility of the interior fluid, respectively. The corresponding energy is given by

$$V_{a+v} = \sum_{j \in 1 \ldots N_t} \frac{k_d (A_j - A_0)^2}{2A_0} + \frac{k_a (A - A_0^{tot})^2}{2A_0^{tot}} + \frac{k_v (V - V_0^{tot})^2}{2V_0^{tot}}, \tag{5.166}$$

where N_t is the number of triangles in the membrane network, A_0 is the triangle area, and k_d, k_a and k_v are the local area, global area and volume constraint coefficients, respectively. The terms A_0^{tot} and V_0^{tot} are the specified total area and volume, respectively.

The MS-RBC model is multiscale, as the RBC can be represented on the spectrin level, where each spring in the network corresponds to a single spectrin tetramer with the equilibrium distance between two neighboring actin connections of ∼75 nm. On the other hand, for more efficient computation, the RBC network can also be highly coarse-grained with the equilibrium spring lengths of up to 500 ∼ 600 nm. The RBC membrane interacts with the fluid particles through DPD forces, and the temperature of the system is controlled through the DPD thermostat. The internal and external fluids are modelled by collections of free DPD particles and their separation is enforced by bounce-back reflections of these particles at the RBC membrane surface. The MS-RBC has been successfully applied in RBC simulations, such as RBC dynamics in Poiseuille flow [28], RBC thermal fluctuations [29] and RBCs in diseases like malaria [31] and sickle cell disease [49, 68].

Modeling Blood Flow in Health

DPD simulations have proven effective in modeling the collective dynamics and microrheology of RBCs in shear flow. The simulations for shear flow can accurately predict the dependence of blood viscosity on shear rate, see Fig. 5.10a. A novel feature is the inclusion of attractive cell–cell interactions which allows to investigate cell aggregation and formation of rouleaux. Simulations in larger tubes with diameters ranging from 10 to 40 μm successfully reproduced several hemodynamic phenomena, including cell migration towards the flow centerline, cell-free layer near the wall and blunt velocity profile [51]. Recently, more complex geometries have been considered, e.g. the blood flow in a bifurcating microfluidic channel or complex arterial network [57, 73]. The results quantify the effect of branch location and bifurcation angle variation on blood-plasma separation, which is agreement with experiment.

An important characteristic of the dynamics of an individual RBC in shear flow is the tank-treading frequency. Simulations with continuum models suggest that the membrane viscosity needs to be accounted for in order to agree with the experiments. Indeed, the MS-RBC model with membrane viscosity captures this effect [28]. More recently, the simulations with a two-component RBC model have been demonstrated to capture the observed dependency between TT frequency and shear rate for RBCs with different degrees of confinement [63]: it follows a linear relationship for a narrow channel but a nonlinear one for a wide channel. The simulations also probed the apparent bilayer–cytoskeleton slip for a defective membrane in hereditary spherocytosis and elliptocytosis.

Modeling Blood Flow in Malaria

Malaria is one of the most prevalent human infections worldwide. In malaria, RBCs are hosts of Plasmodium parasites which change the cell biomechanical properties. Progression through the parasite development from ring to trophozoite then to schizont stages leads to *Pf*-RBCs loss of their deformability with a relative membrane stiffening more than tenfold in comparison to healthy ones. Moreover, at the final stage (schizont) of the parasite development, the *Pf*-RBCs often show near-spherical shapes due to the formation of intracellular parasitophorous vacuoles, which further impaires cell deformability. These changes can greatly affect the dynamic and rheological properties of *Pf*-RBCs, alter blood flow and may even cause occlusions of small capillaries. Quantifying cell deformability for various stages of *Pf*-RBCs is significant. Recent efforts have been directed towards this end. For example, Bow et al. [13] employed a MS-RBC model to study the biomechanical properties of *Pf*-RBCs. They investigated a progressive stiffening of *Pf*-RBCs with parasite growth. Ye et al. [109] simulated the flow dynamics of *Pf*-RBCs in shear flow. They found that malaria parasites can perturb blood flow, causing *Pf*-RBCs move towards blood vessel wall and adhere to the subendothelial surface. Recently, Chang et al. [16] developed a two-step multiscale framework

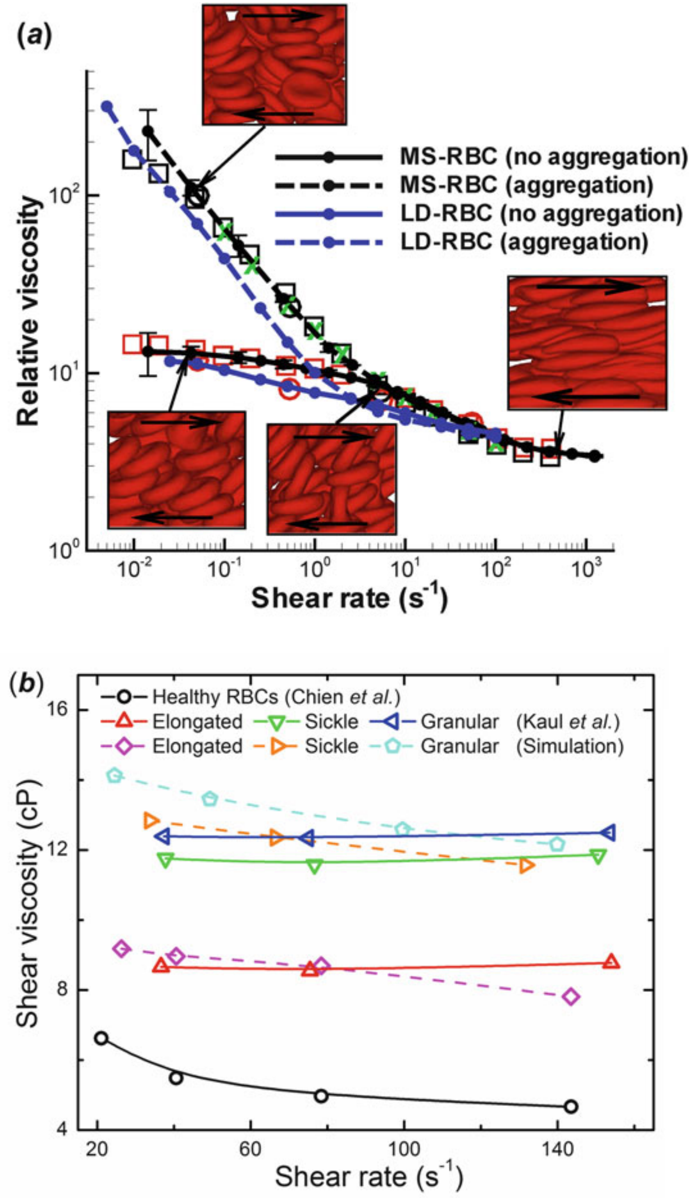

Fig. 5.10 Predicting human blood viscosity in-silico. (**a**) Shear viscosity of normal blood as a function of shear rate; Adapted from [30]. (**b**) Shear viscosity of sickle cell suspension with different cell morphology at different shear rate. Adapted from [68]

for RBC modeling. Using this two-step multiscale framework, they predicted the altered biomechanical properties of RBCs associated with their pathophysiological states, including malaria. They investigated the influence of the nanoscale knob density on RBC deformability and found a decrease in elongation index for *Pf*-RBCs at trophozoite and schizont stages with the increase of knob density, indicating that the nanoscale knobs, being rigid, contribute to cell membrane stiffness.

Modeling Blood Flow in Sickle Cell Anemia (SCA)

SCA is a genetic blood disorder exhibiting heterogeneous cell morphology and abnormal rheology under hypoxic conditions [17, 42]. In sickle cell disease, mechanically fragile but rather stiff RBCs contribute to impaired blood flow and other pathophysiological aspects of the disease. When the flow of blood is relatively slow, cellular reactions occur that lead to adhesion of sickle RBCs to vascular endothelium, resulting in vaso–occlusion and consequent clinical manifestations such as organ damage, pain, and even death. Using the same DPD-based RBC model, Li et al. [68] performed simulations of blood flow in sickle cell disease. The simulation results confirmed the previous experimental measurements that the sickle cell blood exhibit different levels of viscosity for different cell morphologies (Fig. 5.10b): the granular RBC suspension is the most viscous, while the shear viscosity of sickle RBC suspensions containing elongated RBCs shows a dramatic decrease. Moreover, it is known that the origin of SCA can be traced to a common molecular basis, but individual patients with SCA have a highly variable clinical phenotype. For these reasons, Li et al. [68] have recently developed a predictive patient-specific model of SCA. Through the simulations they were able to reveal the role of approved drugs like hydroxyurea on the blood viscosity, which has remained a mystery for a long time.

DPD-based RBC models have also been used to quantify the adhesive properties of sickle RBCs and probe vaso-occlusion phenomena in SCA (Fig. 5.11) [49]. Given the same "adhesive potential", their results validate the hypothesis that heterogeneous cell adhesive dynamics is mainly due to the different cell rigidities and peculiar cell morphologies (Fig. 5.11a) [48]. They also quantified the specific physiological conditions triggering the vaso-occlusion crisis. Under physiological conditions, their simulations show that the interplay of deformable SS2 cells and ISCs can potentially trigger full blood occlusion. In addition, they also employed a DPD-based white blood cell (WBC) model to probe its effect to blood vaso-occlusion. They found that the blood flow undergoes slow down due to the WBC recruitment and the moderate sickle RBC–WBC interaction leads to multiple sickle RBC trapped on the WBCs and the full occlusion (Fig. 5.11b).

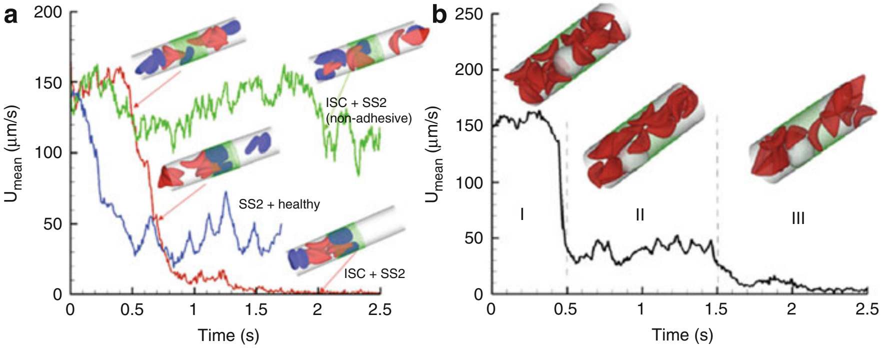

Fig. 5.11 Vaso-occlusion in post-capillaries. (**a**) Instantaneous mean velocity of blood flow in a cylindrical tube of $D = 10\,\mu\text{m}$ infused with different sickle RBC suspensions. The *red curve* represents the resultant velocity infused with SS2 and ISC cell groups. The *inset plots* represent the instantaneous snapshots where SS2 cells adhere to vessel wall, consequently trapping the ISCs and resulting in cell blockage. The *green curve* represents the blood velocity infused with SS2 and ISC cell groups, where adhesive interaction is only applied to the ISC group. The *inset plot* represents a snapshot where transient adhesion is established between ISC and the tube wall. Steady flow is recovered due to the detachment of the cell from the tube wall. The *blue curve* represents the instantaneous velocity of blood flow infused with SS2 and healthy cell groups. Blood flow exhibits a slow down but not a full occlusion. (**b**) Effect of WBCs: instantaneous mean velocity of the blood flow in a tube of $D = 13.4\,\mu\text{m}$. The *inset snapshots* represent blood cells in free motion, WBC adhesion and blood occlusion states. Reproduced from [49], by permission

5.5.3 Dynamics of Polymers in Shear Flow

A polymer is a large molecule composed of many repeated subunits bonded together. The dynamics of a polymer in shear flow is of central importance in biomolecular engineering, materials science, and medicine. Therefore, it is not surprising that the polymer behavior in shear flow has become a subject of intensive experimental, theoretical, and computational studies.

Through the DPD approach, a polymer can be represented by linking collections of DPD particles into chains with appropriate forces arising from different combinations of the following types [100]:

- *Harmonic spring model*: It is one of the most popular polymer models. In the spring model, the consecutive particles in the polymer chain are connected by harmonic springs,

$$F_{ij}^{S} = k_S(1 - r_{ij}/r_0), \tag{5.167}$$

with k_S being the spring constant, and r_0 the equilibrium bond length.

- *Wormlike chain (WLC) model*: It is a continuous model used to characterize the behavior of a semi-flexible polymer.

$$F_{ij}^{WLC} = -\frac{k_B T}{4\lambda_P}\left[\left(1 - \frac{r_{ij}}{L_{SP}}\right)^{-2} + \frac{4r_{ij}}{L_{SP}} - 1\right], \tag{5.168}$$

  where λ_P is an effective persistence length, and L_{SP} is the maximum length of the spring.
- *Finitely extensible nonlinear elastic (FENE) model*: It simplifies the chain of monomers by connecting a sequence of beads with nonlinear springs, which can capture the finite extensibility of a polymer chain. For the FENE chain, the force on particle i due to particle j is,

$$F_{ij}^{FENE} = -\frac{H r_{ij}}{1 - (r_{ij}/r_{max}^2)}, \tag{5.169}$$

  in which H is the spring constant, and r_{max} is the maximum length of the spring.
- *Lennard-Jones chain (LJC) model*: The force for each pair of particles is given by a truncated Lennard-Jones potential,

$$U_{LJ} = 4\epsilon\left[\left(\frac{L}{r_{ij}}\right)^{12} - \left(\frac{L}{r_{ij}}\right)^{6} + \frac{1}{4}\right], \tag{5.170}$$

  where ϵ is the depth of the potential well, and L is the finite distance at which the inter-particle potential is zero.

Industrial and biological applications based on the dynamics of polymer in microfluidic and nanofluidic channels are ubiquitous in past decades. Recent works have focused on the dynamics and flow behaviors of polymers in fluidic channels. Such studies deepen our understanding of the detailed conformational changes of polymers inside the fluidic channels. Dynamic simulation and modeling help in predicting how polymers will behave in fluidic flows and channels. For example, Wijmans and Smit [107] simulate tethered polymers in shear flow using DPD. They found that the polymer chains are able to stretch in the flow direction with respect to the shear rate. Symeonidis and Karniadakis [100] employed DPD to study the λ-phage DNA under shear flow. They presented comparison of WLC models under shear with experimental results and demonstrated the correct static scaling laws for the radius of gyration. Fan et al. [27] simulated the dynamics of macromolecular solutions in shear flow. They found that the velocity profiles of FENE polymer chain suspensions can be fitted using the power-law model.

Dynamics of the translocation of polymers through a narrow channel or a narrow pore is significant in the understanding of several chemical and biological processes such as the transport of protein through membrane channels, motion of DNA and RNA across narrow pores, and infection of virus into the cell nucleus. Therefore, the translocation dynamics of polymer in shear flow have received increasing

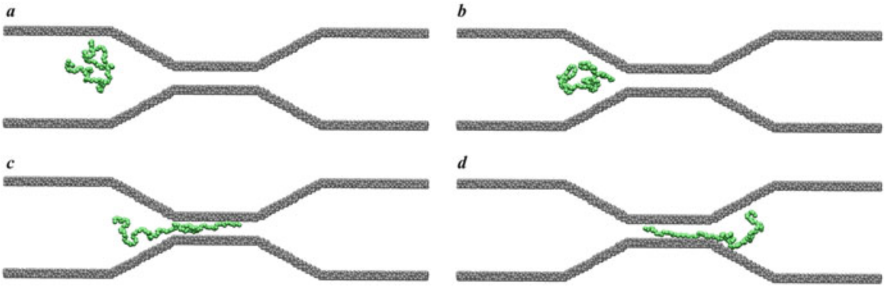

Fig. 5.12 Translocation event produced by a polymer molecule passing through the fluidic channel in single-file conformations in the simulation at (**a**) $t = 110$, (**b**) $t = 160$, (**c**) $t = 180$, and (**d**) $t = 220$. Adapted with permission from [36]

attention in past decades. In the process of polymer translocation through a narrow channel, the number of available configurations of polymer molecules decreases, resulting in an effective entropy barrier for polymer molecules. Therefore, an external driving force such as an external electric field, chemical potential gradient, or a direct pulling force, is needed to overcome this entropy barrier and hasten the translocation. In DPD, an applied pressure gradient, which generates a fluid flow in narrow channel, can drive polymer chains through the narrow channel.

The DPD simulation provides a reliable approach to investigate the conformational changes and dynamic behaviors of polymers in the translocation processes. For example, Guo et al. [36] employed DPD to simulate the dynamics of flow-induced translocation of polymers through a fluidic channel. They found that there are three stages in the translocation process of linear polymer molecule (Fig. 5.12): (1) drift diffusion; (2) capture; and (3) translocation. These simulations can help in clearly understanding the detailed conformational, dynamical, and transport properties of polymer molecules and the events taking place inside the fluidic channels during the process of the polymer translocation.

5.6 Concluding Remarks

Dissipative particle dynamics, as a coarse-grained molecular dynamics method that can be rigorously derived through the Mori-Zwanzig formalism, has been demonstrated to be a powerful and flexible mesoscopic method for simulating the mesoscopic dynamics of complex fluids and various mesoscopic phenomena in soft matter systems. In the past decade, the classical DPD method and its extensions have already been applied successfully to a wide range of problems occurring at the mesoscale. However, there still remain many open questions both in the foundation of DPD and in its applications.

An open question of DPD's foundation is the theoretical derivation of mesoscopic principle from molecular dynamics simulations of unbonded atoms. Unlike bonded atoms in polymers and proteins, unbonded atoms does not move as a group and cannot be packed into a coarse-grained entity. Consequently, the coarse-grained representation of unbonded atoms does not have clear physical definition. Although constraints can be applied to enforce unbonded atoms to move as a group in molecular dynamics simulations for coarse-graining [50, 94], these constraints significantly change the dynamical behavior of the unbonded atoms; hence, these constrained molecular dynamics systems can no longer represent the correct solvents. Therefore, the theoretical derivation of mesoscopic principles for unconstrained and unbonded solvents is an open question.

Another interesting relevant problem of DPD is that memory effects should be included in mesoscopic modeling when the Markovian property breaks down. The classical DPD model was constructed with Gaussian white noise, which assumes that the typical time scales of resolved dynamics and unresolved dynamics are well-separated. However, at small coarse-grained levels, it is expected that the time scale of unresolved dynamics is comparable with that of resolved dynamics, where the correlation of random force cannot simply be replaced by the Dirac delta function. Then, we need to consider non-Markovian dynamics by including memory effects. So far there have been several attempts to include non-Markovian memory into mesoscopic modeling, such as introduction of additional internal variables [104], computing a time-convolution for friction directly [64], using a set of fictitious particles [18], or coupling to the Ornstein-Uhlenbeck process [69].

Finally, DPD application to diverse practical problems requires the development of fast time-evolution algorithms for large-scale simulations and useful boundary methods for modeling biological systems. To this end, many attempts have been made to enhance the capability of DPD simulations. Examples include the open source GPU-accelerated DPD simulators [11, 101] for large-scale simulations, the efficient time-integrators allowing for larger time steps [53, 54], an inflow/outflow boundary method for blood flows [73] and a local detection boundary method for arbitrarily complex geometries [67].

References

1. E. Abu-Nada, Natural convection heat transfer simulation using energy conservative dissipative particle dynamics. Phys. Rev. E **81**(5), 056704 (2010)
2. Y. Afshar, F. Schmid, A. Pishevar, S. Worley, Exploiting seeding of random number generators for efficient domain decomposition parallelization of dissipative particle dynamics. Comput. Phys. Commun. **184**(4), 1119–1128 (2013)
3. M.P. Allen, D.J. Tildesley, *Computer Simulation of Liquids* (Clarendon Press, Oxford, 1989)
4. M. Anand, K. Rajagopal, K.R. Rajagopal, A model incorporating some of the mechanical and biochemical factors underlying clot formation and dissolution in flowing blood. J. Theor. Med. **5**(3–4), 183–218 (2003)

5. M. Arienti, W.X. Pan, X.Y. Li, G. Karniadakis, Many-body dissipative particle dynamics simulation of liquid/vapor and liquid/solid interactions. J. Chem. Phys. **134**(20), 204114 (2011)
6. J.B. Avalos, A.D. Mackie, Dissipative particle dynamics with energy conservation. Europhys. Lett. **40**(2), 141–146 (1997)
7. J.A Backer, C.P Lowe, H.C.J Hoefsloot, P.D Iedema, Poiseuille flow to measure the viscosity of particle model fluids. J. Chem. Phys. **122**(15), 154503 (2005)
8. R.W. Balluffi, S.M. Allen, W.C. Carter, *Kinetics of Materials* (Wiley, Hoboken, 2005)
9. G. Besold, I. Vattulainen, M. Karttunen, J.M. Polson, Towards better integrators for dissipative particle dynamics simulations. Phys. Rev. E **62**(6), R7611–R7614 (2000)
10. X. Bian, S. Litvinov, R. Qian, M. Ellero, N.A. Adams, Multiscale modeling of particle in suspension with smoothed dissipative particle dynamics. Phys. Fluids **24**(1), 012002 (2012)
11. A.L. Blumers, Y.-H. Tang, Z. Li, X.J. Li, G.E. Karniadakis. GPU-accelerated red blood cells simulations with transport dissipative particle dynamics. Comput. Phys. Commun. **217**, 171–179 (2017)
12. J. Bonet, T.S.L. Lok, Variational and momentum preservation aspects of smooth particle hydrodynamic formulations. Comput. Methods Appl. Mech. Eng. **180**(1–2), 97–115 (1999)
13. H. Bow, I.V. Pivkin, M. Diez-Silva, S.J. Goldfless, M. Dao, J.C. Niles, S. Suresh, J. Han, A microfabricated deformability-based flow cytometer with application to malaria. Lab Chip **11**, 1065–1073 (2011)
14. H.B. Callen, *Thermodynamics and An Introduction to Thermostatistics* (Wiley, New York, 1985)
15. Z.H. Cao, K. Luo, H.L. Yi, H.P. Tan, Energy conservative dissipative particle dynamics simulation of natural convection in eccentric annulus. Int. J. Heat Mass Transf. **65**, 409–422 (2013)
16. H.-Y. Chang, X.J. Li, H. Li, G.E. Karniadakis, MD/DPD multiscale framework for predicting morphology and stresses of red blood cells in health and disease. PLOS Comput. Biol. **10**, e1005173 (2016)
17. S. Chien, S. Usami, J.F. Bertles, Abnormal rheology of oxygenated blood in sickle cell anemia. J. Clin. Invest. **49**, 623–634 (1970)
18. A. Davtyan, J.F. Dama, G.A. Voth, H.C. Andersen, Dynamic force matching: a method for constructing dynamical coarse-grained models with realistic time dependence. J. Chem. Phys. **142**(15), 154104 (2015)
19. M.G. Deng, Z. Li, O. Borodin, G.E. Karniadakis, cDPD: a new dissipative particle dynamics method for modeling electrokinetic phenomena at the mesoscale. J. Chem. Phys. **145**(14), 144109 (2016)
20. M.G. Deng, W.X. Pan, G.E. Karniadakis, Anisotropic single-particle dissipative particle dynamics model. J. Comput. Phys. **336**, 481–491 (2017)
21. R. Erban, S.J. Chapman, Reactive boundary conditions for stochastic simulations of reaction-diffusion processes. Phys. Biol. **4**(1), 16–28 (2007)
22. P. Español, Hydrodynamics from dissipative particle dynamics. Phys. Rev. E **52**(2), 1734–1742 (1995)
23. P. Español, Dissipative particle dynamics with energy conservation. Europhys. Lett. **40**(6), 631–636 (1997)
24. P. Español, Fluid particle model. Phys. Rev. E **57**(3), 2930–2948 (1998)
25. P. Español, M. Revenga, Smoothed dissipative particle dynamics. Phys. Rev. E **67**, 026705 (2003)
26. P. Español, P. Warren, Statistical mechanics of dissipative particle dynamics. Europhys. Lett. **30**(4), 191–196 (1995)
27. X.J. Fan, N. Phan-Thien, N.T. Yong, X.H. Wu, D. Xu, Microchannel flow of a macromolecular suspension. Phys. Fluids **15**(1), 11–21 (2003)
28. D.A. Fedosov, B. Caswell, G.E. Karniadakis, A multiscale red blood cell model with accurate mechanics, rheology, and dynamics. Biophys. J. **98**(10), 2215–2225 (2010)

29. D.A. Fedosov, H. Lei, B. Caswell, S. Suresh, G.E. Karniadakis, Multiscale modeling of red blood cell mechanics and blood flow in malaria. PLoS Comput. Biol. **7**, e1002270 (2011)
30. D.A. Fedosov, W.X. Pan, B. Caswell, G. Gompper, G.E. Karniadakis, Predicting human blood viscosity in silico. Proc. Natl. Acad. Sci. USA **108**(29), 11772–11777 (2011)
31. D.A. Fedosov, B. Caswell, S. Suresh, G.E. Karniadakis, Quantifying the biophysical characteristics of *Plasmodium-falciparum*-parasitized red blood cells in microcirculation. Proc. Natl. Acad. Sci. USA **108**, 35–39 (2011)
32. C. Gardiner, *Handbook of Stochastic Methods: For Physics, Chemistry and the Natural Sciences*, 3rd edn. (Springer, New York, 2004)
33. H. Grabert, *Projection Operator Techniques in Nonequilibrium Statistical Mechanics*, vol. 95 (Springer, Berlin/Heidelberg, 1982)
34. R.D. Groot, *Applications of Dissipative Particle Dynamics*. Lecture Notes in Physics, chapter 1, vol. 640 (Springer, Berlin/Heidelberg, 2004), pp. 5–38
35. R.D. Groot, P.B. Warren, Dissipative particle dynamics: bridging the gap between atomistic and mesoscopic simulation. J. Chem. Phys. **107**(11), 4423–4435 (1997)
36. J.Y. Guo, X.J. Li, Y. Liu, H.J. Liang, Flow-induced translocation of polymers through a fluidic channel: a dissipative particle dynamics simulation study. J. Chem. Phys. **134**(13), 134906 (2011)
37. J.-P. Hansen, I.R. McDonald, *Theory of Simple Liquids, Fourth Edition: With Applications to Soft Matter* (Academic, Amsterdam, 2013)
38. C. Hijón, P. Español, E. Vanden-Eijnden, R. Delgado-Buscalioni, Mori–Zwanzig formalism as a practical computational tool. Faraday Discuss. **144**, 301–322 (2010)
39. P.J. Hoogerbrugge, J.M.V.A. Koelman, Simulating microscopic hydrodynamic phenomena with dissipative particle dynamics. Europhys. Lett. **19**(3), 155–160 (1992)
40. M.X. Huang, Z.Q. Li, H.X. Guo, The effect of janus nanospheres on the phase separation of immiscible polymer blends via dissipative particle dynamics simulations. Soft Matter **8**(25), 6834–6845 (2012)
41. J.H. Irving, J.G. Kirkwood, The statistical mechanical theory of transport processes. IV. The equations of hydrodynamics. J. Chem. Phys. **18**(6), 817–829 (1950)
42. D.K. Kaul, H. Xue, Rate of deoxygenation and rheologic behavior of blood in sickle cell anemia. Blood **77**, 1353–1361 (1991)
43. T. Kinjo, S.A. Hyodo, Equation of motion for coarse-grained simulation based on microscopic description. Phys. Rev. E **75**(5), 051109 (2007)
44. J.M.V.A. Koelman, P.J. Hoogerbrugge, Dynamic simulations of hard-sphere suspensions under steady shear. Europhys. Lett. **21**(3), 363–368 (1993)
45. J. Kordilla, W.X. Pan, A. Tartakovsky, Smoothed particle hydrodynamics model for Landau-Lifshitz-Navier-Stokes and advection-diffusion equations. J. Chem. Phys. **141**, 224112 (2014)
46. L.D. Landau, E.M. Lifshitz, *Fluid Mechanics (Volume 6 of A Course of Theoretical Physics)* (Pergamon Press, New York, 1959)
47. A.W. Lees, S.F. Edwards, The computer study of transport processes under extreme conditions. J. Phys. C: Solid State Phys. **5**(15), 1921–1929 (1972)
48. H. Lei, G.E. Karniadakis, Quantifying the rheological and hemodynamic characteristics of sickle cell anemia. Biophys. J. **102**, 185–194 (2012)
49. H. Lei, G.E. Karniadakis, Probing vasoocclusion phenomena in sickle cell anemia via mesoscopic simulations. Proc. Natl. Acad. Sci. USA **110**(28), 11326–11330 (2013)
50. H. Lei, B. Caswell, G.E. Karniadakis, Direct construction of mesoscopic models from microscopic simulations. Phys. Rev. E **81**(2), 026704 (2010)
51. H. Lei, D.A. Fedosov, B. Caswell, G.E. Karniadakis, Blood flow in small tubes: quantifying the transition to the non-continuum regime. J. Fluid Mech. **722**, 214–239 (2013)
52. H. Lei, X. Yang, Z. Li, G.E. Karniadakis, Systematic parameter inference in stochastic mesoscopic modeling. J. Comput. Phys. **330**, 571–593 (2017)
53. B. Leimkuhler, X.C. Shang, On the numerical treatment of dissipative particle dynamics and related systems. J. Comput. Phys. **280**, 72–95 (2015)

54. B. Leimkuhler, X.C. Shang, Pairwise adaptive thermostats for improved accuracy and stability in dissipative particle dynamics. J. Comput. Phys. **324**, 174–193 (2016)
55. H. Li, G. Lykotrafitis, A coarse-grain molecular dynamics model for sickle hemoglobin fibers. J. Mech. Behav. Biomed. **4**(2), 162–173 (2011)
56. H. Li, G. Lykotrafitis, Two-component coarse-grained molecular-dynamics model for the human erythrocyte membrane. Biophys. J. **102**(1), 75–84 (2012)
57. X.J. Li, A.S. Popel, G.E. Karniadakis, Blood-plasma separation in Y-shaped bifurcating microfluidic channels: a dissipative particle dynamics simulation study. Phys. Biol. **9**(2), 026010 (2012)
58. Z. Li, Z. W. Zhou, G.H. Hu, Dissipative particle dynamics simulation of droplet oscillations in AC electrowetting. J. Adhes. Sci. Technol. **26**(12–17), 1883–1895 (2012)
59. H. Li, V. Ha, G. Lykotrafitis, Modeling sickle hemoglobin fibers as one chain of coarse-grained particles. J. Biomech. **45**(11), 1947–1951 (2012)
60. Z. Li, G.H. Hu, Z.L. Wang, Y.B. Ma, Z.W. Zhou, Three dimensional flow structures in a moving droplet on substrate: a dissipative particle dynamics study. Phys. Fluids **25**(7), 072103 (2013)
61. Z. Li, X. Bian, B. Caswell, G.E. Karniadakis, Construction of dissipative particle dynamics models for complex fluids via the Mori–Zwanzig formulation. Soft Matter **10**(43), 8659–8672 (2014)
62. Z. Li, Y.-H. Tang, H. Lei, B. Caswell, G.E. Karniadakis, Energy-conserving dissipative particle dynamics with temperature-dependent properties. J. Comput. Phys. **265**, 113–127 (2014)
63. X.J. Li, Z.L. Peng, H. Lei, M. Dao, G.E. Karniadakis, Probing red blood cell mechanics, rheology and dynamics with a two-component multiscale model. Phil. Trans. R. Soc. A **372**, 20130389 (2014)
64. Z. Li, X. Bian, X.T. Li, G.E. Karniadakis, Incorporation of memory effects in coarse-grained modeling via the Mori–Zwanzig formalism. J. Chem. Phys. **143**(24), 243128 (2015)
65. Z. Li, Y.-H. Tang, X.J. Li, G.E. Karniadakis, Mesoscale modeling of phase transition dynamics of thermoresponsive polymers. Chem. Commun. **51**(55), 11038–11040 (2015)
66. Z. Li, A. Yazdani, A. Tartakovsky, G.E. Karniadakis, Transport dissipative particle dynamics model for mesoscopic advection-diffusion-reaction problems. J. Chem. Phys. **143**(1), 014101 (2015)
67. Z. Li, X. Bian, Y.-H. Tang, G.E. Karniadakis, A dissipative particle dynamics method for arbitrarily complex geometries. arXiv preprint arXiv:1612.08761 (2016)
68. X.J. Li, E. Du, H. Lei, Y.-H. Tang, M. Dao, S. Suresh, G.E. Karniadakis, Patient-specific blood rheology in sickle-cell anaemia. Interface Focus **6**(1), 20150065 (2016)
69. Z. Li, H.S. Lee, E. Darve, G.E. Karniadakis, Computing the non-Markovian coarse-grained interactions derived from the Mori–Zwanzig formalism in molecular systems: application to polymer melts. J. Chem. Phys. **146**(1), 014104 (2017)
70. M. Lisal, J.K. Brennan, Alignment of lamellar diblock copolymer phases under shear: insight from dissipative particle dynamics simulations. Langmuir **23**(9), 4809–4818 (2007)
71. M.B. Liu, G.R. Liu, L.W. Zhou, J.Z. Chang, Dissipative particle dynamics (DPD): an overview and recent developments. Arch. Comput. Meth. Eng. **22**(4), 529–556 (2015)
72. Z.Y. Lu, Y.M. Wang, *An Introduction to Dissipative Particle Dynamics*. Methods in Molecular Biology, chap. 24, vol. 924 (Humana Press, New York, 2013), pp. 617–633
73. K. Lykov, X.J. Li, H. Lei, I.V. Pivkin, G.E. Karniadakis, Inflow/outflow boundary conditions for particle-based blood flow simulations: application to arterial bifurcations and trees. PLoS Comput. Biol. **11**(8), e1004410 (2015)
74. A.D. Mackie, J.B. Avalos, V. Navas, Dissipative particle dynamics with energy conservation: modelling of heat flow. Phys. Chem. Chem. Phys. **1**(9), 2039–2049 (1999)
75. C.A. Marsh, J.M. Yeomans, Dissipative particle dynamics: the equilibrium for finite time steps. Europhys. Lett. **37**(8), 511–516 (1997)
76. C.A. Marsh, G. Backx, M.H. Ernst, Fokker-Planck-Boltzmann equation for dissipative particle dynamics. Europhys. Lett. **38**(6), 411–415 (1997)

77. C.A. Marsh, G. Backx, M.H. Ernst, Static and dynamic properties of dissipative particle dynamics. Phys. Rev. E **56**(2), 1676–1691 (1997)
78. Z.G. Mills, W.B. Mao, A. Alexeev, Mesoscale modeling: solving complex flows in biology and biotechnology. Trends Biotechnol. **31**(7), 426–434 (2013)
79. J.J. Monaghan, Smoothed particle hydrodynamics. Rep. Prog. Phys. **68**(8), 1703–1759 (2005)
80. H. Mori, Transport, collective motion, and Brownian motion. Prog. Theor. Phys. **33**(3), 423–455 (1965)
81. S.V. Nikolov, H. Shum, A.C. Balazs, A. Alexeev, Computational design of microscopic swimmers and capsules: from directed motion to collective behavior. Curr. Opin. Colloid Interface Sci. **21**, 44–56 (2016)
82. W.G. Noid, Perspective: coarse-grained models for biomolecular systems. J. Chem. Phys. **139**, 090901 (2013)
83. J.M. Ortiz de Zárate, J.V. Sengers, *Hydrodynamic Fluctuations in Fluids and Fluid Mixtures* (Elsevier, Amsterdam, 2006)
84. H.C. Öttinger, *Beyond Equilibrium Thermodynamics* (Wiley-Interscience, New York, 2005)
85. I. Pagonabarraga, D. Frenkel, Dissipative particle dynamics for interacting systems. J. Chem. Phys. **115**(11), 5015–5026 (2001)
86. W.X. Pan, I.V. Pivkin, G.E. Karniadakis, Single-particle hydrodynamics in DPD: a new formulation. Europhys. Lett. **84**(1), 10012 (2008)
87. D.Y. Pan, J.X. Hu, X.M. Shao, Lees-Edwards boundary condition for simulation of polymer suspension with dissipative particle dynamics method. Mol. Simul. **42**(4), 328–336 (2016)
88. N. Phan-Thien, N. Mai-Duy, B.C. Khoo, A spring model for suspended particles in dissipative particle dynamics. J. Rheol. **58**(4), 839–867 (2014)
89. C.L. Phillips, J.A. Anderson, S.C. Glotzer, Pseudo-random number generation for Brownian dynamics and dissipative particle dynamics simulations on GPU devices. J. Comput. Phys. **230**(19), 7191–7201 (2011)
90. I.V. Pivkin, G.E. Karniadakis, A new method to impose no-slip boundary conditions in dissipative particle dynamics. J. Comput. Phys. **207**(1), 114–128 (2005)
91. I.V. Pivkin, G.E. Karniadakis, Controlling density fluctuations in wall-bounded dissipative particle dynamics systems. Phys. Rev. Lett. **96**, 206001 (2006)
92. I.V. Pivkin, G.E. Karniadakis, Accurate coarse-grained modeling of red blood cells. Phys. Rev. Lett. **101**, 118105 (2008)
93. I.V. Pivkin, Z. Peng, G.E. Karniadakis, P.A. Buffet, M. Dao, S. Suresh, Biomechanics of red blood cells in human spleen and consequences for physiology and disease. Proc. Natl. Acad. Sci. USA **113**(28), 7804–7809 (2016)
94. M. Praprotnik, L.D. Site, K. Kremer, Adaptive resolution scheme for efficient hybrid atomistic-mesoscale molecular dynamics simulations of dense liquids. Phys. Rev. E **73**, 066701 (2006)
95. R. Qiao, P. He, Simulation of heat conduction in nanocomposite using energy-conserving dissipative particle dynamics. Mol. Simul. **33**(8), 677–683 (2007)
96. M. Ripoll, P. Español, M.H. Ernst, Dissipative particle dynamics with energy conservation: heat conduction. Int. J. Mod. Phys. C **9**(8), 1329–1338 (1998)
97. D. Rossinelli, Y.-H. Tang, K. Lykov, D. Alexeev, M. Bernaschi, P. Hadjidoukas, M. Bisson, W. Joubert, C. Conti, G. Karniadakis, M. Fatica, I. Pivkin, P. Koumoutsakos, The in-silico lab-on-a-chip: petascale and high-throughput simulations of microfluidics at cell resolution, in *Proceedings of the International Conference for High Performance Computing, Networking, Storage and Analysis, SC '15* (Association for Computing Machinery, New York, 2015), pp. 2:1–2:12
98. M.G. Saunders, G.A. Voth, Coarse-graining methods for computational biology. Annu. Rev. Biophys. **42**, 73–93 (2013)
99. T. Shardlow, Splitting for dissipative particle dynamics. SIAM J. Sci. Comput. **24**(4), 1267–1282 (2003)

100. V. Symeonidis, G.E. Karniadakis, B. Caswell, Dissipative particle dynamics simulations of polymer chains: scaling laws and shearing response compared to dna experiments. Phys. Rev. Lett. **95**, 076001 (2005)
101. Y.-H. Tang, G.E. Karniadakis, Accelerating dissipative particle dynamics simulations on GPUs: algorithms, numerics and applications. Comput. Phys. Commun. **185**(11), 2809–2822 (2014)
102. Y.-H. Tang, Z. Li, X.J. Li, M.G. Deng, G.E. Karniadakis, Non-equilibrium dynamics of vesicles and micelles by self-assembly of block copolymers with double thermoresponsivity. Macromolecules **49**(7), 2895–2903 (2016)
103. A. Tiwari, J. Abraham, Dissipative particle dynamics model for two-phase flows. Phys. Rev. E **74**, 056701 (2006)
104. A. Vázquez-Quesada, M. Ellero, P. Español, Smoothed particle hydrodynamic model for viscoelastic fluids with thermal fluctuations. Phys. Rev. E **79**, 056707 (2009)
105. Y.X. Wang, S. Chen, Numerical study on droplet sliding across micropillars. Langmuir **31**(16), 4673–4677 (2015)
106. P.B. Warren, Vapor-liquid coexistence in many-body dissipative particle dynamics. Phys. Rev. E **68**, 066702 (2003)
107. C.M. Wijmans, B. Smit, Simulating tethered polymer layers in shear flow with the dissipative particle dynamics technique. Macromolecules **35**(18), 7138–7148 (2002)
108. S.M. Willemsen, H.C.J. Hoefsloot, P.D. Iedema, No-slip boundary condition in dissipative particle dynamics. Int. J. Mod. Phys. C **11**(5), 881–890 (2000)
109. T. Ye, N. Phan-Thien, B. Khoo, C.T. Lim, Numerical modelling of a healthy/malaria-infected erythrocyte in shear flow using dissipative particle dynamics method. J. Appl. Phys. **115**(22), 224701 (2014)
110. S. Yip, M.P. Short, Multiscale materials modelling at the mesoscale. Nat. Mater. **12**(9), 774–777 (2013)
111. R. Zwanzig, Ensemble method in the theory of irreversibility. J. Chem. Phys. **33**(5), 1338–1341 (1960)
112. R. Zwanzig, Memory effects in irreversible thermodynamics. Phys. Rev. **124**(4), 983–992 (1961)
113. R. Zwanzig, *Nonequilibrium Statistical Mechanics*, vol. 54 (Oxford University Press, Oxford, 2001)